Title
Somatic and dendritic inhibition of hippocampal pyramidal cells

Permalink
https://escholarship.org/uc/item/5t45p4j4

Author
Glickfeld, Lindsey L.

Publication Date
2007

Peer reviewed|Thesis/dissertation

UNIVERSITY OF CALIFORNIA, SAN DIEGO

Somatic and Dendritic Inhibition of Hippocampal Pyramidal Cells

A Dissertation in partial satisfaction of the requirement for the degree

Doctor of Philosophy

in

Neurosciences

by

Lindsey L. Glickfeld

Committee in charge:

> Professor Massimo Scanziani, Chair
> Professor Ed Callaway
> Professor Anirvan Ghosh
> Professor Jeffry Isaacson
> Professor Nicholas Spitzer

2007

The Dissertation of Lindsey L. Glickfeld is approved, and it is acceptable in quality and

form for publication on microfilm:

_____

_____

_____

_____
Chair

University of California, San Diego

2007

iii

TABLE OF CONTENTS

LIST OF FIGURES AND TABLES

ACKNOWLEDGEMENTS

My deepest gratitude to:

VITA

1998-2002   Research Assistant, Stanford University

2002   Bachelor of Sciences, Stanford University

2007   Doctor of Philosophy, University of California, San Diego

PUBLICATIONS

Piedras-Renteria ES, Pyle JL, Diehn M, Glickfeld LL, Harata NC, Cao Y, Kavalali ET, Brown PO, Tsien RW. Presynaptic homeostasis at CNS nerve terminals compensates for lack of a key Ca2+ entry pathway. *PNAS* **101**, 3609-14 (2004).

Murphy GJ, Glickfeld LL, Balsen Z, Isaacson JS. Sensory neuron signaling to the brain: properties of transmitter release from olfactory nerve terminals. *J Neurosci.* **24**, 3023-30 (2004).

Glickfeld LL, Scanziani M. Self-administering cannabinoids. *Trends Neurosci.* **28**,341-3 (2005).

Glickfeld LL, Scanziani M. Distinct timing in the activity of cannabinoid-sensitive and cannabinoid-insensitive basket cells. *Nat Neurosci.* **9**, 807-15 (2006).

Kapfer CK, Glickfeld LL, Atallah BV, Scanziani M. Supralinear increase of recurrent inhibition during sparse activity in the somatosensory cortex. *Nat Neurosci.* **10**, 743-53 (2007).

ABSTRACT OF THE DISSERTATION

Somatic and Dendritic Inhibition of Hippocampal Pyramidal Cells

by

Lindsey L. Glickfeld

Doctor of Philosophy in Neurosciences

University of California, San Diego, 2007

Professor Massimo Scanziani, Chair

The central nervous system is a crystalline-like structure which is constructed through the repeated assembly of stereotyped circuits. These circuits connect a relatively homogenous population of excitatory principal cells with a diverse population of inhibitory interneurons. One of the most striking features of the diversity of the interneurons is the specificity of their axonal arborizations. Each class of interneuron targets a specific subcellular compartment; for instance, different populations of interneurons mediate somatic and dendritic inhibition. However, in order to fully

appreciate the implications of having different compartments under discrete inhibitory control we must know three things about each class of interneuron: its impact on the postsynaptic cell, the patterns of activity through which it is recruited, and its regulation by neuromodulators. We argue that these three properties will allow us to define the role of an inhibitory interneuron in the circuit.

In order to investigate the roles of the diverse population of interneurons, we made intracellular recordings from identified interneurons in slices of the rat hippocampus. Through paired intracellular and extracellular recordings, we found that GABA release from both somatic and dendritic targeting interneurons results in the hyperpolarization of pyramidal cells. Within the groups of somatic and dendritic targeting interneurons there was additional diversity in their intrinsic properties, patterns of excitation, and modulation. By dividing the interneurons according to both the location of their axonal arborization (i.e. somatic or dendritic) and their intrinsic firing patterns (i.e. regular and fast spiking), we were able to define four relatively homogenous populations with distinct patterns of recruitment and impacts on their targets. In addition we found that neuromodulators could independently suppress the different classes of interneurons, suggesting that the network can actively regulate the timing and strength of inhibition.

This work provides evidence for the precise roles of somatic and dendritically targeting interneurons in coordinating network activity. In addition, it proposes a methodology for understanding the role of the diverse population of inhibitory interneurons in the intact cortical circuit.

INTRODUCTION

Inhibition was a necessary concept for explaining the dynamics of circuits long before its synaptic basis was discovered. Sherrington invoked the presence of an antagonistic relationship between excitatory and inhibitory inputs in order to explain the actions of opposing muscles groups during spinal reflexes (Sherrington, 1913). Later, when inhibitory pathways could be isolated and independently stimulated, it was found that excitation and inhibition could interact directly to determine the output of a cell (Kuffler and Katz, 1946; Lloyd, 1946; Marmont and Wiersma, 1938). Thus, when synaptic inhibition in the central nervous system and the circuits behind it were first discovered, their importance for local integration and behavioral output were immediately recognized (Brock et al., 1952; Eccles et al., 1956; Fatt and Katz, 1953; Kuffler and Eyzaguirre, 1955). Since then, there has been enormous progress in understanding the mechanisms and the cellular basis of inhibition: the discovery of transmitters, the cloning of receptors, and the identification of inhibitory interneurons (Colonnier, 1968; Iversen et al., 1971; Kuffler and Edwards, 1958; Schofield et al., 1987).

In contrast to the mechanistic description of inhibition, an understanding of its functional relevance has progressed at a much slower pace. At its most basic level, the presence of synaptic inhibition is required to maintain appropriate levels of network excitability (Dichter and Spencer, 1969; Johnston and Brown, 1981; Traub and Wong, 1982). Yet, inhibition is also necessary for the precise organization of network activity in both space and time. Receptive fields, at all stages of sensory processing, are sharpened

1

through the activity of inhibitory circuits (Kirby and Enroth-Cugell, 1976; Kuffler, 1953; Kyriazi et al., 1996; Wehr and Zador, 2003; Wilent and Contreras, 2005). In some sensory systems, spatial information is encoded temporally; this transformation is achieved through coincidence detection enforced by inhibitory circuits (Fried et al., 2002; Grothe and Sanes, 1994; Saitoh and Suga, 1995). Further, inhibitory circuits can promote synchrony among large ensembles and generate oscillatory rhythms (Cobb et al., 1995; Traub et al., 1996; von Krosigk et al., 1993). Thus, inhibitory circuits actively contribute to many computational processes in the cortex.

Nonetheless, we still do not understand the full range of functions that cortical inhibition can perform. This is due to the diverse population of GABAergic interneurons which generate a heterogeneous source of inhibitory control (Freund and Buzsaki, 1996; Somogyi and Klausberger, 2005). Each class of interneuron, due to its morphology and physiology, likely has a different role in shaping the activity of the entire circuit (Buhl et al., 1996; Freund, 2003; McBain and Fisahn, 2001; Miles et al., 1996; Pouille and Scanziani, 2001). Thus, in order to understand the full computational capacity of the cortex, it is necessary to dissect the role of the diverse population of inhibitory interneurons.

Inhibitory circuits

Excitation and inhibition interact through the activity of cortical circuits. GABAergic interneurons are integrated into stereotyped microcircuits that are the basic building blocks for cortical organization (Szentagothai, 1975). According to Eccles,

these microcircuits can be divided into two basic categories: feed-forward and feedback inhibitory circuits (Eccles, 1969).

Feed-forward inhibition occurs when an afferent excitatory projection provides inhibition to its target by recruiting local inhibitory interneurons (**Fig. I-1a**). This results in a precisely coordinated sequence of excitation followed by inhibition. The short delay between excitation and inhibition, due to the disynaptic recruitment of interneurons, enforces strict temporal precision during cortical processing. Only fast-rising excitatory events are able to reach threshold for spike generation before the onset of the inhibition, thereby reducing the spike jitter of pyramidal cells (Blitz and Regehr, 2005; Gabernet et al., 2005; Mittmann et al., 2005; Pouille and Scanziani, 2001). Feed-forward inhibition also transforms principal cells into coincidence detectors, since the effective summation of excitatory inputs can only occur during a few millisecond window.

Feed-forward inhibitory circuits are activated by all major excitatory pathways in the central nervous system (e.g. (Agmon and Connors, 1991; Andersen et al., 1964; Brock et al., 1952; Buzsaki, 1984; Dubin and Cleland, 1977). Since the same fibers excite both interneurons and principal cells, these circuits ensure that increasing levels of excitation will be accompanied by increasing levels of inhibition. However, feed-forward inhibition can not tonically stabilize a population, since its recruitment requires the activation of afferent inputs (Buzsaki, 1984).

In contrast, feedback inhibition occurs when a population inhibits itself by recruiting local inhibitory interneurons (**Fig. I-1b**). Thus, the degree of feedback inhibition is determined by the output of the population, providing the intrinsic stability that feed-forward inhibitory circuits lack (Buzsaki, 1984). The classic feedback circuit is
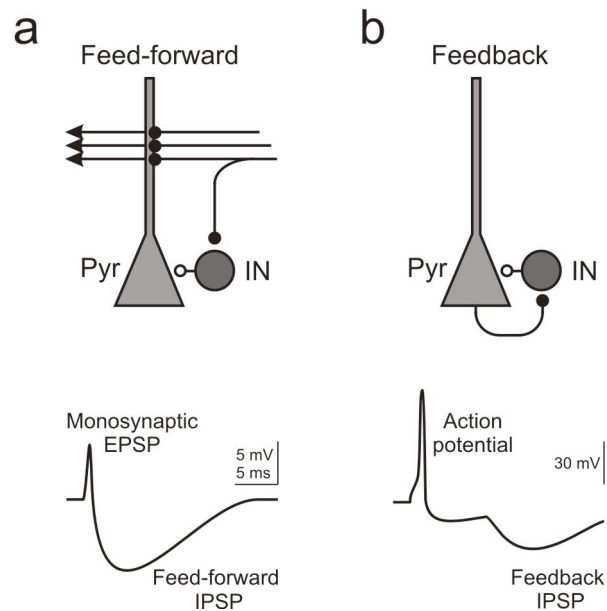
Figure I-1: Feed-forward and feedback inhibitory circuits

(a) Top, schematic of a feed-forward inhibitory circuit where an afferent pathway simultaneously makes excitatory synapses (closed circles) onto the dendrite of a pyramidal cell (Pyr) and an inhibitory interneuron (IN). The IN then makes an inhibitory synapse (open circle) onto the Pyr. Bottom, the resulting synaptic potentials in a Pyr upon activation of the feed-forward inhibitory circuit. The monosynaptic excitatory postsynaptic potential (EPSP), due to the direct release of glutamate onto the pyramidal cell, is cut short by the feed-forward inhibitory postsynaptic potential (IPSP) due to the spiking of feed-forward interneurons.
(b) Top, schematic of a feedback inhibitory circuit where a Pyr makes excitatory synapses onto an IN that makes inhibitory synapses back onto the Pyr. Bottom, the resulting synaptic potentials in a Pyr that is excited above threshold for spiking. The spiking of the Pyr drives the disynaptic feedback inhibtory circuit, evoking a late, feedback IPSP.

that of the Renshaw cell onto motorneurons which limits the excitatory output of the spinal cord (Eccles et al., 1956; Renshaw, 1946). Like feed-forward circuits, recurrent inhibition is ubiquitous, though its function is a bit more obscure (Andersen et al., 1963; Douglas and Martin, 1991; Llinas and Pare, 1991; Windhorst, 1996). Since feedback inhibition follows the activity of its targets, it does not enforce the same millisecond precision that feed-forward inhibition does. Instead, it sets a refractory window which can last for tens of milliseconds (Andersen et al., 1966; Sloviter, 1991). Thus, among other functions, feedback inhibition is likely to underlie the temporal structure of oscillatory activity (Mann et al., 2005).

Lateral inhibition is a specific instance of feed-forward or feedback inhibition in which interneurons inhibit those specific targets which were not excited. Thus, lateral inhibition is an important circuit for the sharpening of receptive fields and increasing signal to noise (Hallett, 1971; Kuffler, 1953; Mori et al., 1999).

The cellular basis of inhibition

Synaptic inhibition in the cortex is mediated by a heterogeneous population of GABAergic interneurons. The most comprehensive characterization of cortical GABAergic interneurons has been done in the hippocampus; there they have been classified according to morphological, immunohistochemical, physiological and pharmacological parameters (Freund and Buzsaki, 1996; Somogyi and Klausberger, 2005). The morphological characterization is predominantly (although not exclusively) based on the distribution of axonal arborizations within hippocampal layers. Since each layer in the CA1 hippocampal region is associated with a specific subcellular domain of

pyramidal cells and an afferent pathway (**Fig. I-2**), the axonal distribution of GABAergic interneurons within these layers can be suggestive of the particular function they exert. The four major compartments of pyramidal cells (the soma, proximal dendrites, distal dendrites, and axon initial segment) each receive inhibition from a specific type of interneuron:

(1) Basket cells are a class of GABAergic interneuron with their axonal arborization restricted to the pyramidal cell layer (**Fig. I-3a**). Individual basket cells form multiple synaptic boutons on the soma of each target cell, generating a powerful inhibitory postsynaptic potential (IPSP) at this key site for integration (Freund and Buzsaki, 1996). Further, the axonal arborizations of basket cells are widely divergent, such that each cell contacts over a thousand pyramidal cells, thereby influencing the activity of an entire network (Cobb et al., 1995; Sik et al., 1995). Somatic inhibition, likely provided by basket cells, is the major source of feed-forward inhibition in the hippocampus (Buhl et al., 1996; Buzsaki, 1984; Pouille and Scanziani, 2001).

(2) Axo-axonic cells specifically impinge on the axon initial segment of pyramidal cells (**Fig. I-3b**). Some reports suggest that since these interneurons directly interact with the action potential initiation zone, they may short-circuit the normal lines of synaptic integration, exerting "veto-power" over pyramidal cell activity (Somogyi et al., 1983).

(3) Bistratified cells target both the basal and apical dendrites of pyramidal cells while avoiding the somatic compartment (**Fig. I-3c**). The extent of their axons matches the innervation pattern of the Schaffer collaterals (Buhl et al., 1996). Given the location

Hippocampal area CA1
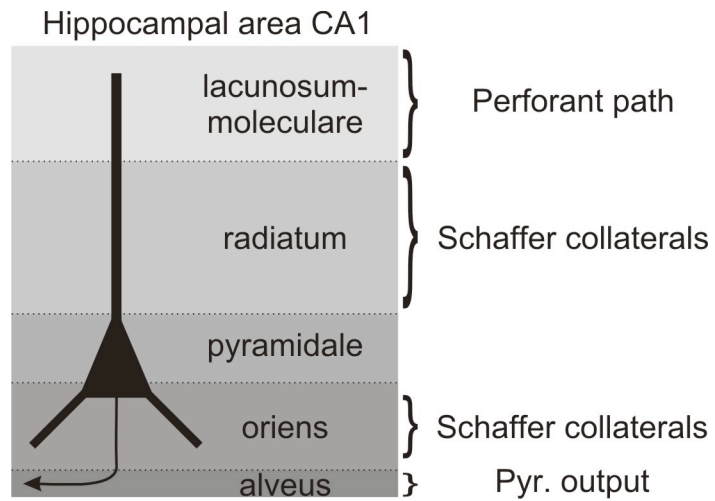
Figure I-2: Lamina of hippocampal area CA1

Schematic illustration of the five strata in area CA1 and the excitatory pathways which innervate them.

of their synapses, it is likely that bistratified cells are more important for governing dendritic integration than the spiking behavior of pyramidal cells (Miles et al., 1996).

(4) Oriens-Lacunosum Molecular (O-LM) neurons target the distal dendritic tufts of pyramidal cells where synapses from the perforant path impinge (**Fig. I-3d**). The distal dendritic tuft of pyramidal cells can respond to strong afferent input with calcium spikes and is thought to act as an independent spike initiation zone (Jarsky et al., 2005). Thus,O-LM neurons may be important in setting the threshold or integration time window for dendritic calcium spikes (Tsubokawa and Ross, 1996). Further, O-LM neurons may gate interactions between inputs from the perforant path and the Schaffer collaterals (Golding et al., 2002). Interestingly, the soma and dendrites of these neurons are restricted to the stratum oriens, over 500 μm from their axonal arborization. Thus, the majority of their inputs are from CA1 pyramidal cells, making them likely mediators of feedback inhibition (Ali and Thomson, 1998; Blasco-Ibanez and Freund, 1995).

Within each of these morphological categories, there is further diversity. For instance, the population of basket cells can be further subdivided into two groups based on their immunohistochemical, physiological and pharmacological properties (Freund, 2003; Pawelzik et al., 2002). One population expresses the calcium binding protein parvalbumin (PV) and fires high frequency, non-adapting trains of action potentials in response to step-depolarizations (fast spiking: FS). Another population expresses the neuropeptide cholecystokinin (CCK) and fires strongly adapting trains of action potentials in response to step-depolarizations (regular spiking: RS). Using anatomy and protein expression alone, the population of GABAergic interneurons in hippocampal area CA1 can be divided into 18 distinct groups (Somogyi and Klausberger, 2005).
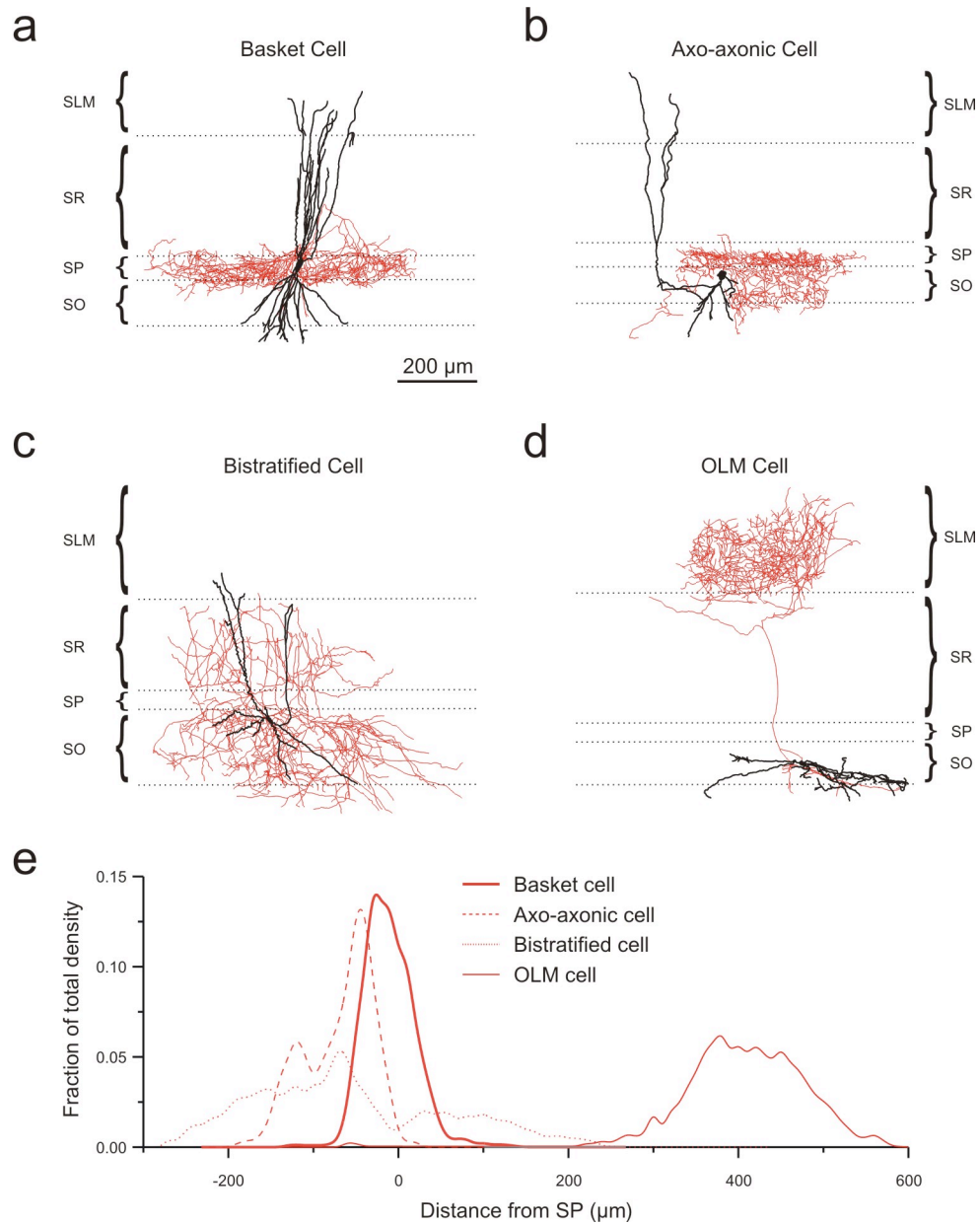
Figure I-3: The cellular basis of inhibition

(a) Reconstruction of the dendrites (black) and axon (red) of a biocytin-filled basket cell. SO, stratum oriens; SP, stratum pyramidale; SR, stratum radiatum; SLM, stratum lacunosum-moleculare. Note the restriction of the axonal arbor to SP.
(b) Reconstruction of an axo-axonic cell.
(c) Reconstruction of a bistratified cell. Note that the axon avoids arborizing in SP.
(d) Reconstruction of an O-LM cell. Note that the axon arborizes in SLM.
(e) Summary of the density of the axonal arborizations of the basket (thick solid line), axo-axonic (dashed line), bistratified (dotted line) and OLM (thin solid line) cells shown in **(a-d)**, plotted along the somato-dendritic axis of the hippocampus.

A role for the diversity of inhibitory circuits

The role of an interneuron is intimately linked to the function of the compartment that it targets (i.e. the soma, dendrite, or axon initial segment). However, its role is also dependent on specific situations that lead to its activation. *In vivo*, the activity of interneurons has been correlated to the ongoing oscillatory rhythms in the hippocampus (Klausberger et al., 2003). While different interneurons of the same class exhibit a stereotyped behavior, interneurons of different classes (basket, axo-axonic and O-LM cells) spike during different phases of an oscillatory rhythm. Thus, different subcellular compartments of pyramidal cells may be selectively inhibited at different times during rhythmic oscillations. Further, the same type of interneuron may participate in one type of oscillation but not another (e.g. theta versus ripple oscillations). This suggests that different interneuron populations are sensitive to the prevailing brain state. Whether these interneurons actively participate in the production of the rhythms or are merely followers of an oscillatory activity generated elsewhere still needs to be established. However, regardless of the underlying causality, the specific pattern of activity of each interneuron type will undoubtedly shape the output of the hippocampus.

In vitro experiments also demonstrate that individual interneuron types are specialized to detect the occurrence of specific patterns of activity (Ali and Thomson, 1998; McBain and Fisahn, 2001; Pouille and Scanziani, 2004). For instance, in response to trains of stimuli, interneurons that target the soma and proximal dendrites (e.g. basket, axo-axonic, and bistratified cells) tend to spike towards the beginning, while interneurons that target the distal dendritic compartment (e.g. O-LM neurons) tend to spike at the end. This pattern recognition is achieved through a confluence of circuit mechanisms: both

their intrinsic membrane properties and the short-term plasticity of their excitatory inputs(Pouille and Scanziani, 2004).

We suggest that each type of interneuron plays a specific role in cortical processing. Two questions are central in establishing the role of individual interneuron types, namely: what are the physiological conditions necessary for their recruitment, and what is the impact of their recruitment on the excitability of the circuit they are embedded in? Thus, in order to fully understand the role of an interneuron, we have developed a integrative approach to studying the circuit. This approach involves systematically determining for each type of inhibitory interneuron: (I) the properties of its inhibitory output, (II) the patterns of activity that make it spike, and (III) the influence of neuromodulators on its activity (**Fig. I-4**). We then can use this data to make predictions about the role of the interneuron and then test this prediction in the intact circuit.

Proposed experiments

The most basic assumption about the role of GABAergic interneurons is that they are inhibitory. However, physiological and immunohistological experiments suggest that the reversal potential for $GABA_A$-mediated currents depends on the post-synaptic compartment (Alger and Nicoll, 1982b; Marty and Llano, 2005; Szabadics et al., 2006). In **Chapter 1**, we will use a non-invasive technique to determine whether the activity of an interneuron induces hyperpolarization, independent of the cellular compartment that it targets.

Basket and bistratified cells are two fundamental sources of GABAergic inhibition. Through somatic inhibition the former determine the output of pyramidal
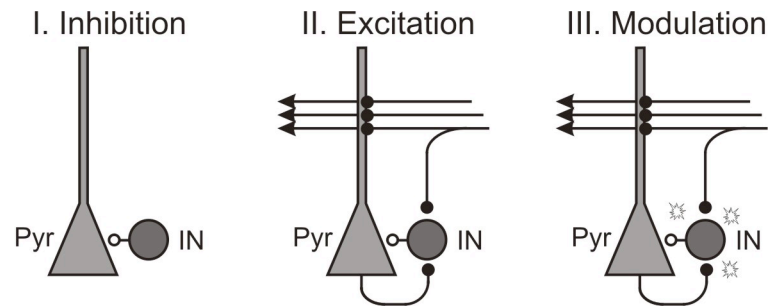
Figure I-4: Determining the role of an interneuron in the circuit

Our strategy for determining the role of an interneuron has three stages:
I.   Determine the properties of the inhibitory synapses from the interneuron (IN) onto the pyramidal cell (Pyr).
II.   Determine the pattern of excitation which preferentially recruits the IN.
III.   Determine the ability of neuromodulators to modulate the inhibition or shift the recruitment of the IN.

cells, while inhibition from the latter interacts directly with inputs from the Schaffer collaterals (Cobb et al., 1995; Miles et al., 1996; Pouille and Scanziani, 2001). Yet, we do not know the function of either of these cell types in the hippocampal circuit. In **Chapters 2** and **3**, we will address the role of basket and bistratified cells, respectively, through the systematic characterization of their outputs, their inputs, and their modulation. Two main aspects are of particular importance: first whether they are activated in a feed-forward or in a feedback manner; and second, the temporal pattern of excitatory activity needed to discharge them. This will enable us to determine the conditions under which basket and bistratified cells are activated and to deduce their impact on the circuit.

EXPERIMENTAL PROCEDURES

Slice preparation and solutions

Hippocampal slices (400 μm) were prepared from 4-6 week-old male Wistar rats

and incubated for one hour in an interface chamber at 34°C in artificial cerebrospinal

fluid (ACSF) containing (in mM): 119 NaCl, 2.5 KCl, 1.3 NaH_2PO_4, 1.3 $MgCl_2$, 2.5

$CaCl_2$, 26 $NaHCO_3$ and 11 glucose (equilibrated with 95% O_2 and 5% CO_2). The slices

were kept at room temperature before being placed in a submerged chamber for

recordings at 32-34°C. Whole cell recordings were performed with patch pipettes (2-4

MΩ) filled with (in mM): 150 K-gluconate, 1.5 $MgCl_2$, 5 HEPES, 1.1 EGTA, and10

phosphocreatine (pH = 7.25; 280-290 mOsm); biocytin (0.2%) and 2 Mg-ATP were

added for interneurons. Extracellular recordings were made with patch pipettes filled

with 3 M NaCl (unless otherwise stated). The drugs used were NBQX, SR95531

('gabazine'), CGP54626, RS-CPP, DAMGO, CTAP, WIN55-212 and AM-251, CPA,

DPCPX (Tocris Cookson). All experiments were conducted in accordance with the

animal use guidelines set out by the University of California, San Diego.

Electrophysiology and stimulation

Data were recorded with Multiclamp 700B and Axopatch 200A amplifiers

(digitization 10 kHz). Voltage measurements were not corrected for the experimentally

determined junction potential (-12 mV). Interneurons within 150 μm of the stratum

pyramidale (in the strata pyrimidale, oriens and radiatum) were visually identified using

infrared DIC videomicroscopy. The spiking pattern of interneurons was determined

14

immediately after achieving whole-cell configuration by a series of depolarizing step current injections (100-1000 ms). The adaptation coefficient was determined by dividing the steady state spike frequency by the initial instantaneous frequency. Stimulation (100 µs) was performed using steel monopolar electrodes (FHC). One radial cut was made to separate CA3 and CA1 regions and a second radial cut was made between CA1 and the subiculum leaving only a portion of the alveus intact (Dingledine and Langmoen, 1980). The Schaffer collaterals were stimulated by placing a stimulation electrode between the two cuts in the stratum radiatum; the perforant path was stimulated by an electrode placed between the two cuts in the stratum lacunosum moleculare; and the alveus was stimulated with an electrode placed in the alveus on the subiculum side of the cut through CA1 (Alger and Nicoll, 1982a; Dingledine and Langmoen, 1980).

The disynaptic nature of IPSCs was confirmed either by being completely abolished by NBQX or by the lack of effect of gabazine on the initial slope of the preceding EPSC.

Cannabinoid sensitivity

Cannabinoid sensitivity of recorded interneurons was determined by depolarizing the postsynaptic pyramidal cell to 0 mV for 5 seconds (depolarization-induced suppression of inhibition (DSI)) while stimulating action potentials in the connected presynaptic interneuron at 0.5 Hz. This protocol was repeated at least three times. Averages were made from five unitary IPSCs before depolarization, two after return to resting conditions, and the five one minute after recovery from depolarization (at least 15, 6, and 15 sweeps respectively were averaged and shown in the figures).

Analysis

Average values in the text and figures are expressed as mean ± s.e.m. The student's *t*-test was used for statistical comparisons unless otherwise stated. Membrane time constants were measured by fitting a single exponential to the late portion of the membrane potential relaxation from a step current injection of -10 to -100 pA. Amplitudes were determined by finding the peak of an EPSC/IPSC as measured from a baseline before the stimulus artifact; if the EPSC/IPSC began before the decay of the previous stimulus, the decay was fit with a single exponential and the baseline extrapolated. The synaptic delay was measured from the peak of the action potential to the 10% rise of the IPSC. Jitter is defined as the standard deviation of the latency of the peak of the action potential.

The extrapolated trains of uIPSCs (**Fig. 3-5**) were generated from the convolution of the uIPSC waveform with the train of APs. The convolution incorporated a scaling factor (to account for short term plasticity) for each AP which was determined manually using the experimentally recorded trains of uIPSCs.

Morphology and immunocytochemistry

Slices were fixed in 4% paraformaldehyde in 0.1 M phosphate buffer (PB), cryoprotected in a 30% sucrose PB solution, and then frozen in a methylbutane on dry ice. In order to recover biocytin-filled interneurons in whole-mount, slices were incubated overnight in 3% Triton, to allow full penetration of the ABC Kit (Vectastain). The neurons were revealed by a DAB reaction (0.5%) with nickel intensification (3%

ammonium nickel sulfate and 100 mM imidazole). Slices were dehydrated in ascending

alcohols and xylenes and mounted in damar resin (Fluka). Interneuron soma, axons and

dendrites were reconstructed on a light microscope at 40X using Neurolucida

(MicroBrightField, Inc). Neuroexplorer was used to quantify the length of the axonal and

dendritic arborizations using 10 µm bins. In order to determine co-localization of CB1R

in recorded basket cell axons we incubated the slices in 3% Triton and rabbit anti-CB1R

(1:1000; from the lab of Ken Mackie) overnight at room temperature. We then incubated

the slices overnight at room temperature in 0.3% Triton, donkey anti-rabbit conjugated

Alexa 594 (1:500) and streptavidin conjugated Alexa-488 (1:1000; Molecular Probes).

Segments of biocytin-immunoreactive axons near the surface of the slice were selected

randomly and confocal stacks (of 0.3 µm thickness) were taken in series with CB1R

immunofluorescence at 60X (Olympus/Fluoview). Co-localization of biocytin and CB1R

immunoreactivity was determined by inspection by a blind observer. Images in **Fig. 2-3**

are the collapse of three 0.3 µm sections.

CHAPTER 1- Unitary Fields Reveal the Hyperpolarizing Effects of Gabaergic

Interneurons

Abstract

GABAergic interneurons are thought to be the main source of synaptic inhibition in the central nervous system. However, in many systems, GABA has been shown to have depolarizing effects on its target. Many of these experiments suggest that the action of GABA may depend on the specific subcellular compartment. Thus, in order to understand the function of local circuit interneurons which target dicrete compartments, it is necessary to determine whether they are excitatory or inhibitory. We recorded from *post hoc* identified interneurons, while simultaneously monitoring the extracellular field potential at the site of the axonal arborization. In response to action potentials in the interneuron, we recorded a positive source from both somatically and dendritically targeting interneurons. This demonstrates that hippocampal GABAergic interneurons can effectively hyperpolarize pyramidal cells irrespective of the compartment that they target.

Introduction

Cortical local circuit interneurons were initially identified as inhibitory in a landmark study by Andersen et al. Through local extracellular stimulation, they evoked a positive (hyperpolarizing) field potential in the pyramidal cell layer, consistent with the location of the dense arborization of basket cell axons (Andersen et al., 1963). Since then, many different types of inhibitory interneurons, each targeting a specific compartment along a pyramidal cell's somato-dendritic axis, have been described (Freund and Buzsaki, 1996; Somogyi and Klausberger, 2005).

However, the inhibitory impact of GABAergic interneurons has come into question. GABA, either released synaptically or applied extracellularly, can effectively depolarize cortical neurons (Alger and Nicoll, 1982b; Gulledge and Stuart, 2003; Perkins and Wong, 1996; Szabadics et al., 2006). In some cases, this GABAergic depolarization is sufficient to induce action potentials in the postsynaptic cell (Szabadics et al., 2006; Woodruff et al., 2006). Interestingly, the action of GABA can be different depending on the postsynaptic compartment. For instance, while GABAergic transmission at the soma of a pyramidal cell is consistently inhibitory, activation of GABA receptors in its dendrites can be excitatory (Alger and Nicoll, 1982b; Perkins and Wong, 1996). Thus, depending on the somato-dendritic compartment that they contact, GABAergic interneurons may either hyperpolarize or depolarize their targets.

The polarity of GABAergic transmission depends on two variables: the chloride reversal potential (E_{Cl}) and the resting membrane potential. Manipulation of either of these two factors could alter the polarity of GABAergic transmission (Coombs et al., 1955; Kuffler and Eyzaguirre, 1955; Rivera et al., 1999). One mechanism to set the

polarity of GABAergic responses is through regulated expression of two types of chloride pumps: NKKC1 and KCC2 (Plotkin et al., 1997; Rivera et al., 1999). These transporters push the intracellular chloride concentration in opposite directions and their differential regulation during development drives a global switch in the polarity of GABAergic transmission (Ben-Ari, 2002). In the adult, precise trafficking of these pumps has been hypothesized to underlie compartment-specific chloride concentrations leading to compartment-specific GABA responses (Hara et al., 1992; Marty et al., 2002; Szabadics et al., 2006).

However, while some groups claim that GABA can have compartment-specific effects, others can not replicate the phenomenon (Lambert et al., 1991). These conflicting results may stem from the non-specificity of the experimental setup. The experiments addressing the depolarizing effects of GABA in the dendrites use either direct GABA application or strong trains of extracellular stimuli (Alger and Nicoll, 1982b; Perkins and Wong, 1996). Thus, it is not clear where the activated GABAergic syapses are located or whether the depolarization is due to the activation of synaptic GABA receptors. Further, intracellular recordings are an unreliable measure of the impact of GABAergic transmission as they may affect the ionic composition.

Here we address the issue systematically by recording from identified interneurons targeting different compartments. In order to leave the intracellular ionic composition and the membrane potential intact, we recorded extracellular field potentials while evoking action potentials in an intracellularly recorded GABAergic interneuron. Irregardless of the location of the interneuron's axonal arborization, the local field potential observed was positive. These data demonstrate that GABAergic synapses onto

either the soma or the dendrites of pyramidal cells can evoke a net hyperpolarization of the population.

Results

The extracellular field potential in the stratum pyramidale (SP) was monitored (using a glass pipette filled with 3 M NaCl) while action potentials were evoked in a basket cell recorded in the whole-cell current clamp configuration (interneurons were identified morphologically *post hoc*; **Fig. 1-1a**). The field potential evoked by the activity of a single basket cell (unitary field potential: uField) was invariably positive (average amplitude: 16.5 ± 1.7; range: $8.2 - 30.5$ µV; $n = 12$; **Fig. 1-1b**). This positive potential could be blocked by the $GABA_A$ receptor antagonist gabazine ($n = 4$), confirming that the event was synaptically generated. Further, the kinetics of the uField were similar to those of intracellularly recorded inhibitory postsynaptic currents (IPSCs) from basket cells onto pyramidal cells (rise: 1.2 ± 0.2, decay tau: 7.5 ± 0.6; $n = 6$), consistent with the uField being proportional to the synaptic current (Glickfeld and Scanziani, 2006; Hefft and Jonas, 2005).

A positive field potential in SP may represent a local active current source indicative of local somatic inhibition or a passive source reflecting dendritic excitation. To distinguish between these two possibilities, we activated adenosine (A1) receptors to hyperpolarize pyramidal cells via activation of G-protein coupled potassium channels (Thompson et al., 1992). If the positive uField represents somatic inhibition, then hyperpolarizing the pyramidal cells should bring their membrane potential closer to the IPSC reversal potential (E_{IPSC}), thereby decreasing the driving force and the amplitude of

Figure 1-1: Basket cells hyperpolarize the somas of pyramidal cells

(a) Schematic of recording configuration. SO- stratum oriens; SP- stratum pyramidale; SR- stratum radiatum; SLM- stratum lacunosum moleculare. *I*clamp- current clamp recording from a basket cell. Field- extracellular electrode in SP.
(b) An action potential (AP) in a basket cell (top; blue trace) evokes an extracellular field (bottom) in SP in control (black trace) which is abolished by 2.5 μM gabazine (red trace).
(c1) An AP in a basket cell (top; blue trace) evokes an extracellular field (bottom) in SP in control (black trace) which is decreased by 1 μM CPA (red trace).
(c2) Voltage clamp recording (V_H = -50 mV) from a pyramidal cell while stimulating extracellularly in SP (10 μM NBQX; black trace) in control and in the presence of 1 μM CPA (red trace).
(d) Left, neurolucida reconstruction of a pyramidal cell for reference. Right, field potential recorded in the different lamina, corresponding to the location on the pyramidal cell, in response to a train of three APs at 50 Hz.

a Basket Cell

SLM

SR Field /clamp

SP

SO

200 μm

b

40 mV
5 ms

10 μV

2.5 μM gabazine

c₁

40 mV
4 ms

20 μV

1 μM CPA

c₂ IPSC in Pyr.

400 pA
8 ms

1 μM CPA

d

40 mV

10 μV
10 ms
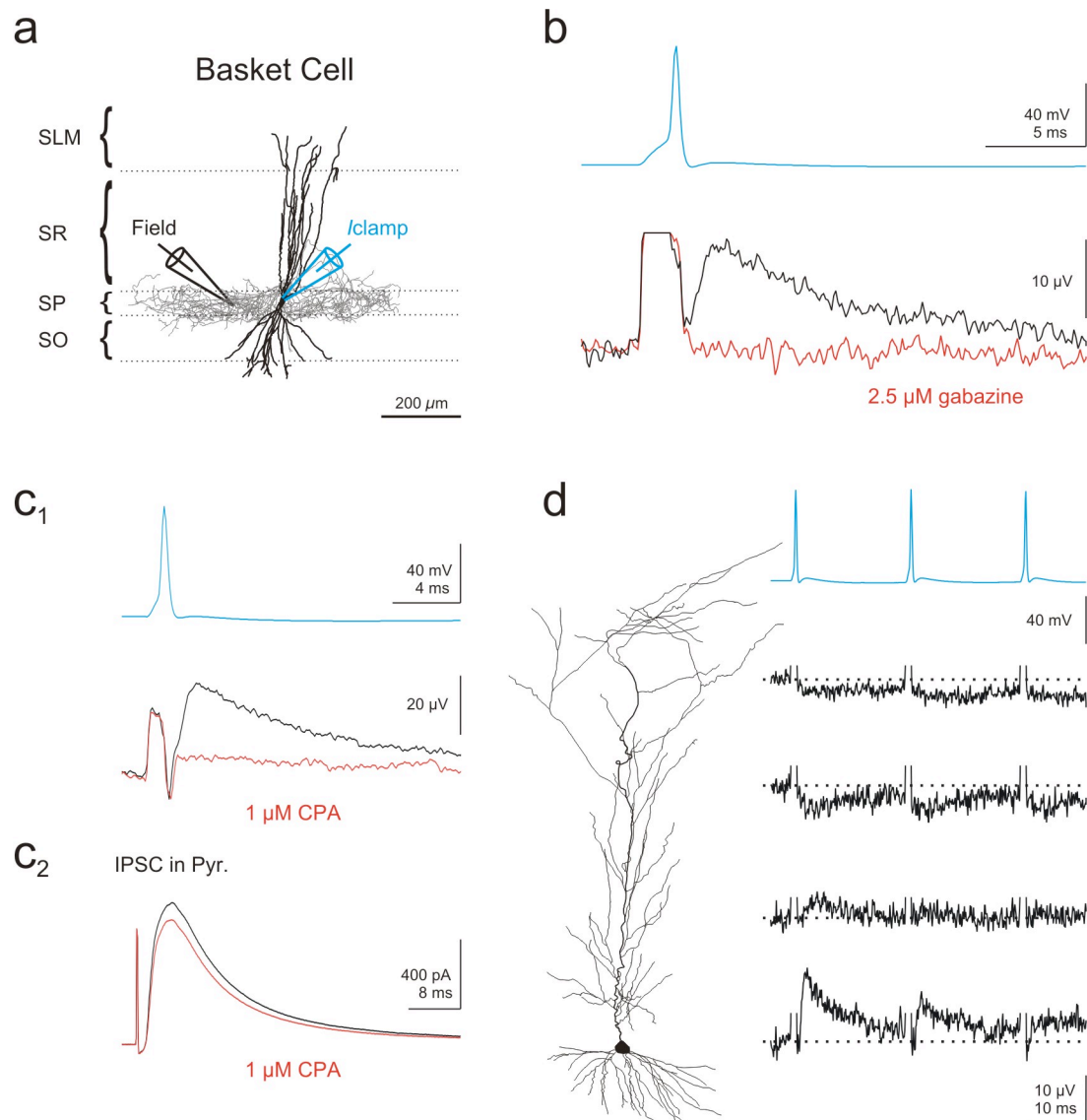
the uField. If however, the uField represents a distally generated depolarization, then hyperpolarization of the pyramidal cells should move them further from E_{IPSC}, thereby increasing the amplitude of the uField. Application of the A1 agonist, CPA (1 µM) decreased the amplitude of the uField in every case (to 41.0 ± 5.9 % of control; $n = 5$; $P < 0.05$) and could be reversed by the A1 receptor antagonist DPCPX (10 µM; to 86.9 ± 2.6 % of control; $n = 2$; **Fig. 1-1c1**). The reduction in amplitude of the uField was not due to a decrease in GABA release by CPA because it had very little effect on evoked IPSCs in an intracellularly recorded pyramidal cell (to 88.0% of control; $n = 1$; **Fig. 1-1c2**). However, CPA did evoke a large outward current (96.2 pA; $n = 1$), consistent with its hyperpolarizing effect (Thompson et al., 1992). This suggests that under our conditions, E_{IPSC} at the soma was hyperpolarized as compared to the resting membrane potential of pyramidal cells.

One concern is that the high NaCl solution in the field recording pipette may leak into the surrounding tissue and locally increase the chloride concentration, rendering E_{IPSC} more negative than is physiological. To address this possibility we performed two series of control experiments. First, we replaced the 3 M NaCl with normal extracellular solution containing 125 mM chloride; this did not affect either the sign or the size of the uField ($n = 2$). Second, we moved the extracellular recording electrode (with 3 M NaCl) out of SP and into the dendritic layers, outside of the basket cell's axonal arborization. If stimulating basket cells generates an active souce in SP even in the absence of the pipette's high chloride concentration, then a passive sink should be recorded in the stratum radiatum (SR). Indeed, as we moved the pipette away from SP and into SR, the amplitude of the uField decreased and then inverted ($n = 2$; **Fig. 1-1d**). The reversal of

the uField demonstrates that the source recorded in SP was not due to the leaking of chloride from the pipette. Thus, the polarity of the uField indicates the presence of a local source, implying the hyperpolarization of the population of pyramidal cells in response to the activity of a single basket cell.

In a separate set of experiments, we recorded from oriens-lacunosum moleculare (O-LM) neurons (**Fig. 1-2a**) which target the distal dendrites of pyramidal cells. The local field potential was monitored in the stratum lacunosum-moleculare (SLM) while action potentials were evoked in the O-LM neuron. In all cases, the O-LM neuron evoked a positive uField (average amplitude: 10.1 ± 2.2; range: $4.8 - 15.0$ µV; $n = 4$; **Fig. 1-2b**). The positive potential could be blocked by gabazine ($n = 2$), suggesting that it was synaptically mediated. Further, like the uField from the basket cells, it was suppressed by the pharmacological hyperpolarization of pyramidal cells (to $42.5 \pm 6.1\%$ of control; $n = 3$; $P < 0.05$; **Fig. 1-2c**). Thus, interneurons that target the dendritic compartment can hyperpolarize pyramidal cells.

Discussion

Using extracellular recordings, we investigate two types of GABAergic interneurons which target compartments at the extreme ends of the pyramidal cell: the soma and the distal apical dendrites. Both interneurons generated a positive source a the site of their axonal arborizations. Thus, we suggest that the effect of synaptic GABAergic transmission is hyperpolarizing along the entire somato-dendritic axis of hippocampal pyramidal cells.
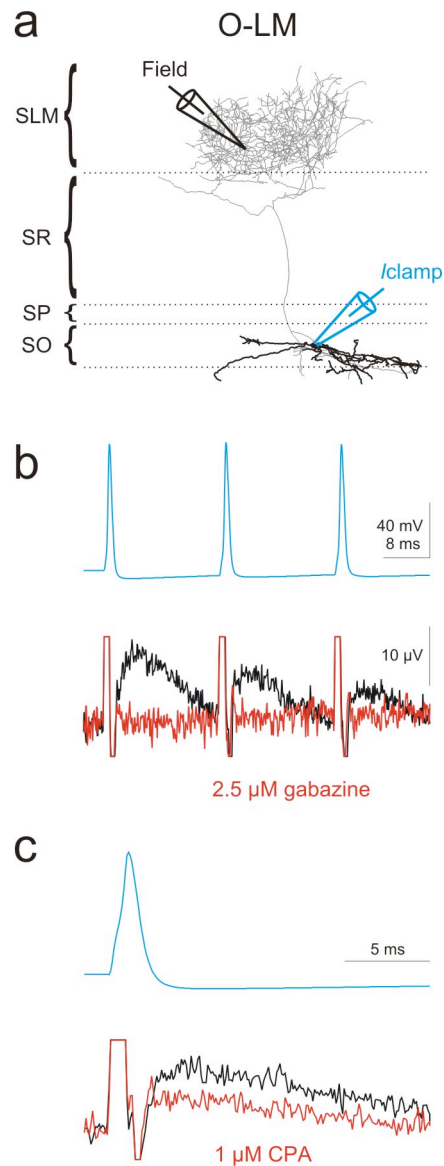
Figure 1-2: O-LM cells hyperpolarize the distal dendrites of pyramidal cells

(a) Schematic of recording configuration. *I*clamp- current clamp recording from an O-LM cell. Field- extracellular electrode in SLM.
(b) APs in an O-LM cell (top; blue trace; 50 Hz) evokes an extracellular field (bottom) in SLM in control (black trace) which is abolished by 2.5 μM gabazine (red trace).
(c) An AP in an OLM cell (top; blue trace) evokes an extracellular field (bottom) in SLM in control (black trace) which is decreased by 1 µM CPA (red trace).

Extracellular field recordings have long been used in the hippocampus to monitor both the synaptic and spiking activity of populations of cells (Andersen et al., 1963; Bliss and Lomo, 1973; Grastyan et al., 1959). Extracellular recordings have many intrinsic advantages for studying synaptic transmission. First, extracellular recordings have a minimal impact on the intracellular properties of the recorded population. Thus, we can be sure that the membrane potential and ionic gradients are as close to the native state as is possible in a slice preparation. Second, recordings of the extracellular potential is the poor man's voltage clamp. The local field potential accurately reports the amplitude and polarity of local currents independent of passive membrane properties. Finally, the extracellular pipette monitors activity from a large population of pyramidal cells; thus, the recording is an estimate of the average population response and is insensitive to the vagaries in the responses of individual neurons.

By pairing extracellular recordings with intracellular recordings, we can monitor the impact of a single cell. After *post hoc* recovery of filled interneurons, we can identify the precise location of the axonal arborization with respect to the location of our recording electrode. Thus, we can independently determine the effect of different types of interneurons which target discrete locations along the somato-dendritic axis of pyramidal cells. Further, unitary field (uField) recordings, in comparison to synaptically connected pairs, are easily and reliably found. As such, this could be a useful tool for many purposes in synaptic and circuit physiology.

uFields recorded in the layer targeted by the axonal arbor of the activated interneuron were invariably positive, indicating the presence of an active source. This was confirmed by pharmacological controls. Hyperpolarization of the pyramidal cell

population, through activation of the metabotropic adenosine receptor, decreased the amplitude of the uField. Given that activation of adenosine receptors has no direct effect on the amplitude of the inhibitory postsynaptic current (IPSC), the decreased amplitude in the uField is due to a decrease in the the driving force for the IPSC (Thompson et al., 1992). This suggests that the resting membrane potential is positive to the IPSC reversal potential (E_{IPSC}), consistent with a hyperpolarizing effect of GABAergic transmission.

One drawback to extracellular recordings is that we do not know the postsynaptic source of the field potential. In addition to pyramidal cells, there are two other cellular populations in the hippocampus: GABAergic interneurons and glia. The field potentials are not likely to be due to interneurons for two reasons. First, interneurons represent a small minority of the population as compared to pyramidal cells (~10%; (Freund and Buzsaki, 1996)) and thus should not dominate the field potential. Second, the membrane potential of interneurons has been previously shown to be very close to E_{IPSC} and should therefore not contribute to the field potential (Banke and McBain, 2006). While glia do express GABA receptors (MacVicar et al., 1989), the field potential is unlikely to result from their activation. First, unlike pyramidal cells and interneurons, the processes of glia do not extend through all lamina of the hippocampus (Ogata and Kosaka, 2002), such that they would not support the reversed field potential observed in the dendritic layers. Second, glia tend to have extremely negative resting membrane potentials which are likely more hyperpolarized than E_{IPSC}, and would therefore have depolarizing responses to GABA (MacVicar et al., 1989).

While we find that GABAergic synaptic transmission can effectively hyperpolarize the dendrites, previous obeservations have suggested that the action of

GABA on dendrites is excitatory (Alger and Nicoll, 1982b; Perkins and Wong, 1996). Several reasons may account for the discrepancy with our observations. For one, these protocols preferentially activate extracellular receptors which could have different ion permeabilities and thus a more depolarized E_{IPSC}. In contrast, our protocol of evoking a uField likely activates only synaptic receptors. However, even when we give high frequency trains of action potentials, the uField does not reverse polarity (ten stimuli at 100 Hz, data not shown).

More recent reports of the excitatory effects of individual interneurons are more difficult to rectify with our findings (Szabadics et al., 2006; Woodruff et al., 2006). Since the uField only reports the average effect of an interneuron in the population, it leaves open the possibility that there may be some variability in the response of individual pyramidal cells. For instance, a minority of the population may be more hyperpolarized or have a higher chloride concentration, and thereby have an excitatory response to GABAergic input. Such a situation may explain the instances of excitatory effects of interneurons on individual pyramidal cells. In addition, it is possible that there is a difference in the effect of GABAergic transmission in different cortical areas due to differences in intrinsic properties. While we and others find that the resting membrane potential of hippocampal pyramidal cells is depolarized to E_{IPSC} measured at the soma (Banke and McBain, 2006), previous studies have concluded that the cortical pyramidal cells rest near or hyperpolarized to E_{IPSC} (Connors et al., 1988; Gulledge and Stuart, 2003; Martina et al., 2001).

The approach used here relies on the relatively dense and spatially confined axonal arborizations made by basket and O-LM cells, and the precise alignment of the

hippocampal pyramidal cells. Under such conditions, the activity of a single axon generates local synaptic currents that are sufficiently large to be picked up by a field electrode. The activity of interneurons with more loose axonal arbors or axons spread over several layers may not generate local currents that can be recorded with a field electrode. Indeed, bistratified cells, which target the basal and apical dendrites of pyramidal cells fall into this category. Thus, we are currently lacking data on the polarity of inhibition in the proximal dendrites. It will also be important to test the effect of axo-axonic cells, which target the axon initial segment of pyramidal cells, given the recent reports of their excitatory role (Szabadics et al., 2006). Nonetheless, we have convincingly demonstrated that interneurons targetting both the soma and distal dendrites of hippocampal pyramidal cells are inhibitory.

CHAPTER 2- Distinct Timing in the Activity of Fast-spiking and Regular-spiking Basket

Cells

Abstract

Basket cells are powerful sources of somatic inhibition, yet their precise spike timing in relation to other neurons in the circuit is poorly understood. Here we find that two populations of basket cells, fast-spiking (FS) and regular-spiking (RS), are differentially recruited in the hippocampal circuit. Despite receiving the same afferent inputs, the synaptic and biophysical properties of the two cell types are tuned to detect different features of activity. FS basket cells responded reliably and immediately to subtle and repetitive excitation. In contrast, RS basket cells responded later and did not follow repetitive activity, but were better suited to integrate the consecutive excitation of independent afferents. This temporal separation in the activity of the two basket cell types generated distinct epochs of somatic inhibition. Further, since FS and RS basket cells express receptors to opioids and cannabinoids, respectively, these epochs of inhibition are under differential neuromodulatory control.

Introduction

The function of each type of GABAergic interneuron is determined by the interplay between the excitation it receives from its inputs, its intrinsic electrophysiological properties, the inhibition it exerts on its targets. Individual interneuron types are preferentially recruited by specific activity patterns of their inputs and, due to their distinct axonal projections, inhibit specific regions along the somato-dendritic axis of their targets (Ali et al., 1998; Ali and Thomson, 1998; Freund and Buzsaki, 1996; Losonczy et al., 2002; McBain and Fisahn, 2001; Pouille and Scanziani, 2004). The participation of distinct classes of interneurons during complementary phases of hippocampal oscillations *in vivo* provides additional evidence of the differential recruitment of cell types (Klausberger et al., 2003; Klausberger et al., 2004; Klausberger et al., 2005). Further, GABAergic interneurons are under the control of neuromodulators which can alter the strength and timing of inhibition in the circuit (Cohen et al., 1992; Freund, 2003; Katona et al., 1999; Oleskevich and Lacaille, 1992; Pitler and Alger, 1992).

Basket cells are a class of GABAergic interneuron that synapse specifically on the somata of their targets (Andersen et al., 1963). From this privileged location, basket cells can perform a variety of temporally precise operations which include the synchronization of neural ensembles, the pacing of rhythmic activity and the control of spike timing and synaptic integration (Bartos et al., 2002; Cobb et al., 1995; Fricker and Miles, 2000; Mann et al., 2005; Miles et al., 1996; Pouille and Scanziani, 2001). In the hippocampus, there are two types of basket cells which can be distinguished according to their physiological, immunohistochemical and pharmacological properties (Freund, 2003).

One type, the fast-spiking (FS) basket cells, responds to a step-depolarization with a non-adapting train of action potentials and expresses the calcium binding protein parvalbumin; the other type, the regular-spiking (RS) basket cells, shows strong spike-frequency adaptation in response to a step-depolarization and expresses the neuropeptide cholecystokinin. A substantial fraction of cannabinoid receptors (CB1Rs) in cortical areas are located on the synaptic terminals of RS basket cells (Bodor et al., 2005; Freund, 2003; Katona et al., 1999; Tsou et al., 1999; Wilson et al., 2001). When exposed to endocannabinoids, as during depolarization of the postsynaptic pyramidal cell, CB1Rs inhibit GABA release, effectively reducing the magnitude of somatic inhibition onto that pyramidal cell (Pitler and Alger, 1994; Wilson and Nicoll, 2001). Opioids are also powerful modulators of inhibition in the hippocampus (Cohen et al., 1992) and some evidence suggests that μ-opioid receptors (μORs), are expressed by parvalbumin positive basket cells (Drake and Milner, 2002; Stumm et al., 2004). Yet, despite the strategic position of basket cell terminals, the specific role played by the two types of basket cells, and therefore opioids and cannabinoids, in controlling network activity is poorly understood.

Thus, we investigated the role of RS and FS basket cells in hippocampal circuit activity. We found that RS and FS basket cells are indeed independently modulated by cannabinoids and opioids, respectively. When we stimulated either the Schaffer collaterals or the perforant pathway, RS basket cells received weak and very transient excitation which, however, they integrated over long time windows and across many afferents. This makes them ideally suited to detect the sequential activation of independent excitatory inputs. In contrast, FS basket cells, received stronger and more

persistent excitation which they integrated only over very narrow time windows, thereby faithfully reporting the timing of ongoing hippocampal activity. Because of their sensitivity to distinct activity patterns, RS and FS basket cells were recruited at different times. Hence, endocannabinoids regulate the inhibition resulting from global changes in activity while opioids can modulate the more precise inhibitory control.

Results

We made whole-cell current clamp recordings from hippocampal basket cells (ascertained by *post hoc* morphological analysis). In order to identify the regular-spiking (RS) and fast-spiking (FS) types, we injected sqare current pulses and compared their spike-frequency adaptation and their action potential (AP) width (**Fig. 2-1a-b**). FS basket cells showed significantly less spike-frequency adaptation (adaptation coefficient- RS: 0.34 ± 0.02; FS: 0.85 ± 0.02; $P < 0.0001$; $n = 42$ and 37) and shorter action potentials (AP width at half-amplitude- RS: 0.76 ± 0.03 ms; FS: 0.32 ± 0.01 ms; $P < 0.0001$; $n = 44$ and 40) than RS basket cells. The two types of basket cells also clearly differed in their membrane time constant (RS: 25.6 ± 1.7 ms; FS: 9.9 ± 0.4 ms; $P < 0.0001$; $n = 20$ and 33; **Fig. 2-1c**) and input resistance (RS: 150.7 ± 10.7 MΩ; FS: 59.9 ± 4.5 MΩ; $P < 0.0001$; $n = 25$ and 38; **Fig. 2-1c**). The axonal and dendritic arborizations of both types of basket cells were overlapping (**Fig. 2-1d**). While their axons were restricted to the pyramidal cell layer, their dendrites spanned all lamina of the hippocampus.

Through paired recordings with pyramidal cells ($V_H = -50$ mV), we found a high rate of connectivity for both RS and FS basket cells (RS: 54.7 %, $n = 95$ pairs with 46
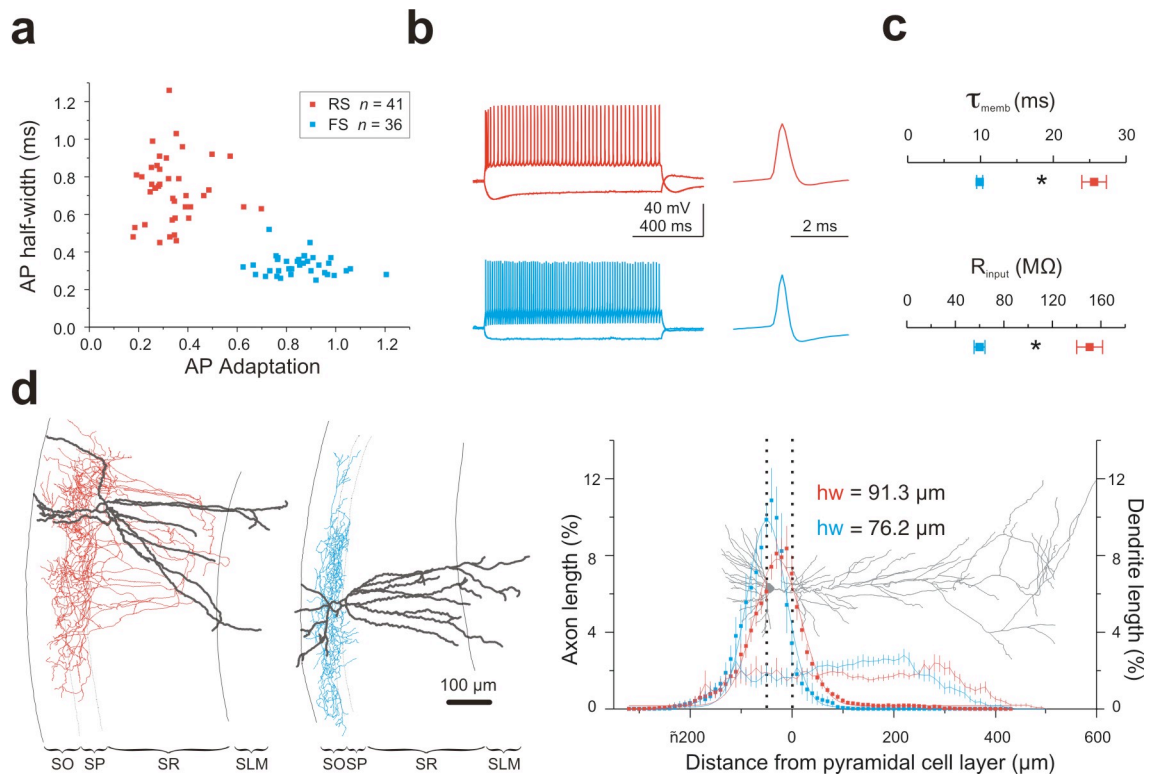
Figure 2-1: Identification of RS and FS basket cells

(a) Plot of action potential (AP) adaptation and AP half-width for the population of recorded basket cells. The basket cells cluster into two groups which we call regular-spiking (RS; red; *n* = 42) and fast-spiking (FS; blue; *n* = 36).
(b) Left: examples of RS (top, red) and FS (bottom, blue) spiking patterns in response to a step current injection (-200 pA and +400 pA). Right: AP on an extended time scale.
(c) Summary of membrane time constant (top) and input resistance (bottom) for RS (red; *n* = 20 and 33) and FS (blue; *n* = 22 and 38) basket cells. Asterisks represent statistical significance.
(d) Top: reconstructions of RS (left; axon red, dendrite grey) and FS (right; axon blue, dendrite grey) basket cells (different cells than those in **Fig. 2-1b**). SO- stratum oriens; SP- stratum pyrimidale; SR- stratum radiatum; SLM- stratum lacunosum-moleculare. Bottom: axonal (squares; *n* = 16 and 11) and dendritic (thin lines; *n* = 13 and 11) density distributions of reconstructed basket cells. Axonal distributions are fit by Gaussians (thick lines; hw = half width). Dotted vertucak kubes represent SP. Grey pyramidal cell for reference).

basket cells; FS: 64.4 %, n = 73 pairs with 41 basket cells). The unitary inhibitory

postsynaptic currents (uIPSCs) that they evoked on their targets were indistinguishable in

terms of peak conductance (RS: 1.25 ± 0.16 nS; FS: 1.51 ± 0.23 nS; P > 0.3; n = 43 and

41; **Fig. 2-2a-b**), decay time constant (RS: 7.7 ± 0.5 ms; FS: 6.7 ± 0.3 ms; P > 0.1; n = 34

and 30; **Fig. 2-2b**), and paired pulse ratio (0.79 ± 0.06; 0.71 ± 0.02; P > 0.3; n = 21 and

12; **Fig. 2-2b**). However, they had distinct rise times (RS: 0.92 ± 0.05 ms; FS: 0.69 ±

0.05 ms; P < 0.001; n = 42 and 38 **Fig. 2-2b**) and synaptic conduction delays (RS: 1.6 ±

0.1 ms; FS: 0.7 ± 0.1 ms ; P < 0.0001; n = 27 and 24; **Fig. 2-2c**), similar to interneurons

expressing cholecystokinin and parvalbumin, respectively, in the dentate gyrus (Hefft and

Jonas, 2005). Thus, the output, in terms of its location, strength and kinetics, is very

similar for both basket cell types.

Modulation of basket cells

The uIPSCs from RS, but not FS, cells were suppressed by depolarization of the

postsynaptic pyramidal cell (to 0 mV for 5 s; depolarization-induced suppression of

inhibition: DSI; **Fig. 2-3a-c**). The suppression could be blocked by the specific

cannabinoid receptor type 1 (CB1R) antagonist AM251 (5 μM; n = 4; **Fig. 2-3d**),

consistent with the depolarization inducing release of endocannabinoids (Wilson and

Nicoll, 2001). Further, the antibody against CB1R co-localized with the axons of RS but

not FS basket cells (n = 5 and 4, respectively; **Fig. 2-3e**). Thus, RS basket cells can be

selectively modulated by endocannabinoids (Wilson et al., 2001).

In contrast, uIPSCs mediated by RS basket cells were not sensitive to the μ-opioid

receptor (μOR) agonist DAMGO as the weak suppression (100 nM; to 82.1 ± 7.7 % of
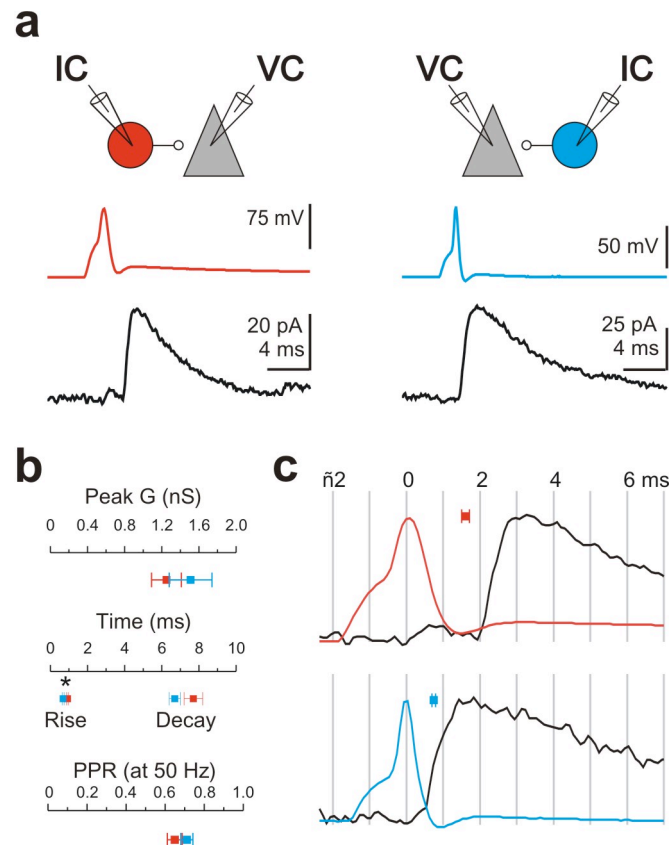
Figure 2-2: Unitary properties of basket cell inputs

(a) Top: schematic of the recording configuration: IC, current clamp; VC, voltage clamp. Bottom: current and voltage traces: unitary IPSCs (uIPSCs) recorded in a pyramidal cell (black traces; VH: −50 mV) in response to an AP triggered in a presynaptic basket cell (upper traces; same basket cells as shown in **Fig. 2-1d**).
(b) Summary graphs of peak conductance (top), rise time and decay time constant (middle), and paired pulse ratio (50 Hz; bottom) of uIPSCs evoked by RS (red; n = 43, 42, 34, and 21) and FS (blue; n = 41, 38, 30, and 12) basket cells.
(c) APs from cells in **(a)** and corresponding uIPSC in the postsynaptic pyramidal cell (black) on an expanded time scale (vertical lines are separated by 1 ms). Square symbols: average latencies (between action potential peak and uIPSC onset) for RS (top, n = 27) and FS (bottom, n = 24) basket cells.

38

Figure 2-3: Selective modulation of RS basket cells by cannabinoids

(a) APs in a presynaptic basket cell (top) trigger uIPSCs in a pyramidal cell (bottom; black traces; same paired recording as shown in **Fig. 2-2a**). Pyramidal cell depolarization (0 mV; 5 s) transiently suppresses the uIPSC (green traces) from RS (left) but not FS (right) basket cells.
(b) Distribution of the uIPSC amplitudes after depolarization (54 pairs). Suppression: red bars ($n = 28$); lack of suppression: blue bars ($n = 26$). The amplitude of the residual IPSC is the average of the uIPSCs collected 3 and 5 s after the end of the depolarization (and hence show a variable degree of recovery).
(c) Summary of the time-course of uIPSC suppression for RS ($n = 28$) and FS ($n = 26$) basket cells . Recovery is fitted with a single exponential ($\tau = 10.2$ s).
(d) Left: depolarization-induced suppression (top) is abolished by the CB1R antagonist AM 251 (5 µM; bottom). Right: summary graph ($n = 4$).
(e) Biocytin-filled axons (top), CB1R antibodies (middle) and their superposition (bottom) in RS (left) and FS (right) basket cells. White arrows mark boutons of the recorded interneuron. Scale bar 5 µm. Note the colocalization of biocytin and CB1R in the RS basket cell.

a

75 mV

50 mV

Control
Recovery
20 pA
4 ms
After depol.

25 pA
4 ms

b

Number of cells

15

10

5

0

RS
(*n* = 28)

FS
(*n* = 26)

10   30   50   70   90   110   130   150

Residual unitary IPSC (%)

c

0 mV

Normalized uIPSC

1.2

0.8

0.4

0.0

Tau = 10.2 s

ñ20   ñ10   0   10   20   30   40   50

Time from depolarization (s)

d

Control
Recovery
After depol.

5 µM AM251

20 pA
20 ms

Residual unirary IPSC (%)

120

80

40

0

Con   AM251

e

RS

Biocytin

CB1R

FS

Biocytin

CB1R
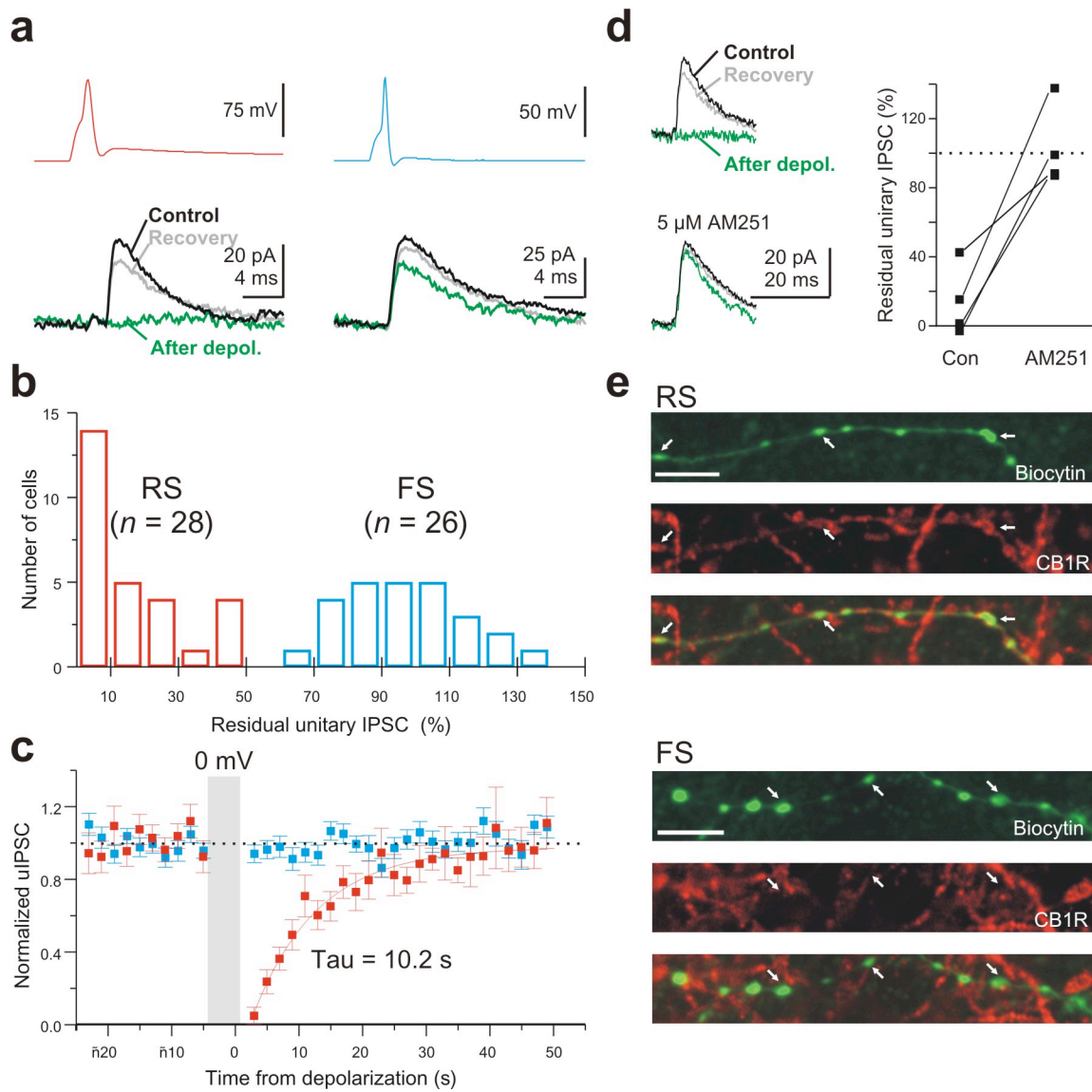
control; $n = 8$; $P = 0.06$; **Fig. 2-4a-b**) did not recover in the presence of the μOR specific

antagonist CTAP (500 nM; to 84.8 ± 10.6 % of control; $n = 8$; $P = 0.89$ compared to

DAMGO). Conversely, uIPSCs mediated by FS basket cells were strongly supressed by

DAMGO (to 26.5 ± 3.2 % of control; $n = 12$; $P < 0.0001$; **Fig. 2-4a-b**); further, this

suppression was reversed by the antagonist CTAP (84.3 ± 3.2; $n = 12$; $P < 0.0001$; **Fig. 2-4b**). These paired recordings indicate that CB1Rs and μORs are segregated on the

presynaptic terminals of two non-overlapping basket cell populations.

In addition, application of DAMGO resulted in the hyperpolarization of the

membrane potential of FS basket cells (from -58.1 ± 1.2 mV in control to -65.1 ± 0.5 mV

in DAMGO; $n = 3$; $P < 0.05$; **Fig. 2-4c**) but had no effect on the membrane potential of

RS basket cells (from -58.2 ± 0.2 mV in control to -58.1 ± 0.4 mV in DAMGO; $n = 3$; $P > 0.1$; **Fig.2-4c**). Accordingly, application of DAMGO evoked a large outward current in

voltage clamped FS (V_H: -40 mV; 159.3 ± 14.3 pA; $n = 7$; $P < 0.00001$; **Fig. 2-4d**) but

not RS basket cells (17.2 ± 9.0 pA; $n = 5$; $P > 0.1$; **Fig. 2-4d**).

On the other hand, the cannabinoid receptor agonist, WIN55-212 (1 μM), did not

evoke any measurable current in either FS (V_H: -50 mV; -0.1 ± 3.9 pA; $n = 6$; $P > 0.9$;

Fig. 2-4e) or RS basket cells (0.9 ± 2.5 pA; $n = 6$; $P > 0.7$; **Fig. 2-4e**). However, CB1Rs

were activated since the uIPSCs mediated by RS basket cells were suppressed (1 μM;

29.0 ± 16.0 % of control; $n = 5$; $P < 0.05$; **Fig. 2-4f**). Application of the CB1R antagonist

AM251 (5 μM) reversed the suppression of WIN55-212 and increased the amplitude of

the uIPSC above control levels suggesting a tonic activation of CB1Rs (to 244.0 ± 59.7

% of control; $n = 5$; $P < 0.05$ compared to WIN55-212; **Fig. 2-4f**; (Losonczy et al.,

2004)). Furthermore, consistent with their lack of sensitivity to DSI, WIN55-212 did not

41

Figure 2-4: Complementary actions of opioids and cannabinoids

(a) APs in a presynaptic basket cell (top) trigger uIPSCs in a pyramidal cell (bottom; black traces). The μ-opioid receptor (μOR) agonist DAMGO (100 nM; gray trace) suppresses the uIPSC from FS (right) but not RS (left) basket cells.
(b) Summary time course of the normalized uIPSC amplitude, from RS (red; $n = 8$) and FS (blue; $n = 12$) basket cells, upon application of DAMGO and the antagonist CTAP (500 nM).
(c) Summary time course of the membrane potential of RS (red; $n = 3$) and FS (blue; $n = 3$) basket cells, upon application of DAMGO and CTAP.
(d) Summary time course of the holding current ($V_H = -40$ mV) of RS (red; $n = 5$) and FS (blue; $n = 7$) basket cells, upon application of DAMGO and CTAP.
(e) Summary time course of the holding current ($V_H = -50$ mV) of RS (red; $n = 6$) and FS (blue; $n = 7$) basket cells, upon application of the cannabinoid receptor agonist, WIN55-212 (1 μM), and the antagonist AM251.
(e) Summary time course of the normalized uIPSC amplitude of RS (red; $n = 6$) and FS (blue; $n = 7$) basket cells, upon application of WIN55-212 and AM251.
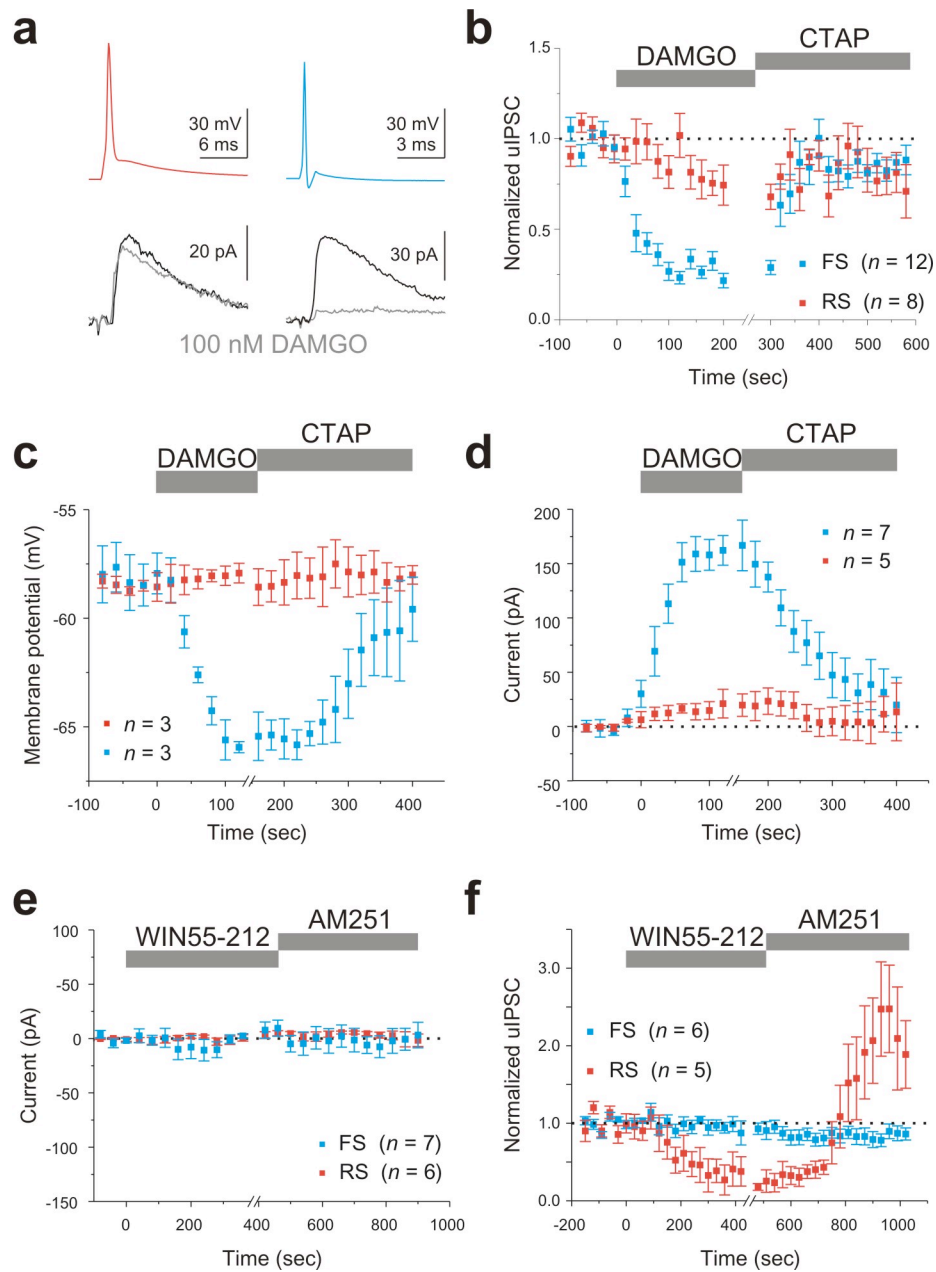
affect the amplitude of the uIPSCs mediated by FS basket cells (95.2 ± 7.0 % of control; $n = 6$; $P > 0.5$; **Fig. 2-4f**).

Taken together, these results show that µORs and CB1Rs are expressed on two distinct basket cell populations. µOR activation both suppresses GABA release from and hyperpolarizes FS basket cells; CB1R activation, on the other hand, exclusively suppresses GABA release without affecting the membrane potential of RS basket cells.

Target specific excitation of basket cells

The similar anatomical distribution (**Fig. 2-1d**) and physiological properties (**Fig. 2-2**) of synapses formed by RS and FS basket cells onto pyramidal cells suggests that the inhibitory impact of the two basket cell types is similar. However, RS and FS basket cells may be differently excited by their afferents. To test this possibility, we compared the amplitude and dynamics of excitatory postsynaptic currents (EPSCs) evoked by afferent stimulation onto RS and FS basket cells.

The amplitude of EPSCs evoked with an extracellular stimulation electrode may vary strongly between experiments depending on stimulation intensity, exact position of the stimulation electrode, electrical properties of the stimulation electrode and quality of the stimulated tissue, all parameters that will affect the number of stimulated fibers. These sources of variability preclude a meaningful comparison of EPSC amplitudes recorded during different experiments. In order to make this comparison, we used a reliable readout of the stimulation conditions during each experiment: the simultaneously recorded, postsynaptic pyramidal cell. By normalizing the amplitude of the evoked EPSC recorded in a basket cell with the EPSC recorded simultaneously in the pyramidal

cell voltage clamped at the same potential, we can control for the sources of variability mentioned above and compare the relative amount of excitation received by RS and FS basket cells across experiments.

We stimulated the three major excitatory pathways in area CA1, the perforant path, the Schaffer collaterals, and the CA1 pyramidal cell axons, by placing stimulation electrodes in the stratum lacunosum moleculare, the stratum radiatum, and the alveus, respectively. Consistent with the extent of their dendritic arborizatons, these three pathways converged onto individual RS and FS basket cells (**Fig. 2-5a**). This suggests that each basket cell can potentially participate in both feed-forward and feedback inhibition.

Despite the fact that RS and FS basket cells were excited by the same afferents, the amplitude and the short-term plasticity of evoked EPSCs were markedly different between the two cell types. Stimulation of the Schaffer collaterals (in the presence of the $GABA_A$ receptor antagonist gabazine or at the IPSC reversal potential to isolate glutamatergic transmission) evoked much larger EPSCs in FS basket cells than in the simultaneously recorded postsynaptic pyramidal cells. The peak amplitude of Schaffer collateral mediated EPSCs was 8.15 ± 1.50 times larger onto FS basket cells as compared to their pyramidal cell targets ($P < 0.005$; $n = 16$ pairs; **Fig. 2-5b**). In contrast, when recording from RS basket cells and their postsynaptic pyramidal cells, Schaffer collateral stimulation elicited EPSCs that were of similar amplitude (1.09 ± 0.36 times larger in RS basket cells; $P > 0.05$; $n = 16$ pairs; **Fig. 2-5b**). Comparison of the normalized EPSCs recorded in the RS and FS basket cells indicates that stimulation of Schaffer collaterals
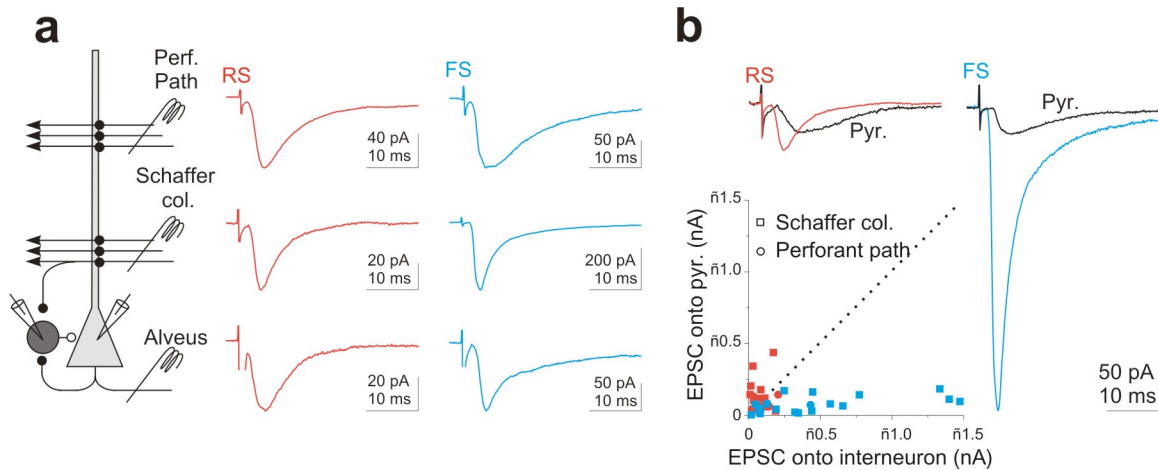
Figure 2-5: Distinct excitation of RS and FS basket cells

(a) Left: schematic of recording configuration. Monosynaptic EPSCs recorded in a RS (middle, blue traces) and FS (right, red traces) basket cell by stimulating three excitatory pathways. EPSCs in this panel and in **(b)** recorded in the presence of gabazine (2.5 μM) or at the IPSC reversal potential (–85 mV).

(b) Top: EPSC recorded simultaneously in connected basket (RS- red traces; FS- blue traces) to pyramidal cell (black traces) pairs in response to Schaffer collaterals stimulation. Same cells as in **(a)**. Bottom: scatter plot of the amplitude of Schaffer collateral (squares) and Perforant path (circles) EPSCs recorded in RS (red: Schaffer collaterals, $n = 16$; Perforant path, $n = 7$) and FS (blue: Schaffer collaterals, $n = 16$; Perforant path, $n = 5$) versus their paired pyramidal cells; unity line is dotted.

evokes EPSCs that are 7.5 times larger in FS as compared to RS basket cells ($P <$ 0.0001).

This difference in amplitude is unlikely to be due to a stronger postsynaptic attenuation of Schaffer collateral evoked EPSCs in RS as compared to FS basket cells because the rise times of the evoked EPSCs were indistinguishable (10-90% EPSC rise-time: RS: 1.16 ± 0.14 ms; FS: 1.02 ± 0.11 ms; $P > 0.4$; $n = 11$ and 18).

Short-term plasticity of EPSCs evoked by repetitive Schaffer collateral stimulation was also different between RS and FS basket cells. In fact, EPSCs depressed significantly more in RS as compared to FS basket cells at all frequencies tested (**Fig. 2-6a** and **Table 2-1**). Hence, FS basket cells receive stronger and more persistent excitation as compared to RS basket cells, suggesting that they are the primary mediators of feed-forward inhibition to CA1 pyramidal cells.

We next tested whether the differences in the magnitude and dynamics of excitation between the two types of basket cells is specific to Schaffer collateral inputs or whether it extends also to the two other major excitatory pathways: the perforant path and the CA1 pyramidal cell axon collaterals. As with the Schaffer collateral input, stimulation of the perforant path evoked larger (1.21 ± 0.30 times larger in RS basket cells; 3.35 ± 0.95; $P < 0.05$ times larger in FS basket cells; $n = 7$ and 5; **Fig. 2-5b**) and less depressing (**Fig. 2-6b** and **Table 2-1**) EPSCs on FS than RS basket cells.

Similarly, stimulation of the alveus elicited EPSCs that depressed significantly more in RS as compared to FS basket cells (**Fig. 2-6c** and **Table 2-1**). Since CA1 pyramidal cells form few, if any, recurrent synapses with other CA1 pyramidal cells
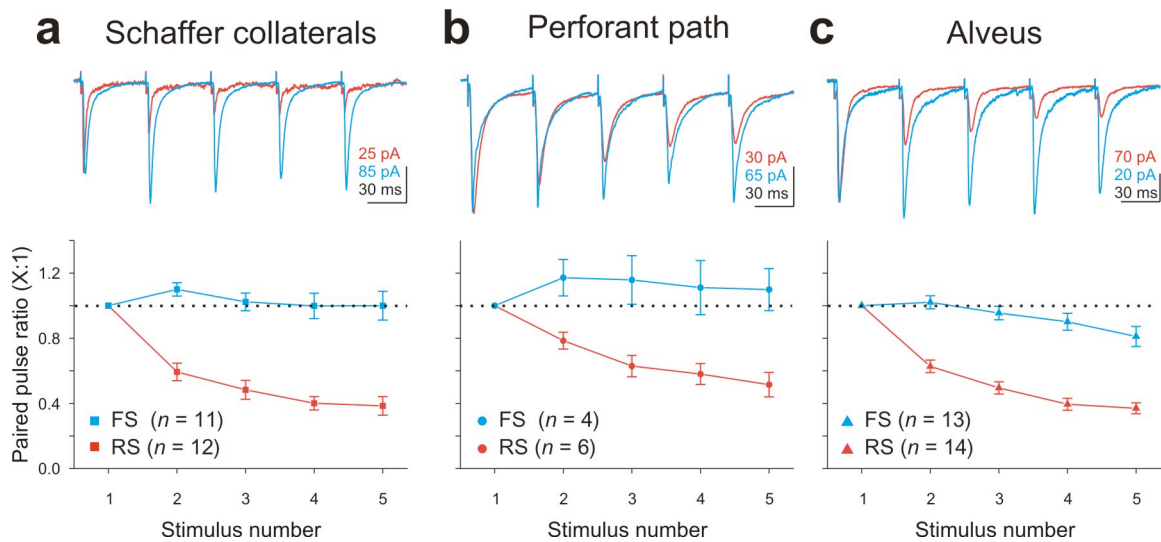
Figure 2-6: Distinct dynamics of excitation of RS and FS basket cells

(a) Top: current traces in response to Schaffer collateral stimulation at 20 Hz in RS (red) and FS (blue) basket cells (scaled to the first EPSC). Bottom: summary graph of normalized EPSC amplitudes plotted against stimulus number (red: RS, $n = 12$; blue: FS, $n = 11$). FS cell is same as in **Fig. 2-5**. All EPSCs in this figure were recorded in presence of gabazine (2.5 µM) or at the IPSC reversal potential (−85 mV).
(b) Same as **(a)** for the perforant pathway (red: RS, $n = 6$; blue: FS, $n = 4$). Both basket cells are same as in **Fig. 2-5**.
(c) Same as **(a)** for the alveus (red: RS, $n = 15$; blue: FS, $n = 13$).

Table 2-1: Short-term plasticity of excitation onto RS and FS basket cells

Ratio of the fifth to the first EPSC evoked by stimulating the three main afferents at three different frequencies. The number of cells is given in parentheses. All within pathway comparisons between RS and FS basket cells are significantly different ($P < 0.05$).

	10 Hz (stim5/stim1)		20 Hz (stim5/stim1)		50 Hz (stim5/stim1)	
Pathway	RS	FS	RS	FS	RS	FS
Schaffer col.	0.49 ± 0.04 (17)	0.99 ± 0.05 (15)	0.38 ± 0.06 (12)	1.00 ± 0.09 (11)	0.25 ± 0.04 (11)	0.96 ± 0.13 (10)
Alveus	0.48 ± 0.04 (19)	0.86 ± 0.06 (17)	0.37 ± 0.03 (14)	0.81 ± 0.06 (13)	0.30 ± 0.04 (14)	0.68 ± 0.08 (12)
Perforant Path	0.60 ± 0.04 (7)	1.18 ± 0.16 (4)	0.52 ± 0.08 (6)	1.10 ± 0.13 (4)	0.38 ± 0.07 (6)	0.93 ± 0.10 (4)

(Deuchars and Thomson, 1996), no reference EPSC could be recorded in response to alveus stimulation in the postsynaptic pyramidal cells. This prevented the comparison of the relative magnitude of excitation produced by CA1 pyramidal cells onto the two basket cell types. These data clearly show that RS basket cells receive significantly weaker and more depressing excitation from their major excitatory inputs than FS basket cells.

The difference in EPSC amplitude recorded in RS and FS basket cells could be due to a difference in any of the following physiological and morphological parameters: 1) quantal size, i.e. the amplitude of the EPSC evoked by the release of a single vesicle of transmitter; 2) quantal content, i.e. the average number of transmitter vesicles that are released by an individual afferent onto the recorded neuron in response to an action potential, or 3) convergence, i.e. the probability that an individual afferent forms a synapse onto the recorded neuron. The quantal amplitude can be determined by measuring the amplitude of spontaneous, action potential independent EPSCs (miniature EPSCs or mEPSCs). The quantal content can be estimated by comparing the amplitude of spontaneous action potential dependent events (apEPSCs) with the quantal amplitude. In order to measure the quantal amplitude and quantal content in RS and FS basket cells, we first recorded spontaneously occurring EPSCs (sEPSCs; **Fig. 2-7a**). The median amplitude of sEPSCs was about 70% larger in FS than RS basket cells (FS: -37.2 ± 7.9 pA; RS: -22.5 ± 2.6 pA; Kolmogorov-Smirnov test $P < 0.0001$; $n = 3$ each; **Fig. 2-7b**). sEPSCs are composed of both mEPSCs and apEPSCs. In order to isolate the mEPSCs, we applied tetrotodoxin (TTX; 1 µM) to block action potentials (**Fig. 2-7c**). TTX

Figure 2-7: Quantal synaptic properties of RS and FS basket cells

(a) Spontaneous EPSCs (sEPSCs) recorded in RS (red) and FS (blue) basket cells.
(b) Cumulative distribution of sEPSC amplitudes for RS (red, $n = 3$) and FS (blue, $n = 3$) basket cells. Inset: summary of the average median sEPSC amplitude.
(c) Miniature EPSCs (mEPSCs) recorded in the same cells as in **(a)** (1 µM TTX)
(d) Same as **(b)** for mEPSCs in RS (red, $n = 3$) and FS (blue, $n = 3$) basket cells.
(e) Equation (top) used to determine the average quantal content (QC; bottom) for RS (red, $n = 3$) and FS (blue, $n = 3$) basket cells. A_S: average amplitude of sEPSCs; $\#_S$: number of sEPSCs over a given time period; A_M: average amplitude of mEPSCs; $\#_M$: number of mEPSCs over a given time period.
(f) Cumulative distribution of mEPSC interevent interval for RS (red, $n = 3$) and FS (blue, $n = 3$) basket cells. Inset: summary of the average median mEPSC interevent interval.

a

RS

FS

240 pA
20 ms

b

sEPSCs

Cumulative fraction

Amplitude (pA)

Amplitude (pA)

c

1 μM TTX

d

mEPSCs

Cumulative fraction

Amplitude (pA)

Amplitude (pA)

e

$$QC = \frac{(Amp_{sEPSCs})(\#_{sEPSCs}) - (Amp_{mEPSCs})(\#_{mEPSCs})}{(Amp_{mEPSCs})(\#_{mEPSCs} - \#_{sEPSCs})}$$

Quantal content

f

mEPSCs

Cumulative fraction

Interval (ms)

Interevent Interval (s)
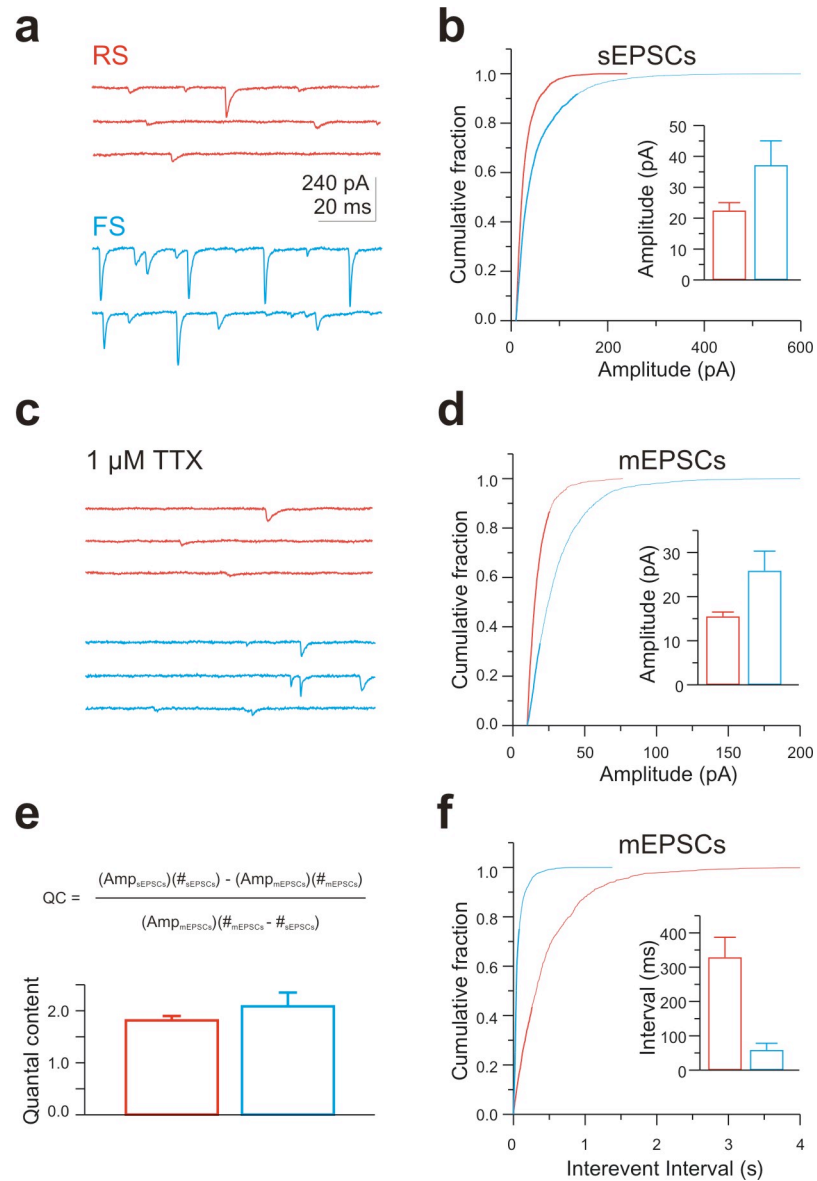
increased the average inter-event interval (FS: from 18 ± 6 ms to 59 ± 20 ms; RS: from

78 ± 32 ms to 329 ± 58 ms; $n = 3$ each), indicating that a substantial fraction of the events

recorded under control conditions were apEPSCs in both cell types. The median

amplitude of mEPSCs was also about 70% larger in FS than RS basket cells (FS: -25.9

± 4.4 pA; RS: -15.5 ± 1.0 pA; Kolmogorov-Smirnov test $P < 0.0001$; $n = 3$ each; **Fig. 2-**

7d). The mean amplitude of apEPSCs (A_{AP}) was determined by using the following

equation:

$$A_{AP} = (A_S \#_S - A_M \#_M)/(\#_S - \#_M),$$

where A_S and A_M are the average amplitudes of sEPSC and mEPSCs, respectively, and $\#_S$

and $\#_M$ are the number of sEPSC and mEPSC, respectively, collected over an identical

time period (from 0.3 to 4.3 min) in control conditions (for sEPSCs) and immediately

afterwards in the presence of TTX (for mEPSCs). The quantal content was determined by

dividing A_{AP} by A_M and was found to be very similar in the two cell types (FS: 2.1 ± 0.3;

RS: 1.8 ± 0.1; $P > 0.3$; $n = 3$ each; **Fig. 2-7e**). Thus, under our experimental conditions an

action potential in an excitatory axon triggers, on average, the release of two vesicles of

glutamate independent of whether it impinges on RS or FS basket cells.

Further, the larger evoked EPSCs observed on FS basket cells can not be

accounted for by a difference in quantal content and only partially by a difference in

quantal amplitude. These results suggest that much of the difference in evoked EPSC

amplitude is likely due to a difference in convergence, a possibility supported by the 5-6

times higher mEPSC frequency in FS basket cells (FS: 59 ± 20 ms; RS: 329 ± 58;

Kolmogorov-Smirnov test $P < 0.0001$; $n = 3$ each; **Fig. 2-7f**).

Transient recruitment of RS basket cells

The strongly depressing EPSCs evoked onto RS basket cells suggests that their recruitment during ongoing hippocampal activity may be very transient as compared to FS basket cells. We tested this by first comparing the spike timing of the two basket cells during trains of stimuli and second by determining the contribution of RS basket cells to the inhibition of pyramidal cells during these trains.

We recorded from basket cells in the whole-cell, current clamp configuration and repetitively stimulated the alveus (five stimuli at 20 Hz) at an intensity that was at threshold to trigger an action potential after the first stimulus in the train. The probability of the alvear input triggering an action potential in RS basket cells decreased sharply with repetitive stimulation (from $57 \pm 9\%$ after the first stimulus to 0 after the fifth stimulus; $P < 0.001$; $n = 4$; **Fig. 2-8a**). In contrast, in FS basket cells the spiking probability remained more sustained during the train (from $69 \pm 4\%$ after the first stimulus to $32 \pm 16\%$ after the fifth stimulus; $P > 0.05$; $n = 4$; **Fig. 2-8a**). Thus, we predict that RS basket cells will only transiently contribute to disynaptic inhibition of pyramidal cells during repetitive stimulation of the alveus.

This hypothesis was tested by evoking disynaptic inhibitory postsynaptic currents (IPSCs) in pyramidal cells via alveus stimulation. To quantify the relative contribution of RS basket cells to the disynaptic IPSC we briefly depolarized the pyramidal cell, thereby suppressing GABA release from RS basket cells via endocannabinoid signaling. The contribution of RS basket cells to the disynaptic IPSC recorded in pyramidal cells was essentially restricted to the very first stimulus in a series (DSI first stim: $30 \pm 9\%$; DSI fifth stim: $-3 \pm 8\%$; $P < 0.05$; $n = 3$; **Fig. 2-8b**). In contrast, interneurons mediating the

Figure 2-8: Transient recruitment of RS basket cells

(a) Left: ten superimposed voltage traces from RS (top, red) and FS (bottom, blue) basket cells during 20 Hz alveus stimulation at threshold for spiking on the first stimulus. APs have been truncated. RS cell is same as shown in **Fig 2-3e**. Right: spiking probability plotted for each stimulus in the train, normalized to the probability of spiking in response to the first stimulus in RS ($n = 4$) and FS ($n = 4$) basket cells.
(b) Upper traces: disynaptic IPSCs recorded in a pyramidal cell in response to repetitive alveus stimulation (five stimuli at 20 Hz) before (black trace) directly after (green trace) and upon recovery from (gray trace) depolarization (0 mV; 5 s). Insets show the first and fifth responses scaled. Lower traces: left, the DSI sensitive component was isolated by subtracting the green from the black trace (upper panel); right, the CB1R antagonist AM251 blocked suppression of the IPSC. The glutamate receptor antagonist NBQX (10 µM) abolished the IPSCs confirming their disynaptic nature.
(c) Upper traces: monosynaptic IPSCs (five stimuli at 20 Hz) in the presence of NBQX with the stimulation electrode placed near the pyramidal cell body. Lower traces: left, DSI sensitive component was isolated as in **(b)**; right, the CB1R antagonist blocked suppression of the IPSC.
(d) DSI plotted against stimulus number for monosynaptic (black; $n = 3$) and disynaptic (red; $n = 3$) IPSCs.

a

RS

FS

20 mV
20 ms

IC

b

Disynaptic inhibition

Control

Recovery

After depol.

1st pulse

5th pulse

10 ms

VC

100 pA
20 ms

DSI sensitive component

100 pA
40 ms

AM251

NBQX

c

Direct inhibition
(NBQX)

Control

Recovery

After depol.

1st pulse

5th pulse

10 ms

VC

100 pA
20 ms

DSI sensitive component

AM251

100 pA
40 ms

d

Disynaptic inhib. ($n = 3$)
Direct inhib. ($n = 3$)
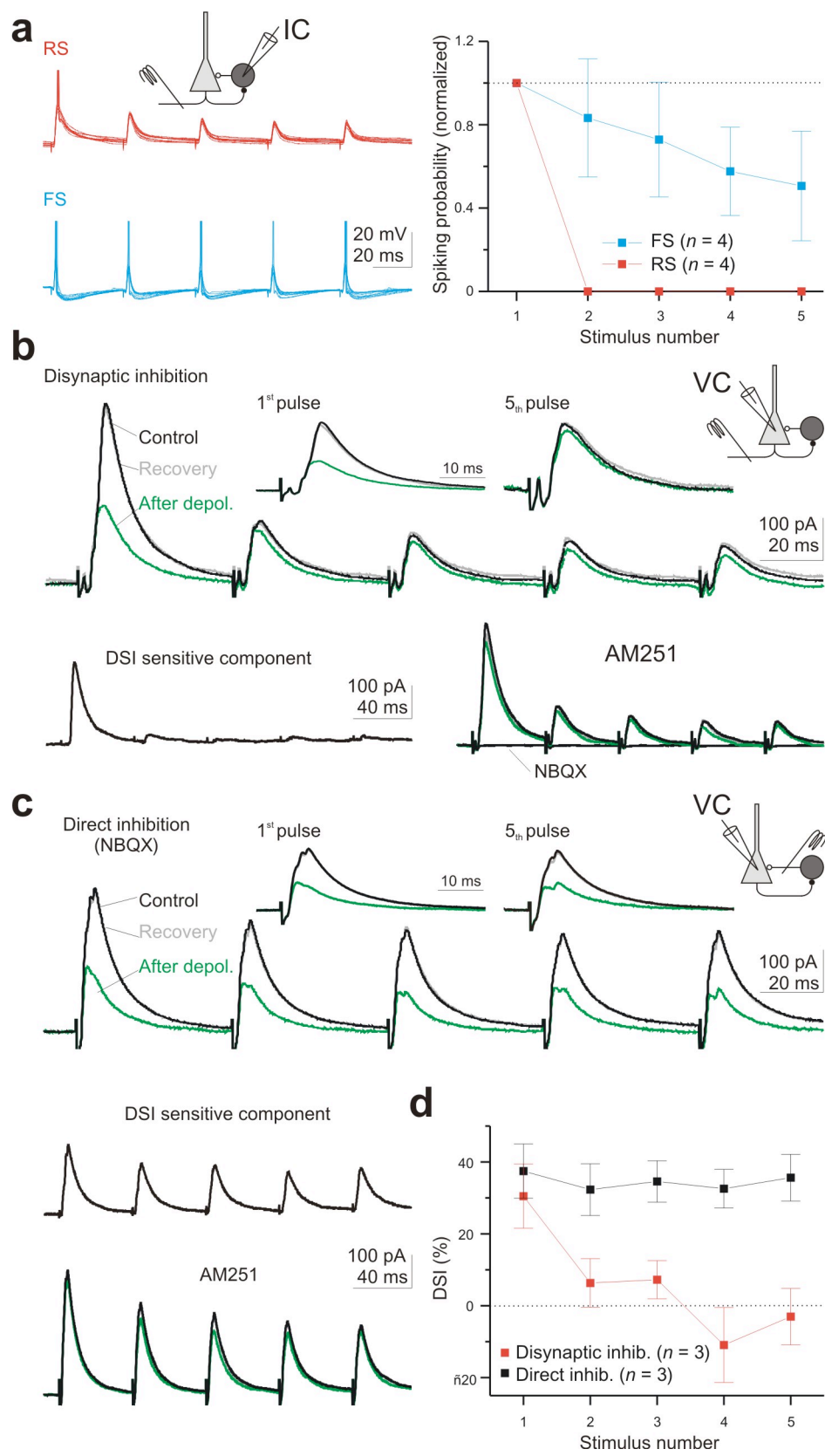
cannabinoid insensitive component (which may include FS basket, axo-axonic and bistratified cells), appear to be recruited repetitively during the stimulus train. The transient contribution by RS basket cells was not due to the depression of GABA release from their terminals because direct stimulation of the GABAergic axons (in the presence of NBQX) elicited monosynaptic IPSCs whose endocannabinoid sensitive component remained unaltered during the entire train of stimuli (DSI first stim: $37 \pm 8\%$; DSI fifth stim: $36 \pm 7\%$; $P > 0.4$; $n = 3$; **Fig. 2-8c-d**). Hence, these data demonstrate that while repetitive activation of excitatory afferents only transiently recruits RS basket cells, FS basket cells are able to spike throughout a train of stimuli.

Selective inhibitory circuits between basket cells

Since RS basket cells respond poorly to the repetitive activation of a single pathway, they may be preferentially recruited when two or more independent pathways are active in succession. Since the ability of a neuron to integrate independent inputs depends critically on the amount of inhibition that it receives (Pouille and Scanziani, 2001), we compared the magnitude of disynaptic inhibition onto RS and FS basket cells. For this, we stimulated excitatory afferents and used the disynaptic IPSC recorded in pyramidal cells as a reference in the same manner as we did when comparing the amplitude of EPSCs (**Fig. 2-9a**).

FS basket cells received larger disynaptic IPSCs as compared to pyramidal cells in response to both Schaffer collateral (FS: 361.5 ± 83.0 pA vs. Pyr: 166.4 ± 21.4 pA; $P < 0.05$; $n = 13$; **Fig. 2-9b**) and alveus stimulation (FS: 206.2 ± 31.4 pA vs. Pyr: 95.9 ± 22.1 pA; $P < 0.05$; $n = 12$; **Fig. 2-9b**). The onset of the disynaptic IPSC (10% of peak
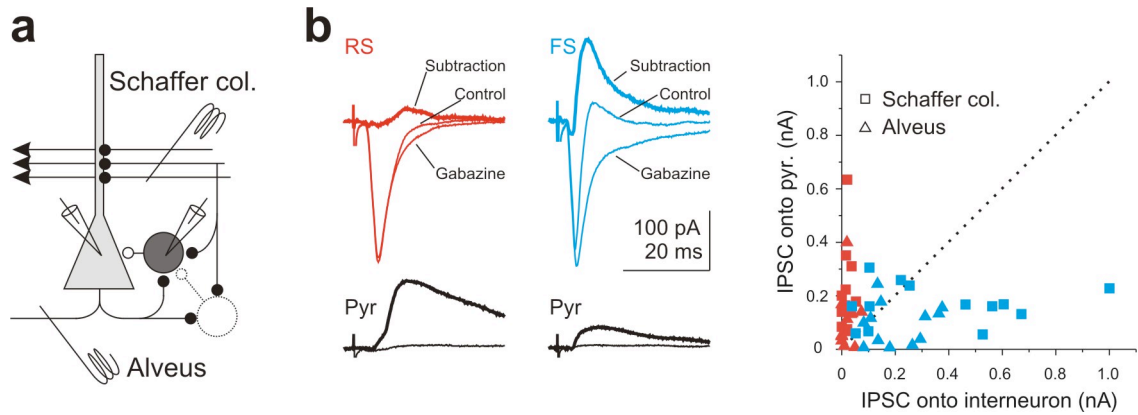
Figure 2-9: Strong disynaptic inhibition of FS basket cells

(a) Recording configuration.
(b) Left: current traces from RS (left, red traces) and FS (right, blue traces) basket (top) and pyramidal cell (bottom, black traces) pairs in response to alveus stimulation in control, gabazine, and their algebraic subtraction (thick traces). RS cell is same as shown in **Fig. 2-3d**. Right: scatter plot of IPSCs onto paired basket and pyramidal cells (Schaffer collaterals (squares): *n* = 11 and 13; alveus (triangles), *n* = 12 and 12 for RS and FS basket cells, respectively).

amplitude) recorded in FS basket cells occurred with 1.64 ± 0.11 ms delay ($n = 25$) with respect to the onset of the monosynaptic EPSC, consistent with its disynaptic origin (Pouille and Scanziani, 2001).In contrast, RS basket cells received a much smaller disynaptic IPSCs as compared to pyramidal cells in response to stimulation of either pathway (Schaffer collaterals: RS: 17.1 ± 4.9 pA vs. Pyr: 242.8 ± 50.3 pA; $P < 0.005$; $n = 12$; Alveus: RS: 22.8 ± 6.7 pA vs. Pyr: 107.5 ± 29.4 pA; $P < 0.05$; $n = 12$; **Fig. 2-9b**). The onset of the small disynaptic IPSC occurred with a 2.89 ± 0.35 ms delay ($n = 13$) with respect to the onset of the monosynaptic EPSC.

The absence of disynaptic inhibition onto RS basket cells could be due to either a lack of inhibitory synapses or to a failure of the stimulus to recruit the correct population of interneurons. Thus, we wanted to determine whether basket cells inhibit each other. In order to test the strength of basket cells' inputs onto other basket cells, monosynaptic IPSCs (10 μM NBQX) were evoked with a stimulation electrode placed in the pyramidal cell layer (to preferentially activate basket cell axons) and recorded simultaneously in voltage clamped basket and pyramidal cells. The amplitude of IPSCs recorded in basket cells were normalized by the amplitude of the IPSC recorded simultaneously in pyramidal cells to control for differences in the number of stimulated inhibitory axons between experiments. On average, the amplitude of the IPSC recorded in FS basket cells was not significantly different than the amplitude of the IPSC recorded simultaneously in pyramidal cells (ratio: 1.22 ± 0.21; $n = 8$; $P > 0.5$; **Fig. 2-10a,c**). In contrast, the IPSCs recorded in RS basket cells were much smaller than the IPSCs recorded in pyramidal cells (ratio: 0.14 ± 0.05; $n = 7$; $P < 0.0005$; **Fig. 2-10b,c**). These results indicate that FS
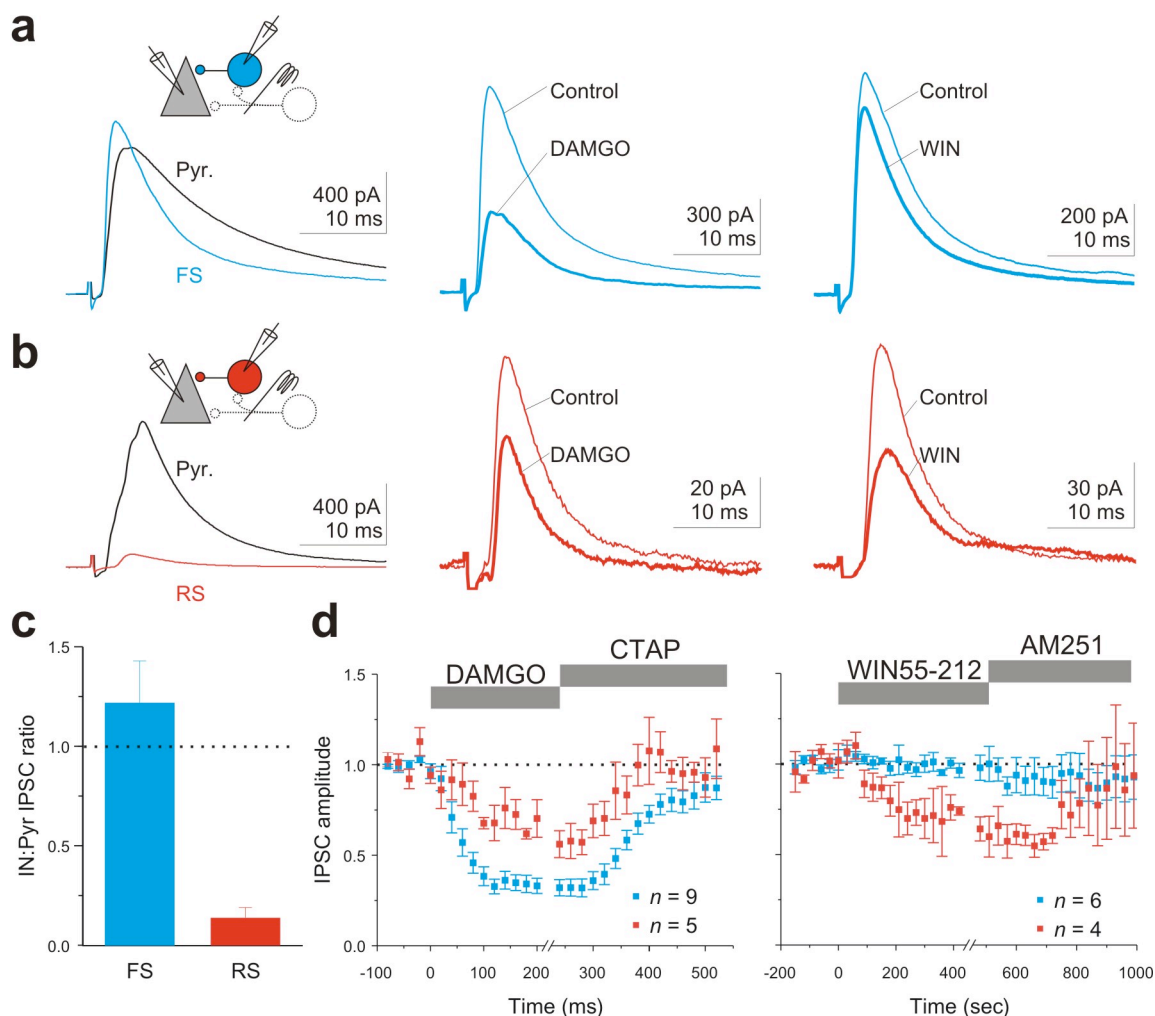
Figure 2-10: Selective inhibitory networks of basket cells

(a) Inset: schematic of the recording configuration. Left, IPSC in a FS (blue trace) basket cell and a simultaneously recorded pyramidal cell (pyr.; black trace; both cells VH = -50 mV) in the presence of NBQX (10 μM). Middle, IPSC from the same FS basket cell in the presence of DAMGO (thick trace). Right, IPSC from the same FS basket cell in the presence of WIN55-212 (thick trace).
(b) Same protocol as in **(a)** in an RS (red trace) basket cell and its paired pyramidal cell.
(c) Summary graph of the ratio of IPSC amplitudes onto simultaneously recorded on RS (red; n = 7) and FS (blue; n = 8) basket and pyramidal cells.
(d) Summary time course of the normalized IPSC amplitude of RS (red; n = 5) and FS (blue; n = 9) basket cells, upon application of DAMGO and CTAP.
(e) Same as **(d)**, upon application of WIN55-212 and AM251 recording from RS (red; n = 6) and FS (blue; n = 4) basket cells.

basket cells receive strong inhibitory input from other basket cells while RS basket cells are only weakly inhibited by basket cells.

In order to determine which basket cells contribute the inhibition onto FS and RS basket cells, we used the μOR and CB1R pharmacology to dissect the IPSCs. The μOR agonist, DAMGO, reduced the amplitude of both the large IPSCs recorded in FS basket cells (to $34.2 \pm 4.2\%$ of control; $n = 9$; $P < 0.0001$; **Fig. 2-10a,d**) as well as the small IPSCs recorded in RS basket cells (to $69.7 \pm 7.3\%$ of control; $n = 5$; $P < 0.05$; **Fig. 2-10b,d**). Since μORs inhibit GABA release from terminals of FS basket cells only (see above) this result suggests that the axons of FS basket cells diverge onto both FS and RS cells. Cannabinoid receptor activation through bath perfusion of WIN55-212 (1 μM), on the other hand, had no effect on the amplitude of the large IPSC recorded in FS basket cells (to $95.7 \pm 1.7\%$ of control; $n = 6$; $P > 0.4$; **Fig. 2-10a,d**). The small IPSCs onto RS basket cells had variable responses to WIN55-212: IPSCs onto three out of four RS cells were suppressed (and two of these could be reversed by the CB1R antagonist AM251), while the fourth showed no effect. Thus, while on average IPSCs onto RS basket cells were not significantly suppressed by WIN55-212 (to $64.7 \pm 14.6\%$ of control; $n = 4$; $P > 0.05$; **Fig. 2-10b,d**) there is likely some contribution of RS basket cells to the very weak inhibition of other RS basket cells.

These data suggest that the only basket cells that inhibit FS basket cells are other FS basket cells. In support of this conclusion, IPSCs onto FS basket cells were inhibited by DAMGO to the same extent as were uIPSCs from FS basket cells onto pyramidal cells (FS uIPSC: to $26.5 \pm 3.2\%$ of control; IPSC onto FS: to $34.2 \pm 4.2\%$ of control; $n = 12$ and 9; $P > 0.1$). Thus, the weak inhibition onto RS basket cells originates from both the

RS and FS basket cells, while the strong inhibition onto FS basket cells comes exclusively from other FS basket cells.

RS basket cells are integrators

We next tested whether this marked difference in the amount of inhibition received by the two basket cell types influences their ability to integrate consecutive inputs. We recorded from basket cells and applied a stimulus to the Schaffer collaterals followed, with a variable delay, by a stimulus to the alveus. The lack of disynaptic inhibition enabled RS basket cells to summate EPSPs originating from the two distinct afferents over much longer time windows than FS cells (summation at 10 ms interval: RS: 0.66 ± 0.07; FS: 0.13 ± 0.06; $P < 0.0001$; $n = 7$ and 10; **2-Fig. 11a**).

The very brief integration window of FS basket cells was, at least in part, due to the presence of inhibition. Accordingly, application of the $GABA_A$ receptor antagonist, gabazine (2.5 μM), increased the integration window of FS basket cells to values comparable with their membrane time constant (summation at 10 ms interval: FS control: 0.13 ± 0.06; gabazine: 0.61 ± 0.05; $P < 0.0005$; $n = 10$ and 5; **Fig. 2-11b**).

We next determined whether these two different integration windows influence summation within physiologically relevant intervals. When Schaffer collateral stimulation is above threshold to trigger action potentials in CA1 pyramidal cells, two consecutive EPSCs are recorded in basket cells: the first is due to direct Schaffer collateral excitation (feed-forward EPSC; **Fig. 2-12a**), the second is due to feedback excitation through the recurrent axon collaterals of CA1 pyramidal cells (feedback EPSC; **Fig. 2-12a**). The amplitude of the population spike (simultaneously recorded in the CA1
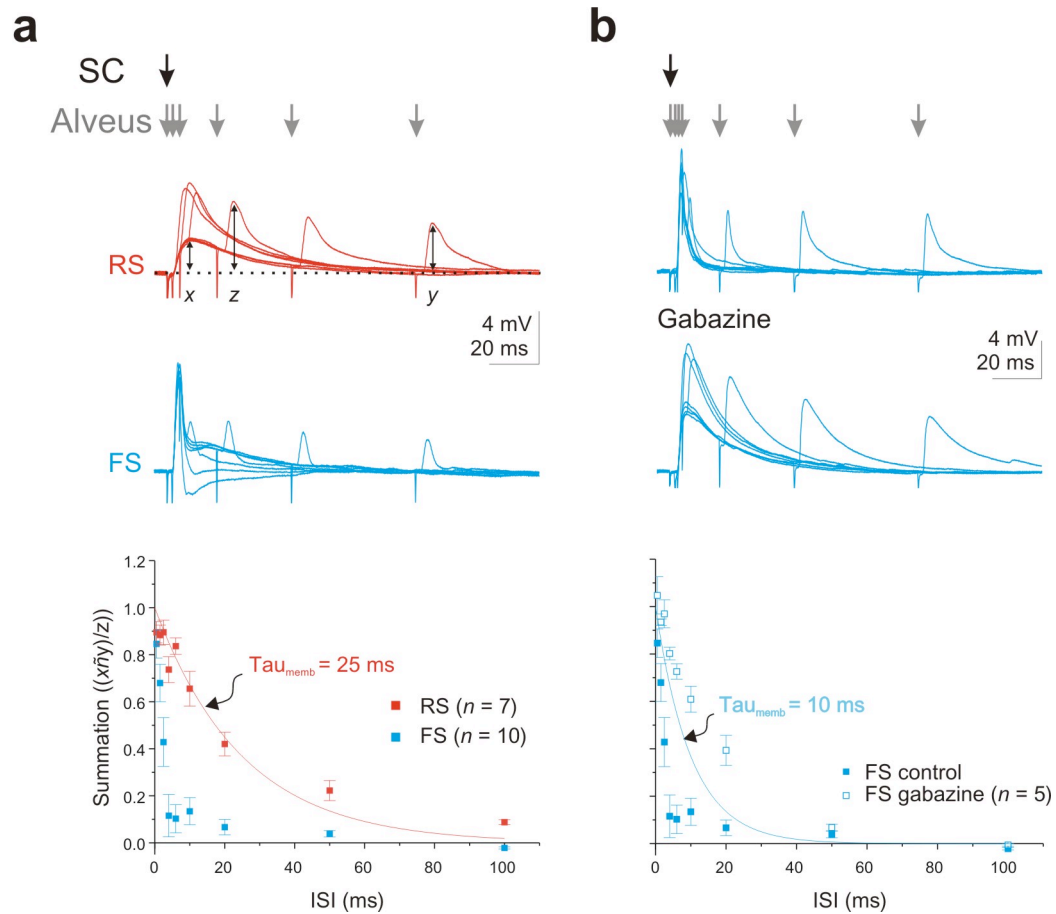
Figure 2-11: Distinct integration time windows in RS and FS basket cells

(a) Top: superimposed average voltage traces from basket cells in response to Schaffer collateral stimulation (black arrow) followed, with increasing delays, by alveus stimulation (gray arrows). Cells are same as in **Fig 2-9b**. Bottom: summation is computed as the peak amplitude of the summed response (x) minus the peak amplitude of the feedback postsynaptic potential (PSP) alone (y), normalized by the peak of the feed-forward PSP (z). The result is plotted against the inter-stimulus interval (ISI) for RS ($n = 7$) and FS ($n = 10$) basket cells. The red line represents the membrane time constant of RS basket cells (tau = 25 ms).

(b) Top: superimposed average voltage traces from a FS basket cell in control (top) and in the presence of gabazine (bottom) for the same protocol as in **(a)**. Bottom: summation is plotted against the ISI in control (closed squares; same data as in **(a)**) and in gabazine (open squares; $n = 5$). The blue line represents the membrane time constant of FS basket cells (tau = 10 ms).

pyramidal cell layer) increased in a sigmoidal manner with the feed-forward EPSC amplitude, as expected (Andersen et al., 1973; Wierenga and Wadman, 2003). In contrast, the amplitude of the late, feedback EPSC increased linearly with the amplitude of the population spike, indicating that this second EPSC is indeed triggered by the spiking of CA1 pyramidal cells (data not shown;(Wierenga and Wadman, 2003)). The average delay between the onset of the feed-forward and feedback EPSC varied between 3 and 5 ms, depending on stimulation intensity (delay at threshold stimulation intensity for feedback EPSC: 4.94 ± 0.73 ms, $n = 7$; delay at maximal stimulation intensity 3.19 ± 0.25 ms; range 2.1 to 4 ms, $n = 7$; **Fig. 2-12a** and shaded region in **Fig. 2-12b**). Notably, this interval is larger than the integration window of FS basket cells but shorter than the integration window of RS basket cells (**Fig. 2-10b**). Our data, thus, indicate that by operating as precise coincidence detectors FS basket cells can process the feed-forward and the immediately following feedback excitation as two separate events. In contrast the succession of feed-forward and feedback EPSPs will summate within the broad integration window of RS basket cells.

Temporal separation in the recruitment of basket cells

The above results suggest that FS basket cells will spike earlier than RS basket cells in response to Schaffer collateral stimulation because the latter must integrate the succession of feed-forward and feedback EPSPs before reaching threshold. Furthermore, if RS basket cells preferentially fire in response to the summation of feed-forward and feedback EPSPs they should contribute to feedback inhibition of CA1 pyramidal cells to a larger extent than to feed-forward inhibition. We tested these two outcomes by first
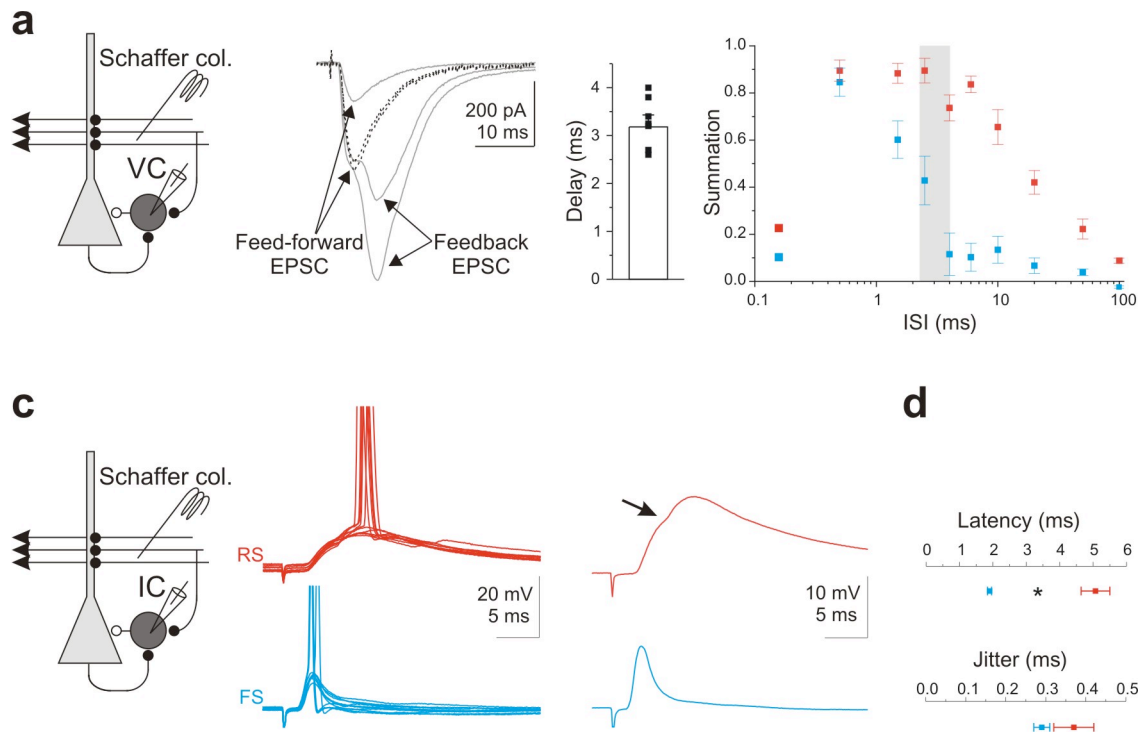
Figure 2-12: Differential activation of RS and FS basket cells by feed-forward and feedback excitation

(a) Left: recording configuration. Center: voltage clamp recording from an interneuron in response to Schaffer collateral stimulation at three different intensities (2.5 µM gabazine). Note the appearance of a late, feedback EPSC at stronger stimulation intensities. Dotted trace: the EPSC recorded at low stim intensity is scaled to the peak of the early component elicited at strong stimulation intensities. Right: delays between feed-forward and feedback EPSCs (*n* = 7).
(b) Same data as in **Fig. 2-11a** plotted on a logarithmic axis. The vertical gray shaded region represents the range of delays recorded in (a).
(c) Left: recording configuration. Middle: ten superimposed current traces from RS (top, red) and FS (bottom, blue) basket cells at threshold for spiking in response to Schaffer collateral stimulation. APs have been truncated. Right, average of responses that failed to elicit an action potentials. Arrow notes discontinuity in the rise of the EPSP in the RS cell due to the onset of feedback EPSP.
(d) Summary of latency to spike (top) and jitter (bottom) in RS (*n* = 4) and FS (*n* = 9) basket cells.

comparing the spike timing of the two basket cell types in response to Schaffer collateral stimulation and second by determining the relative contribution of RS and FS basket cells to feed-forward and feedback inhibition of CA1 pyramidal cells.

When stimulating Schaffer collaterals at threshold for spike generation (RS: spiking probability: $40 \pm 4\%$; membrane potential before EPSP onset: -57.7 ± 1.9 mV; FS: spiking probability: $50 \pm 7\%$; membrane potential before EPSP onset: -57.7 ± 0.8 mV; spiking probability: $P > 0.4$; membrane potential: $P > 0.9$; $n = 4$ and 9; **Fig. 2-12c**), the action potential occurred later in RS basket cells than FS (delay from onset of EPSP: RS: 5.1 ± 0.4 ms; FS: 1.9 ± 0.1 ms; $P < 0.0001$; $n = 4$ and 9; jitter of action potentials: RS: 0.37 ± 0.02; FS: 0.29 ± 0.05 ms; $P > 0.3$; $n = 4$ and 9; **Fig. 2-12c-d**). Furthermore, in RS basket cells, the response triggered by Schaffer collateral stimulation showed a biphasic rising phase, consistent with the integration of the feed-forward/feedback EPSP sequence (**Fig. 2-12c**).

We next recorded from a CA1 pyramidal cell and stimulated the Schaffer collaterals to evoke feed-forward and feedback inhibition. At low stimulation intensities, release of glutamate from the Schaffer collaterals directly excites pyramidal cells (triggering a monosynaptic EPSC, **Fig. 2-13a**) and feed-forward interneurons which, in turn, inhibit the pyramidal cells (triggering a disynaptic feed-forward IPSC). Increasing the stimulation intensity, in order to evoke action potentials in a fraction of the CA1 pyramidal cell population, recruits a population of feedback interneurons which inhibit the pyramidal cells (triggering a trisynaptic feedback IPSC).

Application of the μOR agonist, DAMGO (50-100 nM), selectively reduced the amplitude the feed-forward component of the IPSC (**Fig. 2-13b-c**). In contrast, activation
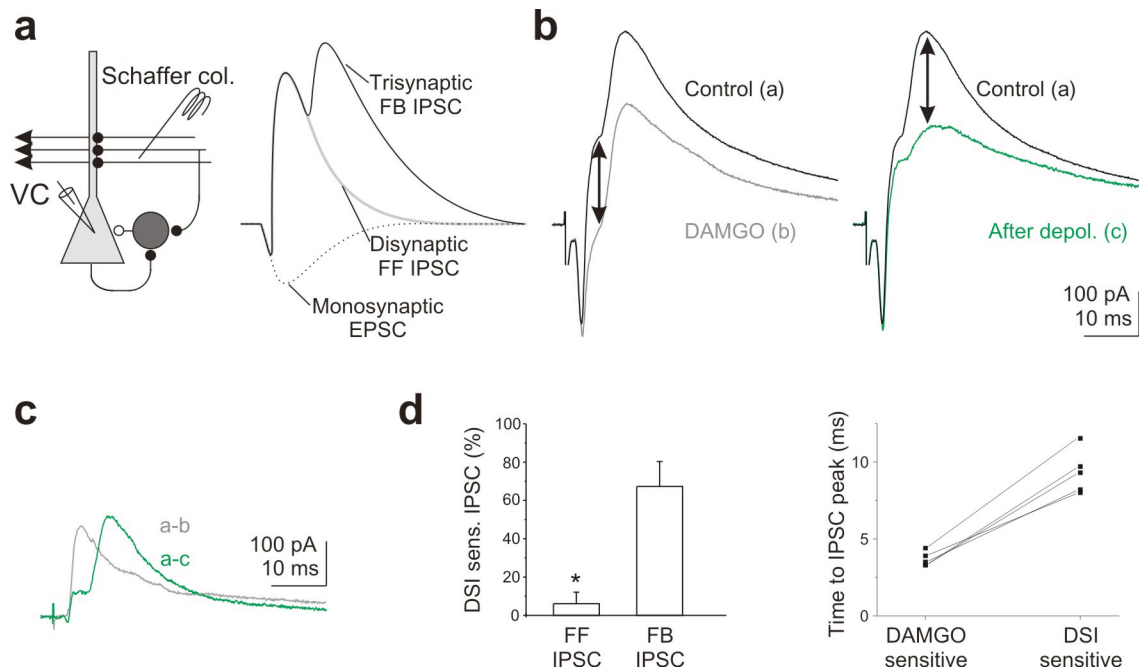
Figure 2-13: Differential contribution of RS and FS basket cells to feed-forward and feedback inhibition

(a) Left: recording configuration. Right: Schematic of response in a pyramidal cell to Schaffer collateral stimulation. Schaffer collaterals release glutamate directly onto pyramidal cells (monosynaptic EPSC: dotted line) and onto feed-forward interneurons which inhibit the pyramidal cells (disynaptic IPSC: gray line). Increasing the stimulus intensity recruits feedback inhibition (trisynaptic IPSC: black line) through the spiking of pyramidal cells.

(b) Left: IPSCs in a pyramidal cell in voltage clamp (VH = -50 mV) in response to stimulation of the Schaffer collaterals in control (black trace) and in the presence of DAMGO (gray trace). Arrow notes selective suppression of feed-forward IPSC. Right, same pyramidal cell in control (black trace) and after depolarization (to 0 mV, 5 s; green trace). Arrow notes selective suppression of feedback inhibition.

(c) Arithmetic subtraction of the traces in **(b)** to reveal the opioid (gray) and DSI (green) sensitive components. Note the different times of the two components.

(d) Left: summary of suppression of the feed-forward and feedback IPSCs by DSI ($n = 5$). Right: summary of the time of the peak of the opioid and DSI sensitive components ($n = 5$).

of CB1Rs, through depolarization of the pyramidal cell and release of endocannabinoids, selectively reduced the amplitude of feedback IPSC (**Fig. 2-13b-c**). Indeed, while RS basket cells only weakly contributed to feed-forward inhibition, they were responsible for the majority of feedback inhibition (percent suppression- feed-forward: $6 \pm 6\%$; feedback: $67 \pm 14\%$; $n = 5$, $P < 0.05$; **Fig. 2-13b,d**). On average, the peak of the opioid and cannabinoid sensitive components were separated by ~6 ms (5.7 ± 0.6 ms; $n = 5$; $P < 0.001$; **Fig. 2-13c-d**) consistent with the difference in spike times of the two basket cells (**Fig. 2-12c-d**).

Thus, by selectively affecting distinct types of basket cells, cannabinoids and opioids independently regulate different phases of inhibition in the hippocampus.

Discussion

Opioids and cannabinoids both modulate inhibitory systems; however, their impact on network activity is distinct. Whereas opioids strongly increase hippocampal excitability and can induce epileptic activity (Lee et al., 1989; Lupica and Dunwiddie, 1991), cannabinoids subtly disrupt the timing without changing the overall rate of activity (Paton et al., 1998; Robbe et al., 2006). This suggests that opioids and cannabinoids affect inhibitory systems in a different manner. Indeed, we find that these drugs independently suppress GABA release from the two populations of somatically targeting hippocampal interneurons: regular-spiking (RS) and fast-spiking (FS) basket cells. RS basket cells were recruited by the sequential activation of independent excitatory inputs, making them ideally suited to detect transitions in global activity. This pattern of

activation was distinct from that necessary to recruit the other major group, FS basket cells, resulting in a clear temporal separation in the activity of the two populations.

RS and FS basket cells are embedded in the same network and receive convergent inputs from the same main excitatory pathways. Thus, the temporal segregation in their activity, as apparent in the preferential participation of the two cell types in feed-forward or feedback inhibition, can not simply be explained by the connectivity. Rather, it is the magnitude and dynamics of excitation, the amount of disynaptic inhibition, and the membrane time constant that determine their specific activity pattern.

On average, evoked EPSCs onto FS basket cells were significantly larger than onto RS cells, independent of whether they originated from Schaffer collaterals or the perforant path, the two major excitatory afferents to the hippocampal CA1 region. This finding is consistent with anatomical data indicating that parvalbumin basket cells receive more excitatory synapses than CCK basket cells (Gulyas et al., 1999; Matyas et al., 2004). Differences in quantal amplitude, release probabilities and number of release sites per axonal input may further contribute to the difference in EPSC amplitude between the two basket cells types. It should be mentioned that the difference in EPSC amplitude might not result in a correspondingly large difference in EPSP amplitude given the lower input resistance of FS basket cells.

Stimulus trains over a broad range of frequencies (10-50 Hz) were more depressing onto RS than FS basket cells. This held true for each of the three major excitatory inputs converging on the two types of basket cells: the Schaffer collaterals, perforant path and CA1 pyramidal cell axons. The depression of excitatory inputs onto RS basket cells could be due to a presynaptic decrease in probabilities of transmitter

release or to a postsynaptic desensitization of the receptors for released glutamate. The coefficient of variation of EPSC amplitude increased during the course of the stimulus train (First pulse: 0.19 ± 0.02; fifth pulse: 0.44 ± 0.06; $n = 9$, $P < 0.005$), suggesting at least some presynaptic contribution to the depression (Faber and Korn, 1991).

Anatomical data demonstrate that CCK basket cells receive more GABAergic synapses than parvalbumin basket cells (Gulyas et al., 1999; Matyas et al., 2004). In contrast, we found that while FS basket cells were strongly inhibited, RS basket cells received almost no inhibition. This apparent discrepancy could be explained by the presence of two interneuron subnetworks in which RS and FS interneurons preferentially target cells in their own class (Bartos et al., 2002; Galarreta et al., 2004; Katsumaru et al., 1988; Sik et al., 1995). Indeed, we find that FS basket cells strongly inhibit each other. Given the stronger excitation received by the FS basket cells, afferent stimulation used in this study was likely to favor the activation of the FS subnetwork, explaining the presence of strong disynaptic inhibition. However, RS basket cells receive very little inhibition from either type of basket cell, consistent with the absence of disynaptic inhibition. Thus, if they are to receive inhibition, it must come from another source (Acsady et al., 1996; Freund, 2003).

The strong inhibition received by FS basket cells, in conjuction with a fast membrane time constant, generates a narrow integration time window. This enabled FS basket cells to discriminate inputs separated by as little as three milliseconds. On the other hand, the weak inhibition and long membrane time constant of RS basket cells enabled them to summate activity over longer intervals. Furthermore, because of the marked depression of their excitatory inputs, RS basket cells were less likely to respond

to repetitive activation of a given set of inputs but were well suited to integrate sequential activity of independent inputs. In behaviorally relevant situations, consecutive activation of independent feed-forward excitatory afferents impinging on a hippocampal RS basket cell in CA1 may occur when the movement of an animal in space triggers the sequential activation of CA3 pyramidal cells with different place fields.

An alternate situation involving the consecutive activity of independent pathway was explored here and results from the convergence of Schaffer collaterals and CA1 pyramidal cell axons onto individual basket cells. Our data showed that an evoked sequence of feed-forward and feedback EPSPs occurred with the optimal interval to be treated as separate events in FS basket cells while they will be integrated by RS basket cells. The strong excitation of FS basket cells by Schaffer collaterals caused them to fire in response to the first event in the sequence and hence provide feed-forward inhibition to their targets. In contrast, the weaker excitation received by RS basket cells required summation of both EPSPs in the sequence to trigger a spike. Hence RS basket cells preferentially contributed to feedback inhibition, rendering this component exquisitely sensitive to endocannabinoids. Feedback inhibitory loops are believed to play an important role in the generation of rhythmic activity (Andersen and Eccles, 1962). Specifically in the hippocampus, perisomatically targeting interneurons have been shown to entrain hippocampal gamma oscillations through feedback inhibition (Csicsvari et al., 2003; Mann et al., 2005). The contribution of RS basket cells to feedback inhibition suggests that these neurons may participate in the modulation of the hippocampal gamma rhythm, a hypothesis supported by recent experimental observations (Hajos et al., 2000).

By detecting distinct features of hippocampal activity, RS and FS basket cells were recruited at different times. The precise time of their recruitment may depend on the spatiotemporal activity pattern of their inputs, on the specific phase of a hippocampal oscillation or, more generally, on behavioral state of the animal. Under specific behavioral conditions, such as exploration or attention, release of neuromodulators may alter the relative excitability of the two basket cells through selective receptor expression (Freund, 2003; Morales and Backman, 2002). Indeed, whereas endogenous opioids are released through activity in afferent pathways (Gall et al., 1984; Gall et al., 1981), endocannabinoids are released from the soma and dendrites of the principal cells (Wilson and Nicoll, 2001). However, investigations of the conditions under which endogenous opioids and cannabinoids are released indicate that both substances are released during periods of increased activity (Fortin et al., 2004; Rocha and Maidment, 2003; Varma et al., 2001; Wagner et al., 1990). Discovery of the precise patterns of activity which lead to the release of endogenous opioids and cannabinoids will further our understanding of the impact of these substances on the circuit.

The relative locations of endogenous agonist and receptor expression are also different for opioids and cannabinoids. CB1Rs, located on the presynaptic terminals of basket cells, are directly apposed to the site of endocannabinoid release (i.e. the soma of pyramidal cells). In contrast, the majority of μORs are at least four microns away from the nearest site of endogenous opioid release (Drake et al., 2002). This, suggests that the effects of opioids will be more diffuse than cannabinoids; however, the extent of the effect of both opioids and cannabinoids will depend on the localization of peptidases and other breakdown mechanisms (Ameri, 1999; Malfroy et al., 1979).

Since opioids selectively modulate feed-forward inhibition, they will decrease the threshold, decrease the synchrony, and increase the integration time window of hippocampal pyramidal cells (Pouille and Scanziani, 2001). Thus, temporary disinhibition via opioids could have important implications for metaplasticity and learning rules in the hippocampus (Bramham and Sarvey, 1996; Xie and Lewis, 1995). In contrast, the selective modulation of feedback inhibition by cannabinoids will increase the tendency of pyramidal cells to burst without affecting their overall activity levels (Robbe et al., 2006). Thus, the ability of opioids and cannabinoids to selectively modulate activity through their specific actions on the two basket cell populations increases the flexibility of the network.

Chapter 2 was published in part in Nature Neuroscience 2006, Glickfeld, Lindsey L.; Scanziani, Massimo. The dissertation author was the primary investigator and author of this paper.

CHAPTER 3- Fast and Slow Inhibition by Two Populations of Dendrite Targeting

Interneurons

Abstract

Dendrites of pyramidal cells are the site of convergence of tens of thousands of excitatory synaptic inputs.   Inhibition of dendrites is, thus, crucial to control the excitation onto pyramidal cells at its source. Here we show that two distinct types of dendrite targeting inhibitory interneurons (so-called bistratified cells) generate two radically opposed modes of inhbition, namely fast and transient or slow and incremental. These two distinct modes of inhibition result, at least in part, from the spatio-temporal profile of GABA at the two synapses. Since the two dendrite targeting interneurons differ in their intrinsic excitability and the type of excitatory input that they receive, they are likely to be active under different conditions. Thus, dendritic excitability can be modulated in a phasic or tonic manner depending on the activated inhibitory circuit.

Introduction

Pyramidal cells receive glutamatergic inputs exclusively on their dendrites (Megias et al., 2001). Through active conductances, passive filtering, and synaptic activity, the dendrites shape excitation before it is integrated at the soma (Magee, 2000; Spruston et al., 1994; Tsay and Yuste, 2004; Williams and Stuart, 2003). Dendritic inhibition is one of these factors that determines the local integration of excitatory inputs. GABAergic inputs to the dendrites have been shown to have diverse effects on dendritic integration: they can shunt local glutamatergic activity, suppress back-propagating action potentials, and inhibit calcium electrogenesis (Larkum et al., 1999; Liu, 2004; Miles et al., 1996; Pouille and Scanziani, 2001; Tsubokawa and Ross, 1996).

Mulitple factors govern the effect of dendritic inhibition on local integration. The kinetics of the inhibitory conductance play a crucial role in dermining the timecourse of integeration (Franks and Lieb, 1994; Liu, 2004; Whittington et al., 1995). Further, the effective interaction of dendritic excitatory and inhibitory inputs falls of sharply with distance (Liu, 2004). Thus, the timing and location of dendritic inhibition is fundamental in determining dendritic processing.

In the hippocampus, there are a population of GABAergic interneurons which selectively inhibit the dendrites of pyramidal cells (Freund and Buzsaki, 1996). Among those interneurons, bistratified cells have elaborate axonal arborizations that target both the basal and apical dendrites of pyramidal cells while avoiding the somatic compartment (Buhl et al., 1996). The extent of the axonal arborization of bistratified cells match well with the innervation pattern of the Schaffer collaterals, one of the two main afferent pathways into area CA1. However, the specific role that bistratified cells play in

determining the spatial and temporal integration of excitatory inputs in pyramidal cells is unknown.

We find that there are two populations of bistratified cells which can be distinguished by their intrinsic properties as fast-spiking (FS) and regular-spiking (RS). These two bistratified cells generate fast and slow dendritic inhibition, respectively. This difference is exaggerated by trains of action potentials during which IPSCs from RS cells summate supralinearly, likely due to the pooling of GABA. Further, trains of action potentials in excitatory afferents depress more onto RS cells than onto FS bistratified cells. Thus, FS cells are reliable and precise sources of inhibition to the dendrites, while RS cells provide disproportionately increasing dendritic inhibition in response to shifts in input pathways.

Results

We made whole-cell current clamp recordings from hippocampal bistratified cells (ascertained through *post hoc* morphological analysis; **Fig 3-1a**). Through injection of square current pulses, we monitored their spiking pattern and found that the population of bistratified cells clustered into two non-overlapping groups (**Fig. 3-1b-c**). One population showed little spike-frequency adaptation (adaptation coefficient- 0.78 ± 0.02; $n = 15$), while the other showed strong adaptation (adaptation coefficient- 0.35 ± 0.02; $n = 19$). To match the current hippocampal nomenclature, we called these two populations fast-spiking (FS) and regular-spiking (RS), respectively (Freund and Buzsaki, 1996). The two types of basket cells also clearly differed in their input resistance (RS: 216.2 ± 14.0 MOhms; FS: 139.7 ± 11.7 MOhms; $P < 0.0005$; $n = 18$ and
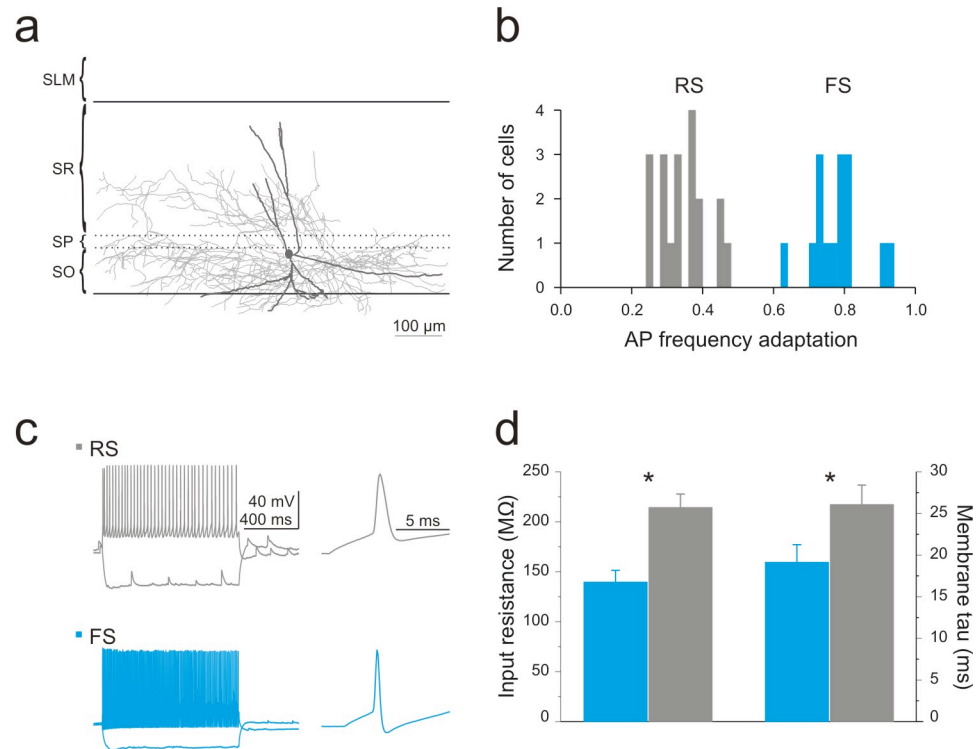
Figure 3-1: Identification of regular-spiking and fast-spiking bistratified cells

(a) Neurolucida reconstruction of a biocytin-filled bistratified cell. Dendrites: dark gray; axon: light gray. SO- stratum oriens; SP- stratum pyrimidale; SR- stratum radiatum; SLM- stratum lacunosum moleculare. Note the arborization of the axon in SO and SR, but not in SP.

(b) Histogram of the action potential (AP) frequency adaptation for the population of recorded bistratified cells ($n = 34$). The population could be divided into two groups: regular-spiking (RS; gray) and fast-spiking (FS; blue).

(c) Left, current clamp recordings from an RS (top, gray) and an FS (bottom, blue) bistratified cell in response to a one second current injection (-200 pA and +400 pA). Right, same step depolarizations on an expanded time scale. The FS cell is the same one as shown in **(a)**.

(d) Summary graph of input resistances and membrane time constants for RS (gray; $n = 18$ and 14) and FS (blue; $n = 15$ and 10) bistratified cells. Asterisk represents statistical significance.

15; **Fig. 3-1d**) and membrane time constant (RS: 26.5 ± 2.5 ms; FS: 19.1 ± 2.1 ms; $P <$

0.05; $n = 14$ and 10; **Fig. 3-1d**).

Two modes of dendritic inhibition

In order to determine the synaptic impact of the two types of bistratified cells, we

made paired recordings with pyramidal cells. The rate of connectivity (RS: 55.2 %

(16/29); FS: 46.7 % (14/30)) and the amplitude of the estimated peak synaptic

conductance (RS: 0.40 ± 0.07 nS; FS: 0.49 ± 0.10 nS; $P > 0.4$; $n = 15$ and 13; **Fig. 3-2a-**

b) was similar for both RS and FS bistratified cells. However, both the 10-90 rise time

(RS: 3.26 ± 0.35 ms; FS: 1.41 ± 0.21 ms; $P < 0.0005$; $n = 14$ and 11; **Fig. 3-2a-b**) and the

decay time constant (RS: 24.1 ± 4.2 ms; FS: 7.9 ± 0.7 ms; $P < 0.0005$; $n = 9$ and 12; **Fig.**

3-2a-b) of the unitary inhibitory post-synaptic currents (uIPSCs) from RS bistratified

cells were strikingly slower than from FS bistratified cells. In accordance with the slower

kinetics, IPSCs from RS bistratified cells carried twice as much charge as FS bistratified

cells (RS: 10.30 ± 1.85 fC/mV; FS: 4.55 ± 0.92 fC/mV; $P < 0.05$; $n = 14$ and 12; **3-Fig.**

2c) despite having the same peak conductance. The difference in rise time could not be

explained as an artifact of series resistance since the average series resistance of the

postsynaptic pyramidal cell was the same for the two populations of bistratified cells (RS:

10.06 ± 1.08 MOhms; FS: 8.34 ± 0.44 MOhms; $P > 0.1$; $n = 15$ and 13). Nor could it be

explained by a difference in the electrotonic distance of the synapses made by RS and FS

bistratified cells. Reconstruction of the population of recorded RS and FS bistratified

cells revealed that the the majority of their axonal arborizations were overlapping (**3-Fig.**
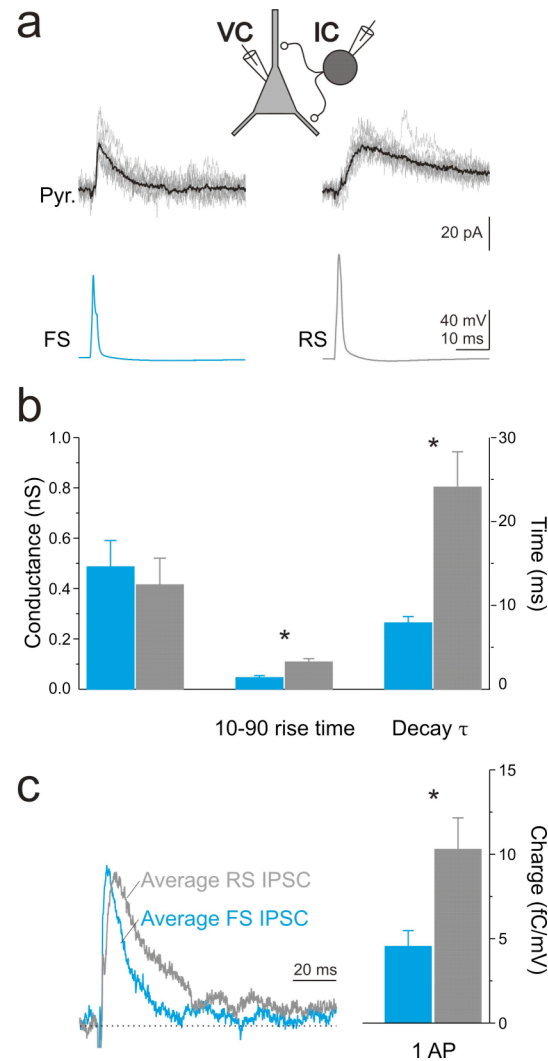
Figure 3-2: Two modes of synaptic inhibition from RS and FS bistratified cells

(a) Top, schematic of paired recording between bistratified and pyramidal cells. VC-voltage clamp; IC- current clamp. Bottom, an AP in an FS (left, blue trace) and an RS (right, gray trace) bistratified cell evokes a unitary inhibitory postsynaptic current (uIPSC) in their paired pyramidals cell (Vh = -50 mV; individual sweeps: gray traces; average: black trace).

(b) Summary graph of the conductances, 10-90 rise times, and decay time constants for uIPSCs from RS (gray; *n* = 15, 14 and 9) and FS (blue; *n* = 13, 11 and 12) bistratified cells.

(c) Left, average of all average uIPSCs, normalized to the peak, from RS (gray; *n* = 14) and FS (blue; *n* = 13) bistratified cells. Right, summary graph of the total charge transfer (normalized for driving force) during RS (*n* = 14) and FS (*n* = 12) uIPSCs

3). Thus, the slow rise time is likely due to either the intrinsic kinetics of the receptors or the spatial profile of the GABA transient.

The difference in charge transfer became even more pronounced when trains of APs were evoked in the presynaptic bistratified cell (**Fig. 3-4a-b**). We find that in response to trains APs (10 at 100 Hz), IPSCs from RS bistratified cells carried seven times as much charge as those from FS bistratified cells (RS: 186.8 ± 43.2 fC/mV; FS: 29.8 ± 8.0 fC/mV; $P < 0.005$; $n = 11$ and 9; **Fig. 3-4b-c**). While, in the absence of any pre- or postsynaptic use-dependent adaptation, a train of ten uIPSCs may be expected to transfer ten times the charge of a single uIPSC, ten APs in a FS bistratified cell evoked only half the expected value, namely five times the charge transfer of a single AP. In contrast, the charge transfer of a train of uIPSCs from a RS bistratified cell generated almost twice the expected charge transfer, namely 18 times that of a single uIPSC.

A possible explanation for this deviation from the expected charge transfer could be a difference in the short-term plasticity of uIPSCs from the two types of bistratified cells. Namely, depression and facilitation of IPSCs from FS and RS bistratified cells, respectively, could achieve this result. Although, we found that the paired pulse ratio (PPR) is significantly higher for RS than for FS basket cells ($IPSC_2/IPSC_1$- RS: 0.86 ± 0.09; FS: 0.57 ± 0.06; $P < 0.05$; $n = 9$ and 8; **Fig. 3-4c**), both showed depression. The paired-pulse depression of FS bistratified cells fully could account for the 50% reduction in expected charge if we assume that the PPR immediately decreases to its steady-state amplitude after the first AP (actual charge: 29.8 ± 8.0 fC/mV; predicted charge: 27.0 ± 8.6 fC/mV; paired t-test: $P > 0.2$; $n = 7$). However, since the PPR in RS bistratified cells
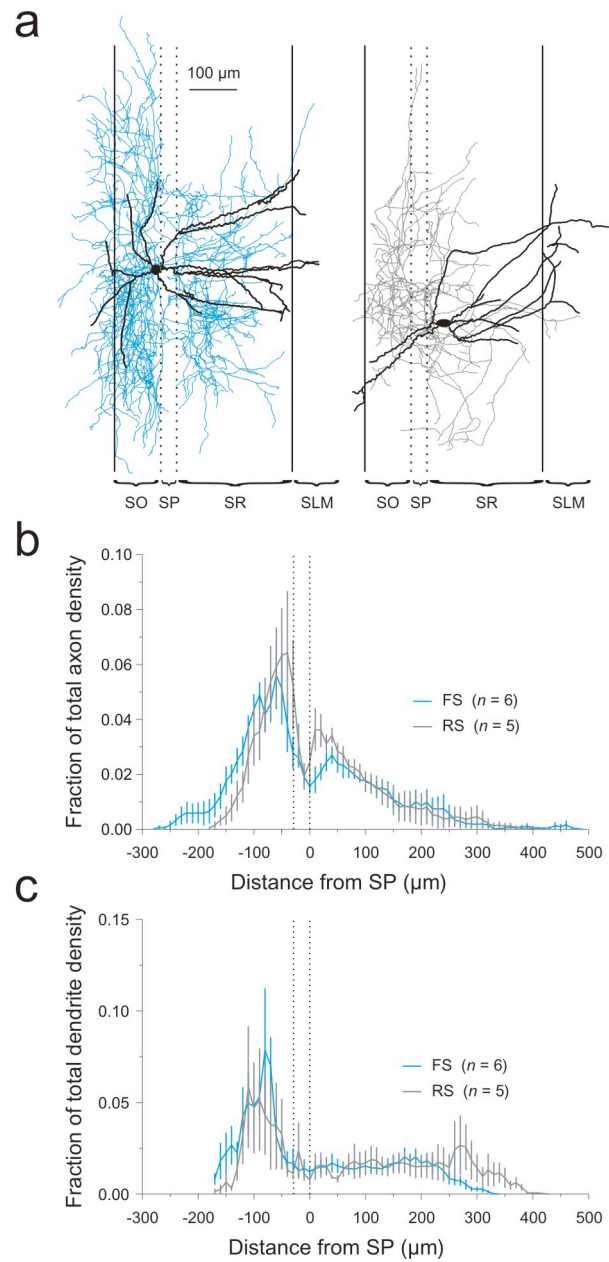
Figure 3-3: Bistratified cells have overlapping axonal and dendritic arborizations

(a) Neurolucida reconstruction of biocytin-filled FS (left: dendrites- black; axon- blue)
and RS (right: dendrites- black; axon- gray) bistratified cells.
(b) Summary graph of the density of the axonal aborizations of FS (blue; $n = 6$) and RS
(gray; $n = 5$) bistratfied cells. The dotted vertical lines represent the pyramidal cell layer.
(c) Same as **(b)** for the dendritic aborizations of FS (blue; $n = 6$) and RS (gray; $n = 5$)
bistratfied cells.
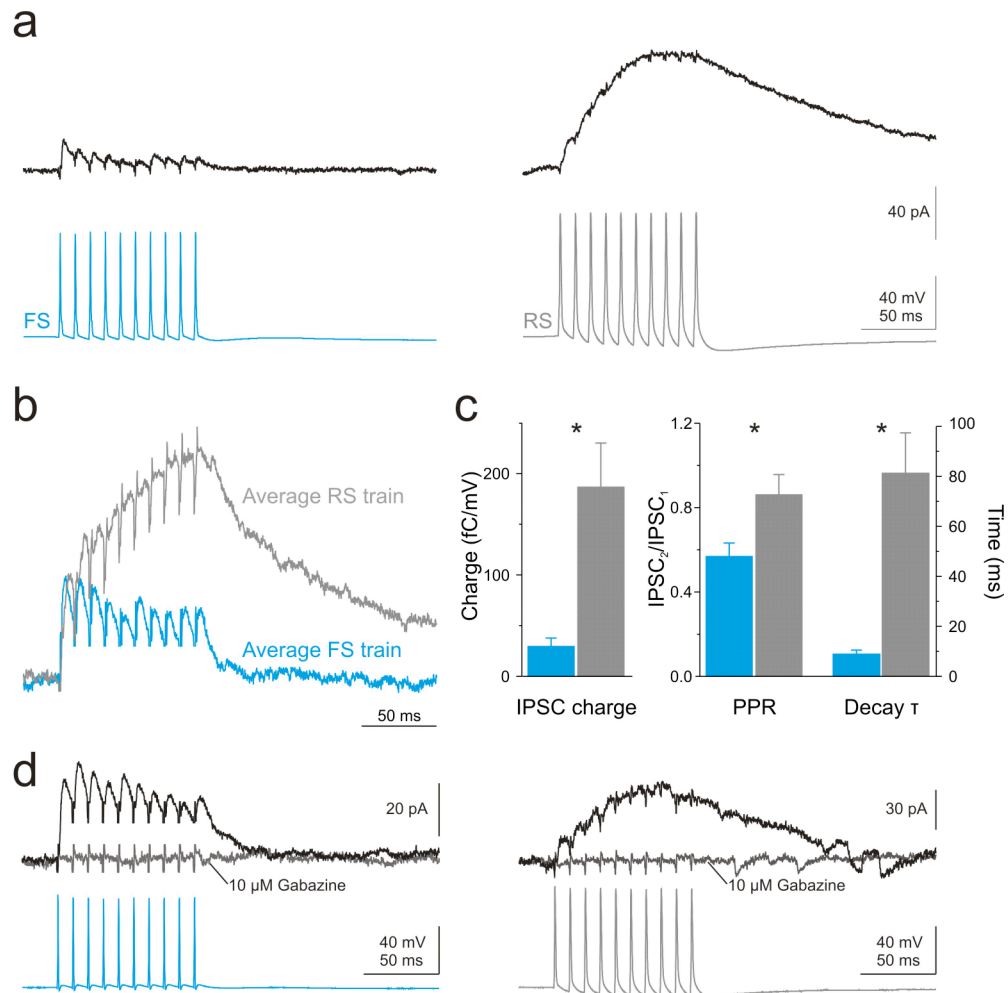
Figure 3-4: Trains of uIPSCs from bistratified cells

(a) Trains of ten APs (100 Hz) in an FS (bottom left, blue trace) and an RS (bottom right, gray trace) bistratified cell evoke a train of uIPSCs in the postsynaptic pyramidal cell (top, black trace). Pairs shown are the same as in **Fig. 3-2a**.
(b) Average of all average trains of uIPSCs, normalized to the peak, from all RS (gray; $n = 11$) and FS (blue; $n = 10$) bistratified cells.
(c) Summary graph of the total charge transfer (normalized for driving force), paired-pulse ratio (PPR), and decay time constants for trains of uIPSCs from RS (gray; $n = 11$, 9 and 9) and FS (blue; $n = 9$, 8 and 8) bistratified cells.
(d) Trains of uIPSCs in a pyramidal cell (top, black traces) in response to ten APs from an FS (bottom left, blue trace) and an RS (bottom right, gray trace) are abolished by the GABAA receptor antagonist, gabazine (10 µM; dark gray traces).

 was not facilitating, it could not account for the observed charge transfer (actual charge: 186.8 ± 43.2 fC/nS; predicted charge: 102.1 ± 29.4 fC/nS; $P < 0.005$; $n = 9$). Thus, the train of uIPSCs from RS basket cells appear to be accumulating extra charge. Accordingly, single IPSCs from RS bistratified cells had faster decay time constants than trains of uIPSCs (one AP: 24.1 ± 4.2 ms; ten APs: 81.3 ± 16.1 ms; paired t-test: $P < 0.005$; $n = 9$; **Fig. 3-4c**). In contrast, the decay of the IPSC from FS bistratified cells was unchanged after a train (one AP: 7.9 ± 0.7 ms; ten APs: 9.0 ± 1.5 ms; paired t-test: $P > 0.4$; $n = 8$; **Fig. 3-4c**).

Metabotropic $GABA_B$ receptors have very slow kinetics and could explain the timecourse of the train of IPSCs. However, application of the $GABA_A$ selective antagonist (gabazine, 10 uM) completely abolished the train of uIPSCs from both RS and FS bistratified cells ($n = 2$ each; **Fig. 3-4d**). Thus, the slow uIPSC from RS bistratified cells is mediated solely by $GABA_A$ receptors.

There are two possible explanations for the change in the decay time constant over the course of the train. First, there may be a slow component of the uIPSC from the RS bistratified cell which is too small to be detected by an exponential fit when only a single AP is evoked, but that comes to dominate the current during a train of APs. Second, the slower component may be activity dependent such that it only arises during the course of the high frequency train, reflecting the buildup of GABA. In order to distinguish between these two hypotheses, we used the waveform of the single uIPSC to extrapolate the response to ten uIPSCs (see methods). If the slow component was present in the single uIPSC, this extrapolation should mimic the experimentally observed ten

82
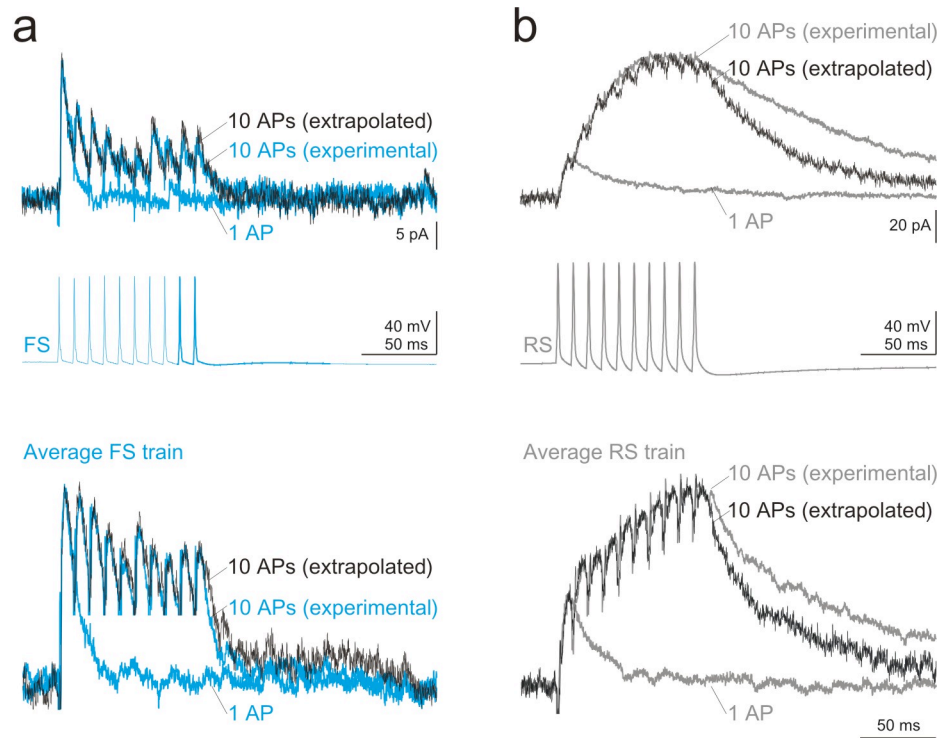
Figure 3-5: Development of a slow component during trains of uIPSCs from RS bistratified cells

(a) Top, same pair as shown in **Fig. 3-2a** and **3-4a** in which single or trains of ten APs in an FS (bottom, blue trace) bistratified cell evoke single (1 AP) or trains of ten (10 APs (experimental)) uIPSCs in its postsynaptic pyramidal cell (top, blue traces). The single uIPSC was scaled and summed to mimic the effect of a train of ten APs (10 APs (extrapolated), black traces; (see methods)). Note the similarity in the decay of the experimental versus the extrapolated train of ten uIPSCs. Bottom, same protocol as above, using the average from all FS uIPSCs (from **Fig. 3-2c** and 3-**4b**).
(b) Same protocol as in **(a)** for the RS bistratified cells. Note the difference in the decay of the experimental versus the extrapolated train of ten uIPSCs.

uIPSCs. However, while the summation of the single uIPSC from an FS bistratified cell successfully reproduced the experimentally observed uIPSC train (**Fig. 3-5a**), the summation of individual uIPSCs from an RS bistratified cell produced a waveform with a much faster decay than the observed uIPSC train (**Fig. 3-5b**). This suggests that the slow component was not present in the single uIPSC, but rather that it was generated in response to the high frequency activity. The presence of a late slow component in RS bistratified cell transmission is consistent with the accumulation of GABA.

Feed-forward and feedback excitation of bistratified cells

Taken together, our data suggests that FS and RS bistratified cells have a very different impact on the dendrites of pyramidal cells. Further, this difference is exaggerated when RS bistratified cells fire trains of APs. Thus, in order to fully appreciate the role of these different inhibitory circuits, we investigated how bistratified cells are recruited.

We stimulated two of the major excitatory pathways in area CA1, the Schaffer collaterals and the CA1 pyramidal cell axons, by placing stimulation electrodes in the stratum radiatum and the alveus, respectively. Both pathways converged onto individual RS and FS bistratified cells (**Fig. 3-6a**), suggesting that each bistratified cell can potentially participate in both feed-forward and feedback inhibition.

The amplitude of excitatory postsynaptic currents (EPSCs) evoked with an extracellular stimulation electrode may vary strongly between experiments depending on stimulation intensity, exact position of the stimulation electrode, electrical properties of the stimulation electrode and quality of the stimulated tissue, all parameters that will
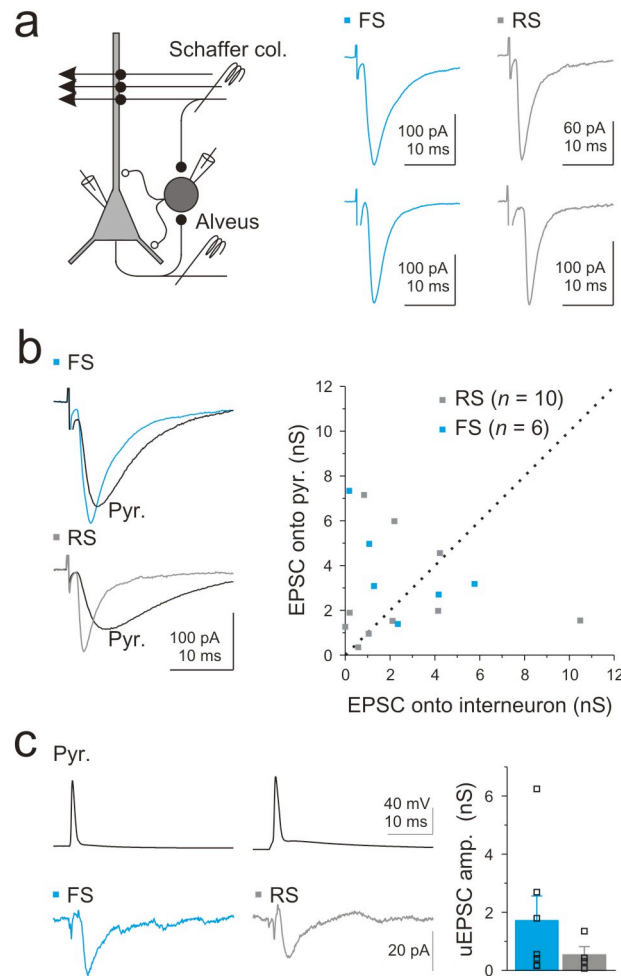
Figure 3-6: Feed-forward and feedback excitation of bistratified cells

(a) Left, schematic of the recording configuration. Monosynaptic EPSCs recorded in an FS (middle) and RS (right) bistratified cell by stimulating the Schaffer collaterals (top) and the alveus (bottom). EPSCs in this panel and in **(b)** recorded in the presence of gabazine (2.5 μM) or at the IPSC reversal potential (−85 mV).

(b) Left, EPSCs recorded simultaneously in bistratified and pyramidal cell pairs in response to stimulation of the Schaffer collaterals. Same cells as in **(a)**. Blue traces: FS; gray traces: RS; black traces: pyramidal cells. Right, scatter plot of the amplitude of EPSCs recorded in RS (gray; $n = 10$) and FS (blue; $n = 6$) versus their paired pyramidal cells; unity line is dotted.

(c) Left, unitary EPSCs (uEPSCs) in FS (blue trace) and RS (gray trace) bistratified cells (Vh = -60 mV) in response to APs in paired pyramidal cells. Right, summary graph of the average amplitude and distribution of uEPSCs onto FS ($n = 7$) and RS ($n = 4$) bistratified cells. RS cell shown is the same cell as in **Fig. 3-1c**.

affect the number of stimulated fibers. These sources of variability preclude a meaningful comparison of EPSC amplitudes recorded during different experiments. In order to make this comparison, we used a reliable readout of the stimulation conditions during each experiment: the simultaneously recorded, postsynaptic pyramidal cell. By normalizing the amplitude of the evoked EPSC recorded in a bistratified cell with the EPSC recorded simultaneously in the pyramidal cell voltage clamped at the same potential, we can control for the sources of variability mentioned above and compare the relative amount of excitation received by RS and FS bistratified cells across experiments.

Stimulation of the Schaffer collaterals (in the presence of the $GABA_A$ receptor antagonist gabazine or at the IPSC reversal potential to isolate glutamatergic transmission) evoked EPSCs of the same amplitude onto RS bistratified cells and simultaneously recorded pyramidal cells ($EPSC_{RS}/EPSC_{Pyr}$: 1.45 ± 0.63; paired t-test: $P > 0.9$; $n = 10$ pairs; **Fig. 3-6b**). Similarly, Schaffer collateral stimulation elicited EPSCs that were of the same amplitude onto FS bistratified cells and their paired pyramidal cells ($EPSC_{FS}/EPSC_{Pyr}$: 0.95 ± 0.33 ; paired t-test: $P > 0.4$; $n = 6$ pairs; **Fig. 3-6b**). Comparison of the normalized EPSCs recorded in the RS and FS bistratified cells indicates that stimulation of Schaffer collaterals excites the two types of bistratified cells to the same extent ($P > 0.5$). Thus, since neither RS nor FS bistratified cells are strongly driven by the feed-forward pathway, they will need to summate many Schaffer collateral inputs in order to spike.

Alternatively, they could be preferentially recruited by feedback excitation. Since CA1 pyramidal cells form few, if any, recurrent synapses with other CA1 pyramidal cells (Deuchars and Thomson, 1996), no reference EPSC could be recorded in response to

alveus stimulation in the postsynaptic pyramidal cells. This prevented the comparison of the relative magnitude of excitation produced by extracellular stimulation of the axons of CA1 pyramidal cells. However, in a subset of cases, the simultaneously recorded pyramidal cell synaptically excited the bistratified cell. While the connectivity from pyramidal cells onto FS bistratified cells (26.9% (7/26)) was slightly higher than onto RS bistratified cells (15.4% (4/26)), the average amplitude of the unitary EPSC (uEPSC) was not significantly different (RS: 0.54 ± 0.28 nS; FS: 1.72 ± 0.84 nS; $P > 0.3$; $n = 4$ and 7; **Fig. 3-6c**). Further, excitation from individual feedback connections is not consistently strong enough to drive bistratified cells to spike either type of bistratified cell.

Target-specific excitation of bistratified cells

Since the inhibitory impact of RS bistratified cells increases disproportionately with trains of APs, we were curious to determine the conditions under which they can be recruited to fire multiple APs. Thus, we challenged them with trains of afferent stimuli. The short-term plasticity of EPSCs evoked by repetitive stimulation of either the Schaffer collaterals or the alveus depressed significantly more in RS as compared to FS bistratified cells at all frequencies tested (**Fig. 3-7a-b** and **Table 3-2**). This trend, although not significant, was maintained in the synaptically connected paired recordings between pyramidal and bistratified cells (uEPSCs; **Fig. 3-7c** and **Table 3-2**).

The depressing EPSCs evoked onto RS bistratified cells suggests that their recruitment during ongoing hippocampal activity may be transient as compared to FS bistratified cells. We tested this by comparing the spike timing of the two bistratified

Figure 3-7: Target specific short-term plasticity of excitation of bistratified cells

(a) Top, EPSCs in response to Schaffer collateral stimulation at 20 Hz in FS (top, blue) and RS (bottom, gray) bistratified cells. Bottom, summary graph of normalized EPSC amplitudes plotted against stimulus number (blue: FS, $n = 3$; gray: RS, $n = 6$). All EPSCs in this figure were recorded in presence of gabazine (2.5 µM) or at the IPSC reversal potential (–85 mV). RS cell shown is the same cell as in **Fig. 3-6a-b**.

(b) Top, EPSCs in response to alveus stimulation at 20 Hz in FS (top, blue) and RS (bottom, gray) bistratified cells. Bottom, summary graph of normalized EPSC amplitudes plotted against stimulus number (blue: FS, $n = 4$; gray: RS, $n = 9$). RS cell shown is the same cell as in **Fig. 3-6a-b**.

(c) Left, uEPSCs in response to APs in pyramidal cells at 20 Hz in FS (top, blue) and RS (middle, gray) bistratified cells. Right, summary graph of normalized uEPSC amplitudes plotted against stimulus number (blue: FS, $n = 7$; gray: RS, $n = 3$). FS cell shown is the same cell as in **(b)**.

(d) Left, ten consecutive voltage traces in FS (blue, top) and RS (gray, bottom) bistratified cells at threshold for AP generation in response stimulation of the alveus at 20 Hz. APs have been truncated. Right, summary graph of normalized spiking probability plotted against stimulus number (blue: FS, $n = 6$; gray: RS, $n = 3$). RS cell shown is the same cell as in **Fig. 3-6c**.
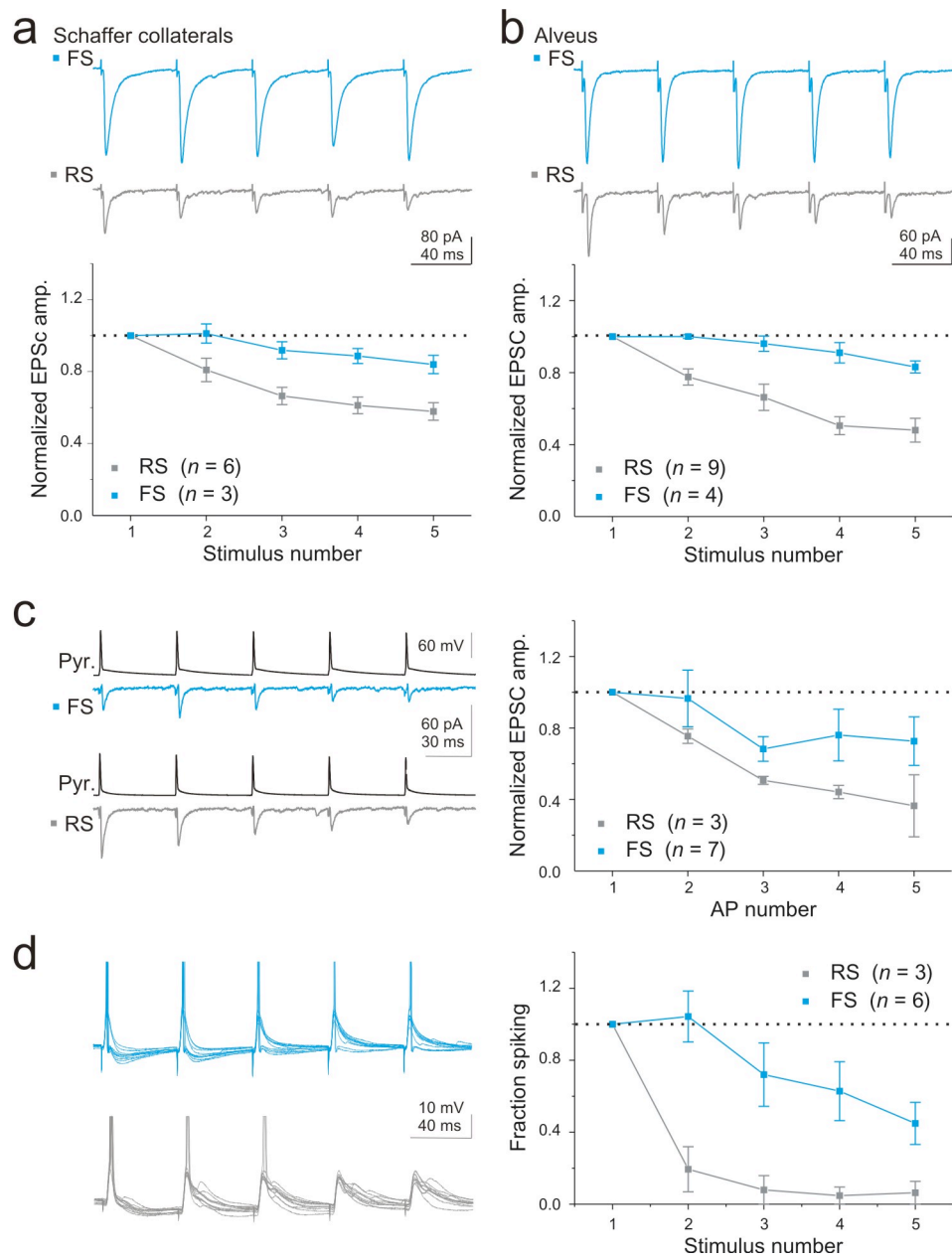
Table 3-2: Short-term plasticity of excitation onto RS and FS bistratified cells

Ratio of the fifth to the first EPSC evoked by stimulating the three main afferents at three different frequencies. The number of cells is given in parentheses. Within pathway comparisons between RS and FS bistratified cells that are significantly different ($P <$ 0.05) are in black.

Pathway	10 Hz (stim5/stim1)		20 Hz (stim5/stim1)		50 Hz (stim5/stim1)	
	RS	FS	RS	FS	RS	FS
Schaffer col.	0.60 ± 0.05 (7)	0.86 ± 0.04 (4)	0.58 ± 0.05 (6)	0.84 ± 0.05 (3)	0.49 ± 0.04 (4)	
Alveus	0.57 ± 0.06 (9)	0.84 ± 0.03 (4)	0.48 ± 0.07 (9)	0.83 ± 0.03 (4)	0.35 ± 0.05 (8)	0.79 ± 0.08 (3)
uEPSC			0.36 ± 0.17 (3)	0.73 ± 0.14 (6)		

cells during trains of stimuli. We recorded from bistratified cells in the whole-cell, current clamp configuration and repetitively stimulated the alveus (five stimuli at 20 Hz) at an intensity that was at threshold to trigger an AP after the first stimulus in the train. The probability of the alvear input to trigger an AP in RS bistratified cells decreased sharply with repetitive stimulation ($50.2 \pm 10.7\%$ after the first stimulus; $12.3 \pm 8.7\%$ after the second stimulus; $4.3 \pm 4.3\%$ after the fifth stimulus; $P < 0.05$; $n = 3$; **Fig. 3-7d**). In contrast, in FS bistratified cells the spiking probability remained more sustained during the train ($47.6 \pm 5.7\%$ after the first stimulus; $48.3 \pm 7.1\%$ after the second stimulus, $P > 0.9$; $22.2 \pm 7.9\%$ after the fifth stimulus, $P < 0.05$; $n = 6$; **Fig. 3-7d**). Thus, RS bistratified cells are much less sensitive than FS bistratified cells to the repetitive activation of a single afferent pathway. Further, this implies that the activation of independent pathways will be necessary to induce RS bistratified cells to fire multiple APs.

Feed-forward and feedback inhibition of bistratified cells

Whether a neuron treats independent inputs as individual events or combines them into a single event depends on the amount of inhibition that it receives (Pouille and Scanziani, 2001). Thus, in order to determine how RS and FS bistratified cells integrate multiple inputs, we compared the magnitude of disynaptic inhibition. For this, we stimulated excitatory afferents and used the disynaptic IPSC recorded in pyramidal cells as a reference in the same manner as we did when comparing the amplitude of EPSCs (**Fig. 3-8a-b**). When we stimulated the Schaffer collaterals or the alveus, we consistently evoked disynaptic inhibition onto both the bistratified cells and the paired pyramidal cell.
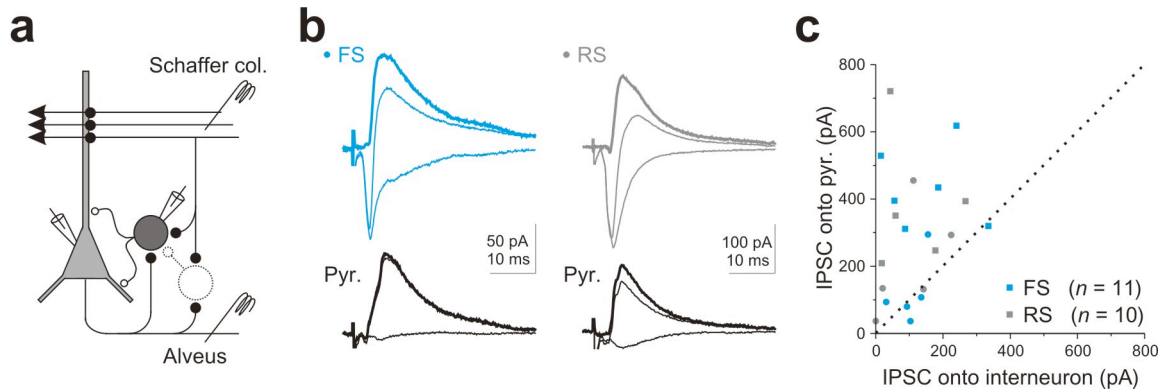
Figure 3-8: Feed-forward and feedback inhibition of bistratified cells

(a) Schematic of recording configuration used in **(b)**.
(b) Current traces from FS (left) and RS (right) bistratified (top) and pyramidal cell (bottom) pairs in response to Alveus stimulation in control, in gabazine, and their algebraic subtraction (thick line).
(c) Scatter plot of IPSCs onto FS (blue; $n = 11$) and RS (gray; $n = 10$) bistratified and pyramidal cells in response to stimulation of the Schaffer collaterals (squares) and alveus (circles). Dotted line represents unity.

While the amplitude of the IPSC onto the pyramidal cell was larger than onto either RS (IPSC$_{RS}$/IPSC$_{Pyr}$: 0.39 ± 0.12; paired t-test: $P < 0.05$; $n = 10$; **Fig. 3-8c**) or FS (IPSC$_{FS}$/IPSC$_{Pyr}$: 0.76 ± 0.24; paired t-test: $P < 0.05$; $n = 11$; **Fig. 3-8b**) bistratified cells, both bistratified cells received the same amount of inhibition ($P > 0.1$).

More importantly, the presence of disynaptic inhibition implies that independent inputs onto bistratified cells will be treated as individual events. Thus, a sequence of independent inputs onto RS and FS bistratified cells could induce them to fire multiple APs.

Discussion

Bistratified cells selectively target the dendrites of pyramidal cells and are thus fundamental in determining the local integration of excitatory inputs. In the hippocampus, there are two populations of bistratified cells which can be discriminated according to their intrinsic properties as regular-spiking (RS) and fast-spiking (FS). These two types of bistratified cells can have dramatically different effects on their targets due to the kinetics of their inhibitory output. While FS bistratified cells have relatively fast unitary inhibitory postsynaptic currents (uIPSCs), RS bistratified cells have extremely slow uIPSCs which accumulate charge during a train of action potentials (APs). However, while FS bistratified cells are recruited throughout a train of stimuli and are thus reliable sources of dendritic inhibition during ongoing hippocampal activity, RS bistratified cells are not effectively recruited by trains of afferent stimuli. Instead they are specifically sensitive to the sequential activation of independent inputs, in response to which they generate a powerful, long-lasting dendritic inhibition.

The presence of two populations of bistratified cells which can be discriminated according to their spiking patterns (as RS and FS), parallels the two populations of somatically targeting interneurons (basket cells; (Freund, 2003)). FS bistratified cells likely correspond to the previously described parvalbumin and somatostatin expressing bistratified cells (Somogyi and Klausberger, 2005). In contrast, the RS bistratified cells could correspond to a number of immunohistochemically defined populations of dendrite targeting neurons; further experiments are necessary to find their place in the literature. While it is possible that there are more than two types of bistratified cells in our sample, the consistent response properties of the population suggest that this is a sufficient division.

The most striking difference between RS and FS bistratified cells are the kinetics of their uIPSCs. Both the rise and decay of the uIPSC from RS bistratified cells are two to three times slower than from FS bistratified cells. The slow kinetics of uIPSCs evoked by RS bistratified cells are reminiscent of $GABA_{Aslow}$, an intrinsically slow conductance due to the prolonged activation of dendritic $GABA_A$ receptors ($GABA_ARs$; (Pearce, 1993)). Thus, while it has long been thought that there are two modes of dendritic inhibition, $GABA_{Aslow}$ and $GABA_{Afast}$, this is the first suggestion of a cellular basis for the phenomenon.

The different kinetics in the uIPSCs from bistratified cells result in a two-fold difference in the charge transfer. In addition, the slow kinetics of the RS uIPSC will be more efficient at charging the membrane, causing a much stronger hyperpolarization.

What mechanism could cause this difference in rise time? There are at least three possibilities. First, it could result from the filtering of a faster conductance. While we

have ruled out the possibility that RS bistratified cells synapse on the more distal dendrites than FS bistratified cells, RS bistratified cells could synapse on higher-order dendritic branches, thereby functionally increasing the electrotonic distance. Second, the GABA receptors underlying the conductance could have intrinsically slower kinetics. And finally, the GABA receptors at RS synapses may be further from the site of GABA release than those at FS synapses. In the extreme case, transmission from RS bistratified cells onto pyramidal cells may be mediated entirely by spillover. These three possibilities are not mutually exclusive; in fact, extrasynaptic transmission is often mediated by receptor subunits that have higher affinity and slower kinetics than synaptic transmission (Arnth-Jensen et al., 2002; Caraiscos et al., 2004; Wei et al., 2003).

In order to better understand the mechanisms behind the slow kinetics of the RS uIPSC, we gave trains of ten APs at 100 Hz to the interneurons. This hugely increased the in charge transfer of RS bistratified cells to seven times that of FS bistratified cells. This effect could be explained by two mechanisms. First, the uIPSCs from FS bistratified cells depressed during the train, such that the charge transfer during a train of ten APs was only five times the transfer of a single AP. Second, the decay time constant of the train of uIPSCs in the RS bistratified cells was three times larger than for a single uIPSC, such that the charge transfer was 18 times the transfer of a single AP. The change in decay time constant was due to the development of slow component that was generated during the train of uIPSCs. We do not think that the slow component is due to the development of asynchronous release, since we do not see an increase in spontaneous IPSCs after the train of APs. Instead, this late, slow component is suggestive of extrasynaptic pooling of GABA and the saturation of uptake mechanisms.

The simplest explanation for both the kinetics of the single uIPSC and the disproportionate increase in charge transfer during a train of APs is the activation of extrasynaptic receptors through spillover. Further experiments are necessary to determine the both the specific $GABA_AR$ subunits and the ultrastructure of bistratified cell synapses. Thus, while the inhibition from FS bistratified cells decreases in efficacy during a train of APs (due to paired-pulse depression), inhibition evoked by the repeated activation of RS bistratified cells becomes increasingly powerful (due to the accumulation of GABA). This led us to seek out the conditions under which RS bistratified cells fire trains of APs.

Stimulation of the Schaffer collaterals and alveus directly excited both RS and FS bistratified cells. Both types of bistratified cells received the same amount of excitation as their paired pyramidal cells during activation of the Schaffer collaterals. Thus, neither bistratified cell will act as a dominant source of feed-forward dendritic inhibition. However, this relationship may evolve during trains of afferent activity within a single pathway. Indeed, inputs onto RS bistratified cells depress more than those onto FS bistratfied cells at many frequencies, suggesting that the inhibition from FS bistratified cells will become dominant during a train.

Further, this implies that repetitive activation of a single input will not be an effective means of making RS bistratified cells fire trains of APs. Instead, they require the sequential activation of independent pathways. Indeed, the presence of feed-forward inhibition supports this function. Feed-forward inhibition enables the RS bistratified cells to discriminate between independent inputs, and thereby fire multiple APs, rather than integrating them as a single event.

The inhibition generated by FS bistratified cells is precisely time-locked to their own excitation. Thus, they are likely to be important in determining the integration time window for local excitatory inputs. Indeed, *in vivo*, FS bistratified cells spike reliably during the depolarizing phase of each theta oscillation (Klausberger et al., 2004). The inhibitory action of RS bistratified cells, on the other hand, generates a more modulatory effect on the dendrites. While the inhibitory conductance evoked by a single IPSC will significantly reduce the excitability of the dendrite, trains of APs could create a memory which lasts well into the next theta cycle.

CONCLUSIONS

In sensory systems, individual neurons are tuned to detect specific features in stimuli. For example, ON retinal ganglion cells respond best to points of light surrounded by dark annuli (Kuffler, 1953). In higher brain areas, these features become increasingly complex, as in an edge, a direction of motion, or a face (Bruce et al., 1981; Hubel and Weisel, 1959; Zeki, 1974). In the hippocampus, neurons increase their firing frequency when the animal is in a specific area, leading them to be called "place cells" (O'Keefe and Dostrovsky, 1971). However, GABAergic interneurons lack this sensitivity and fire with less discrimination to place than principal cells (Wilson and McNaughton, 1993). Thus, it has been thought that interneurons are not feature detectors, but are instead broadly tuned to provide a uniform inhibition to their targets.

Indeed, there is a class of interneuron with an anatomical and physiological profile of a broadly tuned inhibitor. Each fast spiking, parvalbumin positive basket cell powerfully inhibits the somatic compartment of thousands of pyramidal cells (Freund and Buzsaki, 1996). In addition, these basket cells spike reliably on each cycle of oscillations *in vivo* at a wide range of frequencies (Klausberger et al., 2003). This combination of highly divergent output with reliable output creates a uniform inhibition which can synchronize populations of pyramidal cells (Cobb et al., 1995).

Yet, this model for the role of inhibition is clearly incomplete given our current knowledge of inhibitory interneurons. The presence of an anatomically and physiologically diverse population of GABAergic interneurons suggests an equally diverse set of functions for inhibition in circuit processing (McBain and Fisahn, 2001).

Indeed, both *in vivo* and *in vitro* recordings suggest that different types of interneurons have unique response patterns. Different classes of interneurons spike during discrete phases of hippocampal oscillations (Klausberger et al., 2003) and at different times during trains of stimuli (Pouille and Scanziani, 2004). Regular spiking basket cells, like fast spiking, also strongly inhibit the somatic compartment of pyramidal cells; however, these two basket cell types spike under different conditions (Klausberger et al., 2005). Whereas fast spiking basket cells fire on the descending phase of a theta (4-8 Hz) oscillations, before the majority of pyramidal cells, regular spiking basket cells fire on the ascending phase. Moreover, while fast spiking basket cells strongly increase their firing rate during spindle oscillations (120-200 Hz), regular spiking basket cells show no rate modulation during these events.

Thus, interneurons may indeed be feature detectors of a different sort. Rather than responding to every excitatory input, different interneuron types detect specific motifs in the afferent activity. For instance, some interneurons spike specifically at the beginning of a train, thereby detecting an onset; others increase their spiking probability throughout a train, thereby extracting the rate of a stimulus (Pouille and Scanziani, 2004).

This sensitivity to specific patterns of inputs extends into the spatial dimension as well as the temporal. Multiple different afferent pathways converge onto principal cells in the hippocampus, but some interneurons are only responsive to a single pathway (Blasco-Ibanez and Freund, 1995; Buhl et al., 1996; Gulyas et al., 1999). Yet other types of interneurons are sensitive to spatio-temporal patterns and detect the coincident activity of different afferent pathways (Glickfeld and Scanziani, 2006).

Thus, a general role for inhibitory interneurons may be to detect certain features in the afferent activity and then relay this information to the principal cells. This input-output relationship is made more interesting by the specificity with which each cell type makes synapses along the somato-dendritic axis of its target. Different types of interneurons target the axon initial segment (axo-axonic cells), soma (basket cells), proximal dendrites (e.g. bistratified cells) and distal dendrites (e.g. OLM cells) of pyramidal cells (Freund and Buzsaki, 1996). Thus, there is a fundamental relationship between the patterns of ongoing activity and the location of synaptic inhibition. Whether there is further specificity built into the circuit, which allows excitatory axons to modulate their own integration via local inhibition, is not known.

The ability of interneurons to detect features in the ongoing activity is achieved through a unique set of mechanisms for each cell type. Moreover, often there is no one mechanism which is sufficient to explain the selective action of an interneuron. Instead it is the result of the precise tuning of circuit, synaptic and intrinsic properties which generate each response pattern.

Again, the dichotomy of the fast and regular spiking basket cells is a good example of the result of such tuning. Fast spiking basket cells receive highly convergent input from a large number of excitatory neurons which each have large conductances such that activation of only a few are required to reach threshold (Gulyas et al., 1999; Glickfeld and Scanziani, 2006). This combination of strong inputs and high connectivity make these interneurons extremely sensitive to the presence of sparse activity. These excitatory inputs have an intermediate probability of release which eliminates paired pulse plasticity across a wide range of frequencies; thus the response is reliable

independent of previous activity (Glickfeld and Scanziani, 2006). Fast spiking basket cells also have a fast membrane time constant, a fast after-hyperpolarizing potential, and an intense reciprocal connectivity which creates powerful disynaptic inhibition (Glickfeld and Scanziani, 2006). These properties all contribute to a very brief integration time window, which allows individual inputs occurring at high frequency to be treated independently. Finally, the output of fast spiking basket cells has a high probability of release, fast kinetics, and low jitter which maintain a close relationship between the action potential and the inhibitory potential (Hefft and Jonas, 2005; Glickfeld and Scanziani, 2006). Thus, the entire hippocampal circuit is tuned to shape the fast spiking basket cell into a reliable "featureless" detector.

In contrast, despite inhibiting the same population of pyramidal cells, regular spiking basket cells are embedded in a completely different circuit than fast spiking basket cells. They receive many fewer excitatory inputs which each have a relatively weak conductance (Matyas et al., 2004; Glickfeld and Scanziani, 2006). Thus, regular spiking basket cells require a more global circuit activation to drive them to spike. Their activation is facilitated by a long membrane time constant and weak disynaptic inhibition (due to a lack of connectivity with other basket cells) which enable them to summate these weak inputs over a broad window. However, despite being weak, these inputs have a high probability of release, such that repetitive activation of individual inputs undergo strong paired pulse depression (Glickfeld and Scanziani, 2006). Thus, regular spiking basket cells are tuned to detect the transitions in the activation of independent pathways. In addtion, the regular spiking basket cells have a less time-locked output than the fast spiking basket cells; they have a lower probability of release and an stronger propensity

for asynchronous release, both of which increase the saliency of repetitive activation (Hefft and Jonas, 2005).

Thus, there are mechansims at all levels of investigation which have been precisely tuned to make the interneurons sensitive to specific patterns of inputs. Given the wide diversity of interneurons in the cortex, each will have its own unique complement of properties which endow it with an ability to extract a certain feature from the afferent activity. Moreover, the inputs, intrinsic properties, and outputs of each interneuron type are all coordinated to achieve a certain function, creating an internally consistent logic to the system. Thus, by defining these basic properties for each class of interneuron, one can deduce features that it detects and ultimately the role of the interneuron in the circuit.

REFERENCES CITED

Acsady, L., Gorcs, T. J., and Freund, T. F. (1996). Different populations of vasoactive intestinal polypeptide-immunoreactive interneurons are specialized to control pyramidal cells or interneurons in the hippocampus. Neuroscience *73*, 317-334.

Agmon, A., and Connors, B. W. (1991). Thalamocortical responses of mouse somatosensory (barrel) cortex in vitro. Neuroscience *41*, 365-379.

Alger, B. E., and Nicoll, R. A. (1982a). Feed-forward dendritic inhibition in rat hippocampal pyramidal cells studied in vitro. J Physiol *328*, 105-123.

Alger, B. E., and Nicoll, R. A. (1982b). Pharmacological evidence for two kinds of GABA receptor on rat hippocampal pyramidal cells studied in vitro. J Physiol *328*, 125-141.

Ali, A. B., Deuchars, J., Pawelzik, H., and Thomson, A. M. (1998). CA1 pyramidal to basket and bistratified cell EPSPs: dual intracellular recordings in rat hippocampal slices. J Physiol *507 (Pt 1)*, 201-217.

Ali, A. B., and Thomson, A. M. (1998). Facilitating pyramid to horizontal oriens-alveus interneurone inputs: dual intracellular recordings in slices of rat hippocampus. J Physiol *507 (Pt 1)*, 185-199.

Ameri, A. (1999). The effects of cannabinoids on the brain. Prog Neurobiol *58*, 315-348.

Andersen, P., Bland, B. H., and Dudar, J. D. (1973). Organization of the hippocampal output. Exp Brain Res *17*, 152-168.

Andersen, P., and Eccles, J. (1962). Inhibitory phasing of neuronal discharge. Nature *196*, 645-647.

Andersen, P., Eccles, J. C., and Loyning, Y. (1963). Recurrent inhibition in the hippocampus with identification of the inhibitory cell and its synapses. Nature *198*, 540-542.

Andersen, P., Eccles, J. C., and Loyning, Y. (1964). Pathway Of Postsynaptic Inhibition In The Hippocampus. J Neurophysiol *27*, 608-619.

Andersen, P., Gillow, M., and Rudjord, T. (1966). Rhythmic activity in a simulated neuronal network. J Physiol *185*, 418-428.

Arnth-Jensen, N., Jabaudon, D., and Scanziani, M. (2002). Cooperation between independent hippocampal synapses is controlled by glutamate uptake. Nat Neurosci *5*, 325-331.

Banke, T. G., and McBain, C. J. (2006). GABAergic input onto CA3 hippocampal interneurons remains shunting throughout development. J Neurosci *26*, 11720-11725.

Bartos, M., Vida, I., Frotscher, M., Meyer, A., Monyer, H., Geiger, J. R., and Jonas, P. (2002). Fast synaptic inhibition promotes synchronized gamma oscillations in hippocampal interneuron networks. Proc Natl Acad Sci U S A *99*, 13222-13227.

Ben-Ari, Y. (2002). Excitatory actions of gaba during development: the nature of the nurture. Nat Rev Neurosci *3*, 728-739.

Blasco-Ibanez, J. M., and Freund, T. F. (1995). Synaptic input of horizontal interneurons in stratum oriens of the hippocampal CA1 subfield: structural basis of feed-back activation. Eur J Neurosci *7*, 2170-2180.

Bliss, T. V., and Lomo, T. (1973). Long-lasting potentiation of synaptic transmission in the dentate area of the anaesthetized rabbit following stimulation of the perforant path. J Physiol *232*, 331-356.

Blitz, D. M., and Regehr, W. G. (2005). Timing and specificity of feed-forward inhibition within the LGN. Neuron *45*, 917-928.

Bodor, A. L., Katona, I., Nyiri, G., Mackie, K., Ledent, C., Hajos, N., and Freund, T. F. (2005). Endocannabinoid signaling in rat somatosensory cortex: laminar differences and involvement of specific interneuron types. J Neurosci *25*, 6845-6856.

Bramham, C. R., and Sarvey, J. M. (1996). Endogenous activation of mu and delta-1 opioid receptors is required for long-term potentiation induction in the lateral perforant path: dependence on GABAergic inhibition. J Neurosci *16*, 8123-8131.

Brock, L. G., Coombs, J. S., and Eccles, J. C. (1952). The recording of potentials from motoneurones with an intracellular electrode. J Physiol *117*, 431-460.

Bruce, C., Desimone, R., Gross, C.G. (1981). Visual properties of neurons in a polysensory area in superior temporal sulcus of the macaque. J Neurophysiol *46*, 369-84.

Buhl, E. H., Szilagyi, T., Halasy, K., and Somogyi, P. (1996). Physiological properties of anatomically identified basket and bistratified cells in the CA1 area of the rat hippocampus in vitro. Hippocampus *6*, 294-305.

Buzsaki, G. (1984). Feed-forward inhibition in the hippocampal formation. Prog Neurobiol *22*, 131-153.

Caraiscos, V. B., Elliott, E. M., You-Ten, K. E., Cheng, V. Y., Belelli, D., Newell, J. G., Jackson, M. F., Lambert, J. J., Rosahl, T. W., Wafford, K. A.*, et al.* (2004). Tonic inhibition in mouse hippocampal CA1 pyramidal neurons is mediated by alpha5 subunit-containing gamma-aminobutyric acid type A receptors. Proc Natl Acad Sci U S A *101*, 3662-3667.

Cobb, S. R., Buhl, E. H., Halasy, K., Paulsen, O., and Somogyi, P. (1995). Synchronization of neuronal activity in hippocampus by individual GABAergic interneurons. Nature *378*, 75-78.

Cohen, G. A., Doze, V. A., and Madison, D. V. (1992). Opioid inhibition of GABA release from presynaptic terminals of rat hippocampal interneurons. Neuron *9*, 325-335.

Colonnier, M. (1968). Synaptic patterns on different cell types in the different laminae of the cat visual cortex. An electron microscope study. Brain Res *9*, 268-287.

Connors, B. W., Malenka, R. C., and Silva, L. R. (1988). Two inhibitory postsynaptic potentials, and GABAA and GABAB receptor-mediated responses in neocortex of rat and cat. J Physiol *406*, 443-468.

Coombs, J. S., Eccles, J. C., and Fatt, P. (1955). The specific ionic conductances and the ionic movements across the motoneuronal membrane that produce the inhibitory post-synaptic potential. J Physiol *130*, 326-374.

Csicsvari, J., Jamieson, B., Wise, K. D., and Buzsaki, G. (2003). Mechanisms of gamma oscillations in the hippocampus of the behaving rat. Neuron *37*, 311-322.

Deuchars, J., and Thomson, A. M. (1996). CA1 pyramid-pyramid connections in rat hippocampus in vitro: dual intracellular recordings with biocytin filling. Neuroscience *74*, 1009-1018.

Dichter, M., and Spencer, W. A. (1969). Penicillin-induced interictal discharges from the cat hippocampus. II. Mechanisms underlying origin and restriction. J Neurophysiol *32*, 663-687.

Dingledine, R., and Langmoen, I. A. (1980). Conductance changes and inhibitory actions of hippocampal recurrent IPSPs. Brain Res *185*, 277-287.

Douglas, R. J., and Martin, K. A. (1991). A functional microcircuit for cat visual cortex. J Physiol *440*, 735-769.

Drake, C. T., Chang, P. C., Harris, J. A., and Milner, T. A. (2002). Neurons with mu opioid receptors interact indirectly with enkephalin-containing neurons in the rat dentate gyrus. Exp Neurol *176*, 254-261.

Drake, C. T., and Milner, T. A. (2002). Mu opioid receptors are in discrete hippocampal interneuron subpopulations. Hippocampus *12*, 119-136.

Dubin, M. W., and Cleland, B. G. (1977). Organization of visual inputs to interneurons of lateral geniculate nucleus of the cat. J Neurophysiol *40*, 410-427.

Eccles, J. C. (1969). The Inhibitory Pathways of the Central Nervous System, Vol IX (Springfield, Charles C. Thomas).

Eccles, J. C., Fatt, P., and Landgren, S. (1956). Central pathway for direct inhibitory action of impulses in largest afferent nerve fibres to muscle. J Neurophysiol *19*, 75-98.

Faber, D. S., and Korn, H. (1991). Applicability of the coefficient of variation method for analyzing synaptic plasticity. Biophys J *60*, 1288-1294.

Fatt, P., and Katz, B. (1953). The effect of inhibitory nerve impulses on a crustacean muscle fibre. J Physiol *121*, 374-389.

Fortin, D. A., Trettel, J., and Levine, E. S. (2004). Brief trains of action potentials enhance pyramidal neuron excitability via endocannabinoid-mediated suppression of inhibition. J Neurophysiol *92*, 2105-2112.

Franks, N. P., and Lieb, W. R. (1994). Molecular and cellular mechanisms of general anaesthesia. Nature *367*, 607-614.

Freund, T. F. (2003). Interneuron Diversity series: Rhythm and mood in perisomatic inhibition. Trends Neurosci *26*, 489-495.

Freund, T. F., and Buzsaki, G. (1996). Interneurons of the hippocampus. Hippocampus *6*, 347-470.

Fricker, D., and Miles, R. (2000). EPSP amplification and the precision of spike timing in hippocampal neurons. Neuron *28*, 559-569.

Fried, S. I., Munch, T. A., and Werblin, F. S. (2002). Mechanisms and circuitry underlying directional selectivity in the retina. Nature *420*, 411-414.

Gabernet, L., Jadhav, S. P., Feldman, D. E., Carandini, M., and Scanziani, M. (2005). Somatosensory integration controlled by dynamic thalamocortical feed-forward inhibition. Neuron *48*, 315-327.

Galarreta, M., Erdelyi, F., Szabo, G., and Hestrin, S. (2004). Electrical Coupling among Irregular-Spiking GABAergic Interneurons Expressing Cannabinoid Receptors. J Neurosci *24*, 9770-9778.

Gall, C., Brecha, N., Chang, K. J., and Karten, H. J. (1984). Ontogeny of enkephalin-like immunoreactivity in the rat hippocampus. Neuroscience *11*, 359-379.

Gall, C., Brecha, N., Karten, H. J., and Chang, K. J. (1981). Localization of enkephalin-like immunoreactivity to identified axonal and neuronal populations of the rat hippocampus. J Comp Neurol *198*, 335-350.

Glickfeld, L. L., and Scanziani, M. (2006). Distinct timing in the activity of cannabinoid-sensitive and cannabinoid-insensitive basket cells. Nat Neurosci *9*, 807-815.

Golding, N. L., Staff, N. P., and Spruston, N. (2002). Dendritic spikes as a mechanism for cooperative long-term potentiation. Nature *418*, 326-331.

Grastyan, E., Lissak, K., Madarasz, I., and Donhoffer, H. (1959). Hippocampal electrical activity during the development of conditioned reflexes. Electroencephalogr Clin Neurophysiol Suppl *11*, 409-430.

Grothe, B., and Sanes, D. H. (1994). Synaptic inhibition influences the temporal coding properties of medial superior olivary neurons: an in vitro study. J Neurosci *14*, 1701-1709.

Gulledge, A. T., and Stuart, G. J. (2003). Excitatory actions of GABA in the cortex. Neuron *37*, 299-309.

Gulyas, A. I., Megias, M., Emri, Z., and Freund, T. F. (1999). Total number and ratio of excitatory and inhibitory synapses converging onto single interneurons of different types in the CA1 area of the rat hippocampus. J Neurosci *19*, 10082-10097.

Hajos, N., Katona, I., Naiem, S. S., MacKie, K., Ledent, C., Mody, I., and Freund, T. F. (2000). Cannabinoids inhibit hippocampal GABAergic transmission and network oscillations. Eur J Neurosci *12*, 3239-3249.

Hallett, P. E. (1971). Disturbances of rod threshold forced by briefly exposed luminous lines, edges, disks and annuli. J Physiol *215*, 449-476.

Hara, M., Inoue, M., Yasukura, T., Ohnishi, S., Mikami, Y., and Inagaki, C. (1992). Uneven distribution of intracellular Cl- in rat hippocampal neurons. Neurosci Lett *143*, 135-138.

Hefft, S., and Jonas, P. (2005). Asynchronous GABA release generates long-lasting inhibition at a hippocampal interneuron-principal neuron synapse. Nat Neurosci *8*, 1319-1328.

Hubel, D.H., and Wiesel, T.N. (1959) Receptive fields of single neurons in the cat's visual striate cortex. J Physiol *148*, 574-91.

Iversen, L. L., Mitchell, J. F., and Srinivasan, V. (1971). The release of gamma-aminobutyric acid during inhibition in the cat visual cortex. J Physiol *212*, 519-534.

Jarsky, T., Roxin, A., Kath, W. L., and Spruston, N. (2005). Conditional dendritic spike propagation following distal synaptic activation of hippocampal CA1 pyramidal neurons. Nat Neurosci *8*, 1667-1676.

Johnston, D., and Brown, T. H. (1981). Giant synaptic potential hypothesis for epileptiform activity. Science *211*, 294-297.

Katona, I., Sperlagh, B., Sik, A., Kafalvi, A., Vizi, E. S., Mackie, K., and Freund, T. F. (1999). Presynaptically located CB1 cannabinoid receptors regulate GABA release from axon terminals of specific hippocampal interneurons. J Neurosci *19*, 4544-4558.

Katsumaru, H., Kosaka, T., Heizmann, C. W., and Hama, K. (1988). Immunocytochemical study of GABAergic neurons containing the calcium-binding protein parvalbumin in the rat hippocampus. Exp Brain Res *72*, 347-362.

Kirby, A. W., and Enroth-Cugell, C. (1976). The involvement of gamma-aminobutyric acid in the organization of cat retinal ganglion cell receptive fields. A study with picrotoxin and bicuculline. J Gen Physiol *68*, 465-484.

Klausberger, T., Magill, P. J., Marton, L. F., Roberts, J. D., Cobden, P. M., Buzsaki, G., and Somogyi, P. (2003). Brain-state- and cell-type-specific firing of hippocampal interneurons in vivo. Nature *421*, 844-848.

Klausberger, T., Marton, L. F., Baude, A., Roberts, J. D., Magill, P. J., and Somogyi, P. (2004). Spike timing of dendrite-targeting bistratified cells during hippocampal network oscillations in vivo. Nat Neurosci *7*, 41-47.

Klausberger, T., Marton, L. F., O'Neill, J., Huck, J. H., Dalezios, Y., Fuentealba, P., Suen, W. Y., Papp, E., Kaneko, T., Watanabe, M*., et al.* (2005). Complementary roles of cholecystokinin- and parvalbumin-expressing GABAergic neurons in hippocampal network oscillations. J Neurosci *25*, 9782-9793.

Kuffler, S. W. (1953). Discharge patterns and functional organization of mammalian retina. J Neurophysiol *16*, 37-68.

Kuffler, S. W., and Edwards, C. (1958). Mechanism of gamma aminobutyric acid (GABA) action and its relation to synaptic inhibition. J Neurophysiol *21*, 589-610.

Kuffler, S. W., and Eyzaguirre, C. (1955). Synaptic inhibition in an isolated nerve cell. J Gen Physiol *39*, 155-184.

Kuffler, S. W., and Katz, B. (1946). Inhibition at the nerve muscle junction in crustacea. J Neurophysiol *9*, 337-346.

Kyriazi, H. T., Carvell, G. E., Brumberg, J. C., and Simons, D. J. (1996). Quantitative effects of GABA and bicuculline methiodide on receptive field properties of neurons in real and simulated whisker barrels. J Neurophysiol *75*, 547-560.

Lambert, N. A., Borroni, A. M., Grover, L. M., and Teyler, T. J. (1991). Hyperpolarizing and depolarizing GABAA receptor-mediated dendritic inhibition in area CA1 of the rat hippocampus. J Neurophysiol *66*, 1538-1548.

Larkum, M. E., Zhu, J. J., and Sakmann, B. (1999). A new cellular mechanism for coupling inputs arriving at different cortical layers. Nature *398*, 338-341.

Lee, P. H., Obie, J., and Hong, J. S. (1989). Opioids induce convulsions and wet dog shakes in rats: mediation by hippocampal mu, but not delta or kappa opioid receptors. J Neurosci *9*, 692-697.

Liu, G. (2004). Local structural balance and functional interaction of excitatory and inhibitory synapses in hippocampal dendrites. Nat Neurosci *7*, 373-379.

Llinas, R. R., and Pare, D. (1991). Of dreaming and wakefulness. Neuroscience *44*, 521-535.

Lloyd, D. P. C. (1946). Facilitation and inhibition of spinal motoneurons. J Neurophysiol *9*, 421-438.

Losonczy, A., Biro, A. A., and Nusser, Z. (2004). Persistently active cannabinoid receptors mute a subpopulation of hippocampal interneurons. Proc Natl Acad Sci U S A *101*, 1362-1367.

Losonczy, A., Zhang, L., Shigemoto, R., Somogyi, P., and Nusser, Z. (2002). Cell type dependence and variability in the short-term plasticity of EPSCs in identified mouse hippocampal interneurones. J Physiol *542*, 193-210.

Lupica, C. R., and Dunwiddie, T. V. (1991). Differential effects of mu- and delta-receptor selective opioid agonists on feedforward and feedback GABAergic inhibition in hippocampal brain slices. Synapse *8*, 237-248.

MacVicar, B. A., Tse, F. W., Crichton, S. A., and Kettenmann, H. (1989). GABA-activated Cl- channels in astrocytes of hippocampal slices. J Neurosci *9*, 3577-3583.

Magee, J. C. (2000). Dendritic integration of excitatory synaptic input. Nat Rev Neurosci *1*, 181-190.

Malfroy, B., Swerts, J. P., Llorens, C., and Schwartz, J. C. (1979). Regional distribution of a high-affinity enkephalin-degrading peptidase ('enkephalinase') and effects of lesions suggest localization in the vicinity of opiate receptors in brain. Neurosci Lett *11*, 329-334.

Mann, E. O., Suckling, J. M., Hajos, N., Greenfield, S. A., and Paulsen, O. (2005). Perisomatic feedback inhibition underlies cholinergically induced fast network oscillations in the rat hippocampus in vitro. Neuron *45*, 105-117.

Marmont, G., and Wiersma, C. A. (1938). On the mechanism of inhibition and excitation of crayfish muscle. J Physiol *93*, 173-193.

Martina, M., Royer, S., and Pare, D. (2001). Cell-type-specific GABA responses and chloride homeostasis in the cortex and amygdala. J Neurophysiol *86*, 2887-2895.

Marty, A., and Llano, I. (2005). Excitatory effects of GABA in established brain networks. Trends Neurosci *28*, 284-289.

Marty, S., Wehrle, R., Alvarez-Leefmans, F. J., Gasnier, B., and Sotelo, C. (2002). Postnatal maturation of Na+, K+, 2Cl- cotransporter expression and inhibitory synaptogenesis in the rat hippocampus: an immunocytochemical analysis. Eur J Neurosci *15*, 233-245.

Matyas, F., Freund, T. F., and Gulyas, A. I. (2004). Convergence of excitatory and inhibitory inputs onto CCK-containing basket cells in the CA1 area of the rat hippocampus. Eur J Neurosci *19*, 1243-1256.

McBain, C. J., and Fisahn, A. (2001). Interneurons unbound. Nat Rev Neurosci *2*, 11-23.

Megias, M., Emri, Z., Freund, T. F., and Gulyas, A. I. (2001). Total number and distribution of inhibitory and excitatory synapses on hippocampal CA1 pyramidal cells. Neuroscience *102*, 527-540.

Miles, R., Toth, K., Gulyas, A. I., Hajos, N., and Freund, T. F. (1996). Differences between somatic and dendritic inhibition in the hippocampus. Neuron *16*, 815-823.

Mittmann, W., Koch, U., and Hausser, M. (2005). Feed-forward inhibition shapes the spike output of cerebellar Purkinje cells. J Physiol *563*, 369-378.

Morales, M., and Backman, C. (2002). Coexistence of serotonin 3 (5-HT3) and CB1 cannabinoid receptors in interneurons of hippocampus and dentate gyrus. Hippocampus *12*, 756-764.

Mori, K., Nagao, H., and Yoshihara, Y. (1999). The olfactory bulb: coding and processing of odor molecule information. Science *286*, 711-715.

Ogata, K., and Kosaka, T. (2002). Structural and quantitative analysis of astrocytes in the mouse hippocampus. Neuroscience *113*, 221-233.

Oleskevich, S., and Lacaille, J. C. (1992). Reduction of GABAB inhibitory postsynaptic potentials by serotonin via pre- and postsynaptic mechanisms in CA3 pyramidal cells of rat hippocampus in vitro. Synapse *12*, 173-188.

Paton, G. S., Pertwee, R. G., and Davies, S. N. (1998). Correlation between cannabinoid mediated effects on paired pulse depression and induction of long term potentiation in the rat hippocampal slice. Neuropharmacology *37*, 1123-1130.

Pawelzik, H., Hughes, D. I., and Thomson, A. M. (2002). Physiological and morphological diversity of immunocytochemically defined parvalbumin- and cholecystokinin-positive interneurones in CA1 of the adult rat hippocampus. J Comp Neurol *443*, 346-367.

Pearce, R. A. (1993). Physiological evidence for two distinct GABAA responses in rat hippocampus. Neuron *10*, 189-200.

Perkins, K. L., and Wong, R. K. (1996). Ionic basis of the postsynaptic depolarizing GABA response in hippocampal pyramidal cells. J Neurophysiol *76*, 3886-3894.

Pitler, T. A., and Alger, B. E. (1992). Postsynaptic spike firing reduces synaptic GABAA responses in hippocampal pyramidal cells. J Neurosci *12*, 4122-4132.

Pitler, T. A., and Alger, B. E. (1994). Depolarization-induced suppression of GABAergic inhibition in rat hippocampal pyramidal cells: G protein involvement in a presynaptic mechanism. Neuron *13*, 1447-1455.

Plotkin, M. D., Snyder, E. Y., Hebert, S. C., and Delpire, E. (1997). Expression of the Na-K-2Cl cotransporter is developmentally regulated in postnatal rat brains: a possible mechanism underlying GABA's excitatory role in immature brain. J Neurobiol *33*, 781-795.

Pouille, F., and Scanziani, M. (2001). Enforcement of temporal fidelity in pyramidal cells by somatic feed-forward inhibition. Science *293*, 1159-1163.

Pouille, F., and Scanziani, M. (2004). Routing of spike series by dynamic circuits in the hippocampus. Nature *429*, 717-723.

O'Keefe, J., and Dostrovsky, J. (1971). The hippocampus as a spatial map. Preliminary evidence from unit activity in the freely-moving rat. Brain Res *34*, 171-5.

Ramon y Cajal, S. (1893). Estructura del asta de ammon y fascia dentata. Anal Soc Espan Historia Natural *22*, 53-114.

Renshaw, B. (1946). Central effects of centripetal impulses in axons of spinal ventral roots. J Neurophysiol *9*, 191-204.

Rivera, C., Voipio, J., Payne, J. A., Ruusuvuori, E., Lahtinen, H., Lamsa, K., Pirvola, U., Saarma, M., and Kaila, K. (1999). The K+/Cl- co-transporter KCC2 renders GABA hyperpolarizing during neuronal maturation. Nature *397*, 251-255.

Robbe, D., Montgomery, S. M., Thome, A., Rueda-Orozco, P. E., McNaughton, B. L., and Buzsaki, G. (2006). Cannabinoids reveal importance of spike timing coordination in hippocampal function. Nat Neurosci *9*, 1526-1533.

Rocha, L., and Maidment, N. T. (2003). Opioid peptide release in the rat hippocampus after kainic acid-induced status epilepticus. Hippocampus *13*, 472-480.

Saitoh, I., and Suga, N. (1995). Long delay lines for ranging are created by inhibition in the inferior colliculus of the mustached bat. J Neurophysiol *74*, 1-11.

Schofield, P. R., Darlison, M. G., Fujita, N., Burt, D. R., Stephenson, F. A., Rodriguez, H., Rhee, L. M., Ramachandran, J., Reale, V., Glencorse, T. A., and et al. (1987). Sequence and functional expression of the GABA A receptor shows a ligand-gated receptor super-family. Nature *328*, 221-227.

Sherrington, C. S. (1913). Further observations on the production of reflex stepping by combination of reflex excitation with reflex inhibition. J Physiol *47*, 196-214.

Sik, A., Penttonen, M., Ylinen, A., and Buzsaki, G. (1995). Hippocampal CA1 interneurons: an in vivo intracellular labeling study. J Neurosci *15*, 6651-6665.

Sloviter, R. S. (1991). Feedforward and feedback inhibition of hippocampal principal cell activity evoked by perforant path stimulation: GABA-mediated mechanisms that regulate excitability in vivo. Hippocampus *1*, 31-40.

Somogyi, P., and Klausberger, T. (2005). Defined types of cortical interneurone structure space and spike timing in the hippocampus. J Physiol *562*, 9-26.

Somogyi, P., Nunzi, M. G., Gorio, A., and Smith, A. D. (1983). A new type of specific interneuron in the monkey hippocampus forming synapses exclusively with the axon initial segments of pyramidal cells. Brain Res *259*, 137-142.

Spruston, N., Jaffe, D. B., and Johnston, D. (1994). Dendritic attenuation of synaptic potentials and currents: the role of passive membrane properties. Trends Neurosci *17*, 161-166.

Stumm, R. K., Zhou, C., Schulz, S., and Hollt, V. (2004). Neuronal types expressing mu- and delta-opioid receptor mRNA in the rat hippocampal formation. J Comp Neurol *469*, 107-118.

Szabadics, J., Varga, C., Molnar, G., Olah, S., Barzo, P., and Tamas, G. (2006). Excitatory effect of GABAergic axo-axonic cells in cortical microcircuits. Science *311*, 233-235.

Szentagothai, J. (1975). The 'module-concept' in cerebral cortex architecture. Brain Res *95*, 475-496.

Thompson, S. M., Haas, H. L., and Gahwiler, B. H. (1992). Comparison of the actions of adenosine at pre- and postsynaptic receptors in the rat hippocampus in vitro. J Physiol *451*, 347-363.

Traub, R. D., Whittington, M. A., Stanford, I. M., and Jefferys, J. G. (1996). A mechanism for generation of long-range synchronous fast oscillations in the cortex. Nature *383*, 621-624.

Traub, R. D., and Wong, R. K. (1982). Cellular mechanism of neuronal synchronization in epilepsy. Science *216*, 745-747.

Tsay, D., and Yuste, R. (2004). On the electrical function of dendritic spines. Trends Neurosci *27*, 77-83.

Tsou, K., Mackie, K., Sanudo-Pena, M. C., and Walker, J. M. (1999). Cannabinoid CB1 receptors are localized primarily on cholecystokinin-containing GABAergic interneurons in the rat hippocampal formation. Neuroscience *93*, 969-975.

Tsubokawa, H., and Ross, W. N. (1996). IPSPs modulate spike backpropagation and associated [Ca2+]i changes in the dendrites of hippocampal CA1 pyramidal neurons. J Neurophysiol *76*, 2896-2906.

Varma, N., Carlson, G. C., Ledent, C., and Alger, B. E. (2001). Metabotropic glutamate receptors drive the endocannabinoid system in hippocampus. J Neurosci *21*, RC188.

von Krosigk, M., Bal, T., and McCormick, D. A. (1993). Cellular mechanisms of a synchronized oscillation in the thalamus. Science *261*, 361-364.

Wagner, J. J., Caudle, R. M., Neumaier, J. F., and Chavkin, C. (1990). Stimulation of endogenous opioid release displaces mu receptor binding in rat hippocampus. Neuroscience *37*, 45-53.

Wehr, M., and Zador, A. M. (2003). Balanced inhibition underlies tuning and sharpens spike timing in auditory cortex. Nature *426*, 442-446.

Wei, W., Zhang, N., Peng, Z., Houser, C. R., and Mody, I. (2003). Perisynaptic localization of delta subunit-containing GABA(A) receptors and their activation by GABA spillover in the mouse dentate gyrus. J Neurosci *23*, 10650-10661.

Whittington, M. A., Traub, R. D., and Jefferys, J. G. (1995). Synchronized oscillations in interneuron networks driven by metabotropic glutamate receptor activation. Nature *373*, 612-615.

Wierenga, C. J., and Wadman, W. J. (2003). Functional relation between interneuron input and population activity in the rat hippocampal cornu ammonis 1 area. Neuroscience *118*, 1129-1139.

Wilent, W. B., and Contreras, D. (2005). Dynamics of excitation and inhibition underlying stimulus selectivity in rat somatosensory cortex. Nat Neurosci.

Williams, S. R., and Stuart, G. J. (2003). Role of dendritic synapse location in the control of action potential output. Trends Neurosci *26*, 147-154.

Wilson, M.A., and McNaughton, B.L. (1993). Dynamics of the hippocampal ensemble code for space. Science *261*, 1055-8.

Wilson, R. I., Kunos, G., and Nicoll, R. A. (2001). Presynaptic specificity of endocannabinoid signaling in the hippocampus. Neuron *31*, 453-462.

Wilson, R. I., and Nicoll, R. A. (2001). Endogenous cannabinoids mediate retrograde signalling at hippocampal synapses. Nature *410*, 588-592.

Windhorst, U. (1996). On the role of recurrent inhibitory feedback in motor control. Prog Neurobiol *49*, 517-587.

Woodruff, A. R., Monyer, H., and Sah, P. (2006). GABAergic excitation in the basolateral amygdala. J Neurosci *26*, 11881-11887.

Xie, C. W., and Lewis, D. V. (1995). Depression of LTP in rat dentate gyrus by naloxone is reversed by GABAA blockade. Brain Res *688*, 56-60.

Zeki, S.M. (1974). Functional organization of a visual area in the posterior posterior bank of the superior temporal sulcus of the rhesus monkey. J Physiol *236*, 549-73.